# Evaluation of Occupant Volume Strength in Conventional Passenger Railroad Equipment

A thesis

submitted by

Michael E. Carolan

In partial fulfillment of the requirements

for the degree of

Master of Science

in

Mechanical Engineering

TUFTS UNIVERSITY

May, 2008

Adviser:

Professor A.B. Perlman

**THIS PAGE INTENTIONALLY LEFT BLANK**

**Abstract**

To ensure a level of occupant volume protection, passenger railway equipment operating on mainline railroads in the United States must currently be designed to resist an 800,000 pound compressive load applied statically to the underframe. An alternative manner of evaluating the strength of the occupied volume is sought that will ensure the same level of protection for occupants of the equipment as the current test but will allow for a greater variety of equipment to be evaluated.

A finite element (FE) model of the structural components of the railcar has been applied to examine the existing compressive strength test and evaluate selected alternate testing scenarios. Using simplified geometry and material properties in the model, the gross behaviors of the railcar are captured without excessive processing time. This simplified modeling technique was used to construct FE models of a generic single-level railcar and an exemplar multilevel railcar.

Both models can be interpreted to have some single beam-like behaviors. In each model, the existing compressive load results in a significant bending moment as well as the prescribed compressive load. The alternative load cases examined demonstrate that a larger total compressive force may be distributed across the end structure of the railcar and result in similar stress levels throughout the structural frame as are observed from application of the conventional proof load.

**Acknowledgements**

This thesis certainly would not have been possible without the dedication, enthusiasm, and guidance of my adviser, Professor Perlman. From translating "ancient" finite element codes to providing pep talks when the going got tough, Benj was always happy to help. Thank you for your constant collaboration, which enabled me to finish my Master's degree on time.

I certainly would not have been able to finish this work without the assistance of my Volpe Center project leader, David Tyrell. Thank you for working with me on this thesis, as well as keeping my non-thesis work assignments light, so this could be my primary focus.

I'm certainly grateful for the support of my coworkers at the Volpe Center in my pursuit of this degree. In particular, thank you to Brandon Talamini and Jeff Gordon for advice on working with Abaqus, and Michelle Priante and Kari Jacobsen for advice on writing this thesis.

Special thanks to all of my friends and family who helped keep me sane and focused throughout this entire process. My parents were a steady source of reassurance during the entirety of this Master's degree program. And extra special thanks to Sarah, who has made me realize how lucky I am.

**Abstract** ... iii
**Acknowledgements** ... iv
**List of Figures** ... vii
**List of Tables** ... ix
**Nomenclature** ... x
**Introduction** ... 2
**1 Background** ... 7
1.1 Conventional Passenger Car Design ... 7
1.2 Introduction of Multilevel Passenger Car Designs ... 9
1.3 Development of Specifications and Standards ... 12
1.4 Determining Compliance with Strength Standards ... 18
1.4.1 Current Testing Procedures ... 20
1.4.2 Potential Difficulties Associated with the Current Standards ... 24
1.5 Crashworthiness Research Program ... 28
**2 Modeling Approach** ... 32
2.1 Shell Model of Single-level Conventional Car ... 35
2.1.1 Mesh ... 37
2.1.2 Weights ... 40
2.1.3 Material Used ... 41
**3 Results for Conventional Car** ... 43
3.1 Loading Conditions ... 43
3.2 Boundary Conditions ... 44
3.3 Carbody Neutral Axis ... 46
3.4 Standing Car Results ... 48
3.5 Buff Stop Loading Results ... 56
3.6 Alternative Proof Load ... 65
3.6.1 Buffer Beam Loading Results ... 68
3.6.2 AT Plate Loading Results ... 73
3.6.3 Combined Endframe Loading Results ... 80
**4 Results for Multilevel Car** ... 88
4.1 Model Description ... 88
4.1.1 Mesh ... 89
4.1.2 Weights ... 92

4.1.3 Material Used ..... 93
4.2 Boundary Conditions ..... 94
4.3 Standing Car Load ..... 96
4.4 Baseline 800 kip Load ..... 98
4.5 Alternative Loads ..... 102
**5 Summary ..... 109**
**6 Conclusions ..... 112**
**Appendix A – Tied Constraints versus Single Parts ..... 119**
**Appendix B – Calculation of Suspension Spring Stiffness ..... 124**
**Appendix C – Symmetry of Results ..... 126**
**Appendix D – Stress Contour Plots for Various Load Cases ..... 131**
**Appendix E – Beam and Shell Model ..... 142**
**Appendix F – Conventional Single-level Railcar Construction ..... 153**
**References ..... 161**

## List of Figures

Figure 1 - Plan View of Conventional Underframe Structure ..... 7
Figure 2 - Schematic Showing Underframe and Superstructure, Single-level Car ..... 8
Figure 3 - Schematic Application of Static End Load on Single-level Car ..... 9
Figure 4 - Exemplar Profile for Multilevel Passenger Railcar ..... 10
Figure 5 - Cutaway View of Multilevel Car ..... 11
Figure 6 - Schematic Application of Static End Load on Multilevel Car ..... 12
Figure 7 - RPO Car, Circa 1940 ..... 16
Figure 8 - Schematic Representation of Buff Strength Test ..... 21
Figure 9 - Carbody Supports for Compressive Strength Test ..... 22
Figure 10 - Load Application Mechanism for Compressive Strength Test ..... 23
Figure 11 - Line of Draft and Underframe Height, Single-level and Multilevel Cars ..... 26
Figure 12 - Representative Articulated Railcar Design ..... 27
Figure 13 - Single-car Impact Test, Before (Left) and After (Right) Impact ..... 30
Figure 14 - Force-crush Characteristics from Single-car and Two-car Impact Tests ..... 31
Figure 15 - Progression of Shell Mesh for Prismatic Longitudinal Center Sill ..... 36
Figure 16 - Single-level Car Model Geometry ..... 38
Figure 17 - Single-level Car Longitudinal Members ..... 39
Figure 18 - Mesh of Single-level Railcar ..... 40
Figure 19 - Location of Buff Stops in Single-level FE Model ..... 44
Figure 20 - Boundary Conditions Applied to Body Bolster ..... 45
Figure 21 - Contour Plot of Longitudinal Displacement, Cantilevered Conventional Railcar ..... 47
Figure 22 - Neutral Axis Height for Varied Cross-section Locations ..... 48
Figure 23 - Undeformed and Deformed Profiles, AW0 Railcar ..... 49
Figure 24 - Stress Distribution in Center Sill, Standing AW0 Railcar ..... 50
Figure 25 - Stress Distribution in Side Sill, AW0 Railcar ..... 51
Figure 26 - Stress Distribution in Belt Rail, AW0 Railcar ..... 52
Figure 27 - Stress Distribution in Upper Window Rail, AW0 Railcar ..... 53
Figure 28 - Stress Distribution in Roof Rail, AW0 Railcar ..... 54
Figure 29 - Stress Distribution in Purlin, AW0 Railcar ..... 55
Figure 30 - Stress Distribution in Longitudinal Members Over Occupant Volume, AW0 Railcar 56
Figure 31 - Schematic of Stresses from Compression and Bending ..... 57
Figure 32 - Shapes of Deformed Carbody under Gravity and 800 kip Loads ..... 58
Figure 33 - Stress Distribution in Center Sill, 800 kip Load ..... 59
Figure 34 - Stress Distribution in Side Sill, 800 kip Load ..... 60
Figure 35 - Stress Distribution in Belt Rail, 800 kip Load ..... 61
Figure 36 - Stress Distribution in Upper Window Rail, 800 kip Load ..... 62
Figure 37 - Stress Distribution in Roof Rail, 800 kip Load ..... 63
Figure 38 - Stress Distribution in Purlin, 800 kip Load ..... 63
Figure 39 - Stress Distribution in Longitudinal Members, 800 kip Load ..... 64
Figure 40 - Average Occupant Volume Stresses, 800 kip Load ..... 65
Figure 41 - Coupled CEM Railcars ..... 67
Figure 42 - Buffer Beam Compressive Test Setup ..... 69
Figure 43 - Average Stresses in Center Sill, 800 kip and 1,000 kip Loads ..... 70
Figure 44 - Average Stresses in Side Sill, 800 kip and 1,000 kip Loads ..... 71
Figure 45 - Average Occupant Volume Stresses, 800 and 1,000 kip Loads ..... 72
Figure 46 - Stress Distribution in Longitudinal Members, 1,000 kip Load ..... 73
Figure 47 - AT Plate Compressive Test Setup ..... 74
Figure 48 - Stress Distribution in Center Sill, 200 kip Load ..... 75
Figure 49 - Average Stresses in Center Sill, 200 kip and AW0 Loads ..... 76
Figure 50 - Stress Distribution in Side Sill, 200 kip Load ..... 77
Figure 51 - Average Stresses in Side Sill, 200 kip and AW0 Loads ..... 77
Figure 52 - Average Stresses in Superstructure Members, 200 kip and AW0 Loads ..... 78

Figure 53 - Stress Distribution in Longitudinal Members, 200 kip Load ..... 79
Figure 54 - Combined AT Plate and Buffer Beam Compressive Test Setup ..... 81
Figure 55 - Stress Distribution in Center Sill, 1,200 kip Load ..... 82
Figure 56 - Average Stresses in Center Sill, 800, 1,000, 1,200 kip Loads ..... 83
Figure 57 - Stress Distribution in Side Sill, 1,200 kip Load ..... 84
Figure 58 - Average Stresses in Side Sill, 800, 1,000, 1,200 kip Loads ..... 85
Figure 59 - Average Occupant Volume Stresses, 800, 1,000, 1,200 kip Loads ..... 86
Figure 60 - Stress Distribution in Longitudinal Members, 1,200 kip Load ..... 87
Figure 61 - Multilevel Railcar Geometry ..... 90
Figure 62 - Profile of Multilevel Railcar Structure ..... 91
Figure 63 - Mesh of Multilevel Railcar ..... 92
Figure 64 - Boundary Condition Applied to Multilevel Body Bolster ..... 95
Figure 65 - Stress Distribution for Multilevel Car, AW0 Load ..... 96
Figure 66 - Average Stresses in Center Section of Multilevel Car, AW0 Load ..... 97
Figure 67 - Stress Distribution in Center Sill of Multilevel Car, 800 kip Load ..... 98
Figure 68 - Stress Distribution in Side Sill of Multilevel Car, 800 kip Load ..... 99
Figure 69 - Stress Distribution in Multilevel Railcar, 800 kip Load ..... 100
Figure 70 - Average Stresses in Center Section of Multilevel Car, 800 kip Load ..... 101
Figure 71 - Alternative Load Setup for Multilevel Railcar ..... 102
Figure 72 - Average Stresses in Center Section of Multilevel Car, 800 and 1,000 kip Loads ..... 103
Figure 73 - Stress Distributions in Multilevel Railcar, 1,000 kip Load ..... 104
Figure 74 - Average Stresses in Center Section of Multilevel Car, 200 kip and AW0 Loads ..... 105
Figure 75 - Stress Distributions in Multilevel Car, 200 kip Load ..... 106
Figure 76 - Average Stresses in Center Section of Multilevel Car, 800, 1,000, and 1,200 kip Loads ..... 107
Figure 77 - Stress Distributions in Multilevel Railcar, 1,200 kip Load ..... 108
Figure 78 - Average Stresses in Single-level (top) and Multilevel (bottom) Cars ..... 116

## List of Tables

Table 1 - Summary of Previous Finite Element Models ..... 32
Table 2 - Single-level Railcar Weights..... 41
Table 3 - Material Properties Used for Steel ..... 42
Table 4 - Yield Stresses for Structural Members, Shell Model ..... 42
Table 5 - Summary of Boundary Conditions, Single-level Model ..... 46
Table 6 - Multilevel Railcar Weights ..... 93
Table 7 - Material Properties, Multilevel Railcar Model ..... 94

**Nomenclature**

| | |
|---|---|
| AAR | Association of American Railroads |
| APTA | American Public Transportation Association |
| AT Plate | Anti-telescoping plate |
| AW0 | Empty, ready-to-run weight condition |
| CEM | Crash Energy Management |
| CFR | Code of Federal Regulations |
| FE | Finite element |
| FRA | Federal Railroad Administration |
| ICC | Interstate Commerce Commission |
| Kip | Kilopound (1000 pounds) |
| MU | Multiple unit |
| RMS | Railway Mail Service |
| RPO | Railway Post Office |
| SOA | State-of-the-art |
| UIC | International Union of Railways |
| Volpe Center | Volpe National Transportation Systems Center |

# Evaluation of Occupant Volume Strength in Conventional Passenger Railroad Equipment

## Introduction

The objective of this thesis is to examine the existing compressive strength test used to determine structural strength in passenger railroad equipment. With an understanding of the demands of this test, alternative tests may be examined that will enable a wider variety of equipment to be evaluated while ensuring comparable occupant protection. This work was performed using a finite element (FE) model of a generalized conventionally-designed single-level passenger railcar. The model was used to evaluate the occupied volume strength design standard that is applied to North American railroad equipment, the compressive strength requirement. Compliance with this requirement is verified when a vehicle exhibits no permanent deformation under 800,000 pounds of compression applied at the line-of-draft. The model had a number of simplifications made to allow a number of simulations to be run in a short period of time. Once the single-level passenger car model was assembled, the same modeling technique was used to create a model of a multilevel rail vehicle.

The Department of Transportation's Federal Railroad Administration (FRA) promulgates regulations to promote safe inter-city, passenger, and freight rail operation [1]. One of the major concerns addressed by these regulations is the safety of crew and passengers during normal operations as well as during collision events. While rail travel is one of the safest forms of transportation, railroad accidents have historically been high-profile events. Over time, a number of federal regulations as well as rail industry standards have developed to ensure a

baseline level of protection to railcar occupants.

The first priority of a crashworthy railcar is to prevent loss of occupant volume, providing some space for the occupants of the car to ride out the collision [2]. Preservation of the occupant volume has typically been accomplished by the structural strength of the car. If the railcar is sufficiently strong, the occupied volume will be able to withstand the forces of a collision.

The standard that has the greatest influence on the strength of a passenger railcar is known as the "Static End Strength Requirement", located in the Code of Federal Regulations (CFR) at 49CFR238.203 [3]. This requirement states, in part:

> Except as further specified…on or after November 8, 1999 all passenger equipment shall resist a minimum static end load of 800,000 pounds applied on the line of draft without permanent deformation of the body structure.

This requirement has evolved into its current form over the course of the 20th century as the railroads themselves have gone through a number of changes with respect to equipment and services. While this design requirement ensures a strong underframe, it does not dictate the strength of the superstructure. Additionally, this requirement contains implicit requirements for the design of the underframe, which have constrained the ability of railcar manufacturers to introduce new designs to the American market. Finally, accident studies and full-scale crash testing have shown that the loads introduced into the railcar during a collision are dynamic in nature and spread out over a larger area than the prescribed static load applied at the line of draft [4]. The results of these dynamic tests indicate that the carbody is capable of transmitting loads greater than 800

kips when the load is applied over a greater area of the structure.

By utilizing an FE model of a conventional railcar, the 800 kip static end strength test can be simulated and the load path through the car structure can be determined. This information can be used to help in breaking the test down to a set of testing conditions that are better suited to ensuring occupied volume conservation in a variety of rail equipment. The FE model can also be used to evaluate the railcar's behavior when loaded by proposed alternative proof loads.

This thesis begins with a discussion of the structure of conventionally-designed passenger rail equipment. A study of the structure of the railcar leads to an examination of the development of the static strength requirement, to provide an overview of how passenger car structural crashworthiness evolved to where it is today. The background discussion also includes an introduction to non-conventional rail equipment and some of the difficulties associated with this equipment meeting the current testing requirements.

Three distinct modeling techniques were considered. The first technique used beam elements to construct the structural members of the railcar, with shell elements for the roof, wall, and floor skins. This technique oversimplifies the geometry of the car. Detailed models, with complex material behavior and complicated connections between members have high geometric fidelity. However, they require excessive processing time. This technique was determined to be overly sophisticated for evaluating a static load case.

The technique ultimately chosen was a compromise between the two aforementioned approaches. Shell elements represent both the structural members

and the skin of the railcar. The geometries of the members were simplified where possible. Members were connected directly to one another without the use of complicated connectors, and the material behavior was linear elastic. This approach resulted in FE models that adequately captured the overall behavior of the railcar with runtimes on the order of 10 minutes.

Shell models of single- and multilevel cars establish the behavior of the railcar when the 800 kip compressive load is applied. This investigation identifies the stress states in the carbody during the test. The effects of the 800 kip load on the individual structural members of the carbody are investigated in detail.

The FE model of the single-level car captures the overall car behavior as a simple beam. The 800 kip compressive load is applied below the neutral axis of the railcar. This condition results not only in a compressive axial load, but a bending moment as well. The combination of these two effects is a railcar under compression in the underframe but in tension at the roof level.

A series of alternative loading conditions are then applied to the vehicle. These loads include compressive and bending loads designed to load the car in a manner comparable to the current test. The alternative loads, applied across larger areas of the car end, total more than 800 kips but generate similar stress levels in the longitudinal members examined.

The second FE model analyzed for its response to the 800 kip test is a model of a multilevel car. This vehicle behaves similarly to the single-level car, but there are exceptions. The neutral axis location of this vehicle is less evident, as the car features a dramatic change in cross-section to create the partial low-

floor area. The application of the 800 kip compressive load results in compressive stresses in each longitudinal member examined, where the single-level car exhibited tensile stresses at the roof-height members. The alternative loads applied to this model are similar to those applied to the single-level car model, and result in comparable behavior in the multilevel car as the 800 kip compressive load.

# 1 Background

## 1.1 Conventional Passenger Car Design

The conventional design for a passenger railcar for service in North America relies on a strong underframe, as shown schematically in Figure 1 [5]. During normal operations, the largest of the forces transmitted through the vehicle are compressive (buff) and tensile (draft) longitudinal forces associated with the acceleration and deceleration of the railcar. The draft sill is a significant structural member that also provides a housing for the coupler. The draft sill is connected to the body bolster, which provides lateral support to the underframe at the location where the trucks are attached. The longitudinal distance between the two body bolsters is spanned by a center sill and two side sills. The center sill is more structurally significant than the side sills, as the center sill is aligned with the line of draft between the two draft sills.

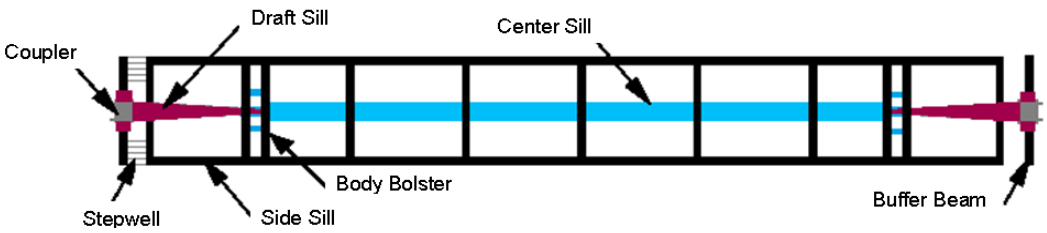


**Figure 1 - Plan View of Conventional Underframe Structure**

Additional longitudinal members in the superstructure contribute to the load path of these buff and draft forces through the car. The superstructure of the railcar is made up of these longerans, vertical members supporting the walls, and the wall skin itself. The members in the superstructure are less structurally

significant than those in the underframe, despite enclosing a large volume of the car. The superstructure and underframe are shown in a schematic elevation of the railcar in Figure 2.

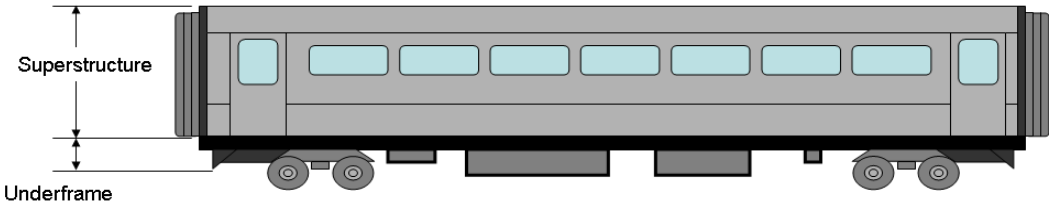


**Figure 2 - Schematic Showing Underframe and Superstructure, Single-level Car**

In addition to the underframe and superstructure of the railcar, there are a number of other significant structures important to the discussion of the proof loading of the railcar. These include the endframes, the trucks, and the coupler and draft gear assemblies. These structures are discussed in a detail in Appendix F – Conventional Single-level Railcar Construction.

A conventional single-level passenger car weighs approximately 100,000 pounds in an empty, ready-to-run configuration [6]. This loading caused by the car weight is known as AW0 condition [18]. This weight includes the trucks, mechanical equipment, and interior fixtures. The structural components of the carbody weigh approximately 24,000 pounds [6]. Typical single-level passenger cars of conventional construction have a coupler-to-coupler length of 85 feet [9].

In order to determine compliance with the static end compression strength requirement, a longitudinal load of 800 kips is applied to the carbody. The test load is applied to the buff stops, the structures within the draft sill that the coupler of the car reacts against. The line of draft is the line of action of the compressive

force running coupler-to-coupler. This load is shown schematically on a representative single-level railcar in Figure 3.

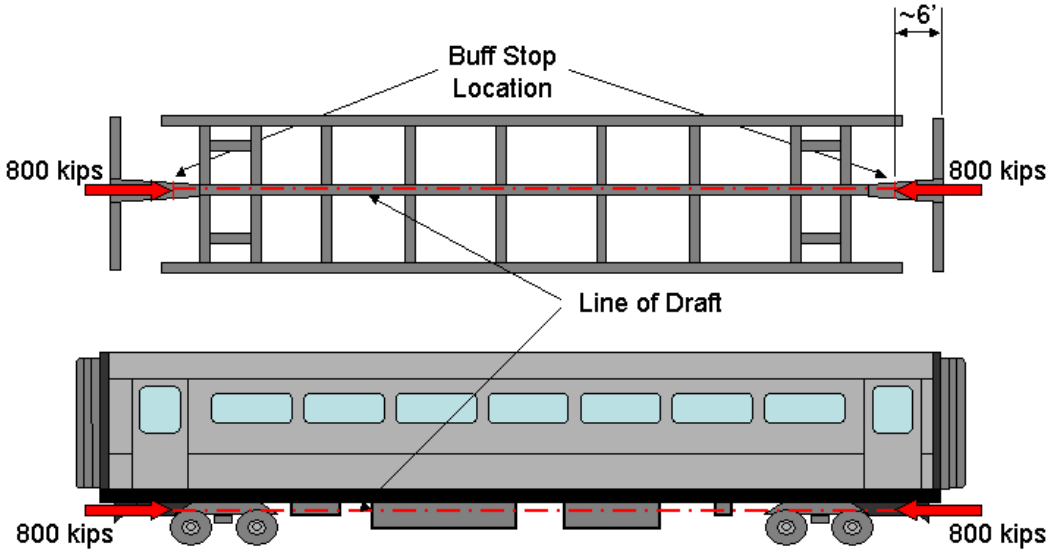


**Figure 3 - Schematic Application of Static End Load on Single-level Car**

## 1.2 Introduction of Multilevel Passenger Car Designs

As railroad corridors have become more densely populated, commuter railroads have found a surging demand for their services. A difficulty with this is the need to increase the number of passengers per train, subject to restrictions on time, space, and weight. Adding more trains is not always an option, as timetables may not permit more traffic on a line. While simply adding more cars to each scheduled train seems an attractive option, both locomotive pulling power and available station space may prevent this from being a reality as well.

An attractive option to a number of railroads has been to increase the number of passengers that can be carried in a given car. To accomplish this, these railroads have started using multilevel equipment. While there are a small

number of discrete designs for this type of equipment being used on North American railroads today, these designs do differ from one another. Rather than elaborate on the small differences employed by different manufacturers, the general similarities between the cars will be discussed in further detail. An exemplar multilevel car is shown in profile in Figure 4.

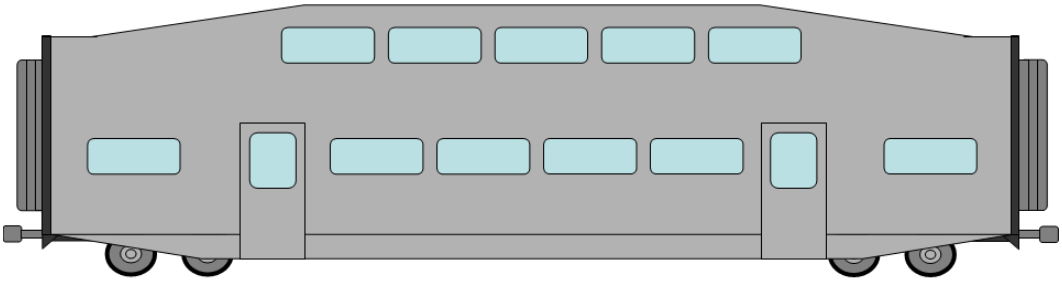

**Figure 4 - Exemplar Profile for Multilevel Passenger Railcar**

The service demands on the multilevel car are the same as on the conventional single-level car. The in-train buff and draft forces developed during service are on the same scale as those developed in the consist made up of single-level cars. The multilevel cars are taller than the single-level cars but are the same length (85 feet) from coupler to coupler [9]. Multilevel cars typically weigh more than single-level cars, which is a result of more carbody structure as well as more interior fixtures. A typical multilevel passenger car weighs approximately 140,000 pounds in AW0 configuration [10].

While both the single-level and multilevel cars feature the same general longitudinal members, there are significant differences in the way these members are arranged in each car. As shown in Figure 5, the multilevel car features seating at three distinct elevations: a mezzanine level over the trucks and draft sills, a

lower level with the underframe as a base, and an upper level with its own supporting structure [10]. To create the dual levels between the two bolsters, it is necessary to depress the lower level, between the body bolsters.

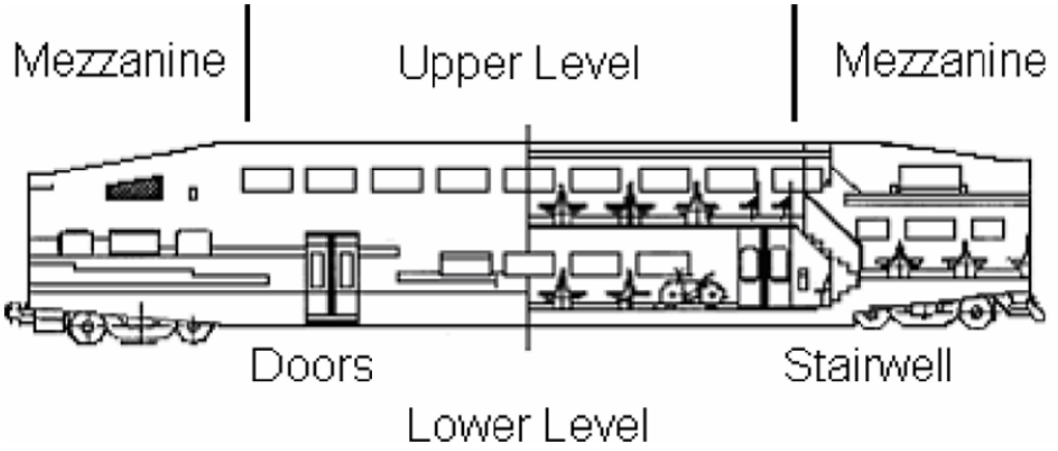


**Figure 5 - Cutaway View of Multilevel Car**

This lowering of the floor of the car in the middle of the vehicle results in an underframe that is not one continuous level, as in the single-level car. Between the body bolsters and the lower level there exists a transition zone, also referred to as a "gooseneck," which connects the side and center sills of the lower level with the side and draft sills of the mezzanine level of the car.

The multilevel passenger car is required to meet the applicable safety standards and regulations, including the compressive end strength requirement. The compressive-strength test is performed in the same manner for both the single- and multilevel cars. This testing procedure is outlined in Section 1.4.1. Figure 6 shows the 800 kip compressive load schematically applied to a multilevel railcar. The approximate vertical location of the underframe is shown in this diagram as a solid yellow line.

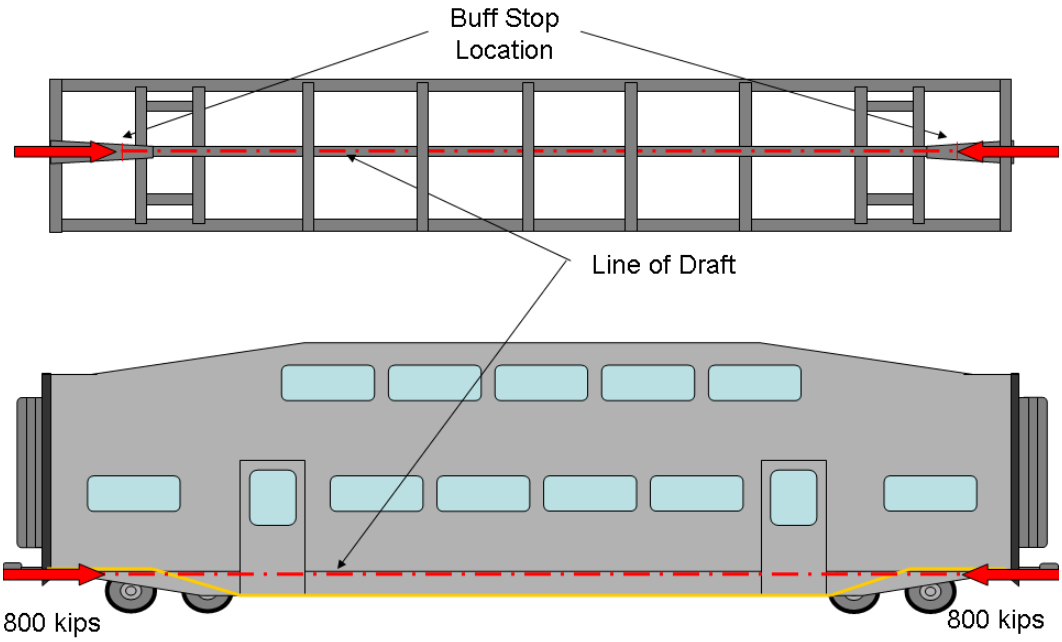


**Figure 6 - Schematic Application of Static End Load on Multilevel Car**

At the mezzanine level of the multilevel car, the position of the compressive load with respect to the center sill is the same as in the single-level car. As the structure goes through the transition zone to the lower level of the car, the center and side sills move to a lower height. The centerline of draft, being an imaginary line of reaction between the two couplers of the car, does not shift as the geometry changes. The result of this is an offset between the position of the underframe and the centerline of draft, such that the centerline of draft is located vertically above the significant structural members of the underframe.

## 1.3 Development of Specifications and Standards

While railroad passenger cars have evolved from the wooden wagons of the 1800's to the modern steel coaches of today, many of the hazards that could affect safe train operation remain the same [11]. Over time, the design of the

railcar has evolved to incorporate protection strategies against these hazards. The evolution of safety features in railcars has historically been a reactionary process, where rail accidents reveal undesirable behavior of existing equipment. New design features are developed to address the behavior, and standards and/or regulations dictate the use of such features in future construction.

In addition to supporting the buff and draft forces during normal operations, the carbody must support the suspension loads, as well as the loads associated with the occupants. The train must not experience any permanent deformation under these conditions. During normal operations, the train cars are subject to impact loads at low speed during yard operations, such as coupling them. Again, the design should be robust enough that permanent damage is not incurred during this operation.

While the majority of railroad equipment will never be subject to emergency loading conditions, it is important that the equipment be designed as though it will be. This broad category of operation subjects the equipment to a number of extreme loading conditions, including medium to high speed impact, high buff forces associated with emergency braking, and vertical loading associated with train cars overriding one another [25]. While it is not possible to design a railcar that is impervious to all potential emergency scenarios, it is good engineering practice to have a design that is robust enough to provide some level of protection to its occupants regardless of the overload type.

In the case of a collision, it is essential that the passengers of the car be given sufficient space within the car that they may “ride out” the collision. A

number of accidents in the early part of the 20th century resulted in the deaths of passengers when the interior space of the car was compromised by another car intruding into it [11]. In 1906, the Pennsylvania Railroad was developing some of the earliest steel passenger railroad cars [11]. These early designs featured center sills that were designed to handle the entire longitudinal load. The car was designed to "withstand…a minimum end force of 200 tons" [11].

During this time period, the United States Post Office operated Railway Post Office (RPO) cars across the United States [4]. These cars housed postal employees who collected, sorted, and bagged mail while the train was en route. In an effort to protect its employees in the event of an accident, the Post Office issued a set of specifications for the construction of RPO cars in 1912, the Railway Mail Service (RMS) Specification [12]. The Post Office was pushing for the adoption of steel railway cars when it generated this standard [11]. This document represents the earliest published crashworthiness specification for passenger railcars in the U.S. [12].

Among the structural requirements included in the Post Office Specification was a minimum compressive load that the underframe was required to resist. This specification was described as follows in a 1919 Interstate Commerce Commission (ICC) railroad accident report:

> In the Railway Mail Service, specifications require a static resistance in the underframe members of 400,000 pounds, the several structural parts to act as a unit, the stresses being restricted to 16,000 pounds per square inch [13].

In later revisions of the specification, a factor of safety of 2 was to be included in calculations of buff strength, so that the minimum effective force to

cause yield was 800,000 pounds [14]. This load was understood to be applied at the rear end of the draft gear, which is the location of the buff stops.

As a requirement, this specification only applied to RPO cars. The United States Post Office did not have the authority to require that railroads develop equivalent standards for railcars in general passenger service. Individual railroads, however, began to include portions of this specification in the designs for their own passenger equipment [12]. During the 1930's, railroads developed "lightweight" steel passenger cars, which raised questions about the structural strength necessary to be compatible with older, "heavyweight" steel car designs [11]. In 1939, the Association of American Railroads (AAR) developed a set of recommended practices for the construction of passenger railcars that included a number of structural specifications from the RMS Specification, known as AAR S-034 [15]. This recommendation was adopted into an AAR standard in 1945, "Specifications for the Construction of New Passenger Equipment Cars," with the strength requirement being an 800,000 pound load applied on the center line of draft with no permanent deformation in the car structure [15]. An RPO car of riveted steel construction, circa 1940, is shown in Figure 7.


**Figure 7 - RPO Car, Circa 1940**

In addition to the 800 kips applied at the buff stops of the railcar, the AAR specification also called for 500 kips applied across the buffer beam and 400 kips applied between the buffer beam and line of draft [20]. However, because the 800 kip load is of greater magnitude and is typically offset further from the carbody's neutral axis than either of the other two compressive loads, the carbody was only typically subjected to the 800 kip compressive test as a means of determining compliance [20].

As railroad equipment evolved, a new type of vehicle began to appear on the North American railroads. The multiple-unit (MU) locomotive is a self-propelled rail vehicle that is also occupied by passengers [16]. A consist composed of multiple-unit locomotives does not require a conventional locomotive to power the train, as each car provides its own motive power, either from an onboard diesel engine or from overhead catenaries or third rail electricity. In response to a number of fatal accidents involving MU equipment, the ICC issued new regulations in 1956 to require MU locomotives to also withstand 800 kips applied at the rear of the buff stops [12]. In 1965, the United States Congress

transferred control over railroad safety from the ICC to the FRA [17]. These MU regulations were incorporated into the CFR, and are currently found at 49CFR229.141.

In 1989, the AAR discontinued publication of its passenger car construction standards [12]. The standards were still employed in the construction of new passenger equipment after this time, but no further changes to the standard were made. In 1995, as mandated by Congress, the FRA began drafting regulations to improve the crashworthiness of passenger rail equipment [1]. The FRA issued these new regulations on the safety of passenger rail equipment in 1999. The rule governing the static compressive strength of passenger cars can be found at 49CFR238.203. This requirement mandates that passenger equipment is to resist 800 kips applied at the line of draft without permanent deformation. This regulation covers all passenger-carrying equipment, including coach cars, multiple unit locomotives, and cab control cars, traveling on the general railroad system. As a part of the CFR, this regulation carries the force of law.

Also in 1999, the American Public Transportation Association (APTA) approved "Standard for the Design and Construction of Passenger Railroad Rolling Stock," SS-C&S-034-99 [18]. The APTA standard incorporates requirements from both the AAR S-034 as well as the CFR. Portions of this standard exceed the requirements of the prior standards. The APTA standard for buff strength also requires 800 kips applied "longitudinally on the centerline of draft to the coupler or drawbar anchor of an empty, ready-to-run car body" [18].

Additionally, there is a requirement for a 500 kip load applied over an area of the "underframe end sill or buffer beam construction." The criterion for passing either test is no permanent deformation.

Outside of the United States, railroad crashworthiness compliance is evaluated in different ways. In Europe, railroad car structural requirements are published by the International Union of Railways (UIC) [19]. The UIC prescribes a number of static structural requirements for passenger railcars, including longitudinal compressive loading requirements. Among the standards is the ability for the railcar to be loaded to 2000 kN (450 kip) at the buffers, 300 kN (67.5 kip) at the lower superstructure longerans, 300 kN (67.5 kip) at the upper superstructure longerans, and 2000 kN (450 kip) inboard of the couplers.

## 1.4 Determining Compliance with Strength Standards

While the RMS specification was required for any cars to be used as Railway Post Office cars, cars for general passenger service could be built to this specification if the builder and purchaser so desired. Demonstrating compliance with the static end strength portion of the specification was also a matter between the manufacturer and the purchaser.

In the early 20$^{th}$ century, there was no requirement for the builder to test the entire passenger car for compliance with the buff strength requirement. In an accident report from 1938, the ICC discusses different methodologies employed in evaluating the structural strength of passenger cars that were subsequently involved in an accident. In the case of one railroad,

> Tests were made of a section of a Cor-Ten steel underframe which was duplicate

> of that used on the…streamlined cars involved in this accident. The section was 8 feet 1/8 inch in length, which represents the greatest unsupported span which occurs at the center of the car…Actual extensometer stress readings were made up to 900,000 pounds, at which point the instrument readings were discontinued, but calculated stresses were applied up to 1,000,000 pounds pressure, at which point it was apparent that the yield point had been reached [14].

The railroad described accepted the results of a test where the compressive load was applied to a section of the center sill. The test demonstrated that with loads applied directly to a section of the center sill, the member could support loads in excess of 800 kips compressive without permanent deformation. The builder based this test on the assumption that the critical location for the compressive loading would be in the center sill, in the region with the fewest lateral members.

This same report includes mention of another test performed on the same type of car, where a different railroad was preparing to purchase this type of equipment.

> For this purpose, the [manufacturer] furnished a complete skeleton car frame, without interior finish, windows, etc, and the test was made in February, 1938…The actual, full-size car frame was subjected to a longitudinal compression test and the report covering this test shows that the center sills began to spread just back of the draft casting when a pressure of 395,000 pounds was indicated by the hydraulic gage…The test was stopped at this point and a plate…was applied to the bottom of the sill, after which the test was continued to a pressure of 909,000 pounds on the hydraulic gage. The report shows that the draft casting failed at 882,000 pounds and the center sill cracked at 909,000 pounds [14].

By conducting the compressive strength test on an entire carbody, the second railroad more closely simulated the loading that the vehicle would be subject to during operations. Additionally, this test revealed a potential vulnerability in the design, which could be addressed with a reinforcing plate in the later design. The ICC report indicates that there was no evidence of this reinforcement being made

to cars from the earlier test.

An American railcar manufacturer constructed the first testing machine capable of performing a compression test on an entire railroad car in 1939 [11]. In 1954, the AAR began performing compression tests on entire cars as a method of determining compliance with its standards [17]. Testing the structure of full cars is still the standard method of demonstration of compliance with the buff strength requirement.

### 1.4.1 Current Testing Procedures

The procedures for conducting a buff strength test are given in detail in APTA SS-C&S 034-99. In addition to the structural load requirements dictated by 49CFR238.203, the APTA standard states that the test article shall be an "empty, ready-to-run car body" [18]. The car builder is not required to outfit the car with interior fixtures, such as seats and lighting, but is required to ballast the car such that the weight of these items is accounted for. A schematic representation of the testing setup is shown below, in Figure 8.

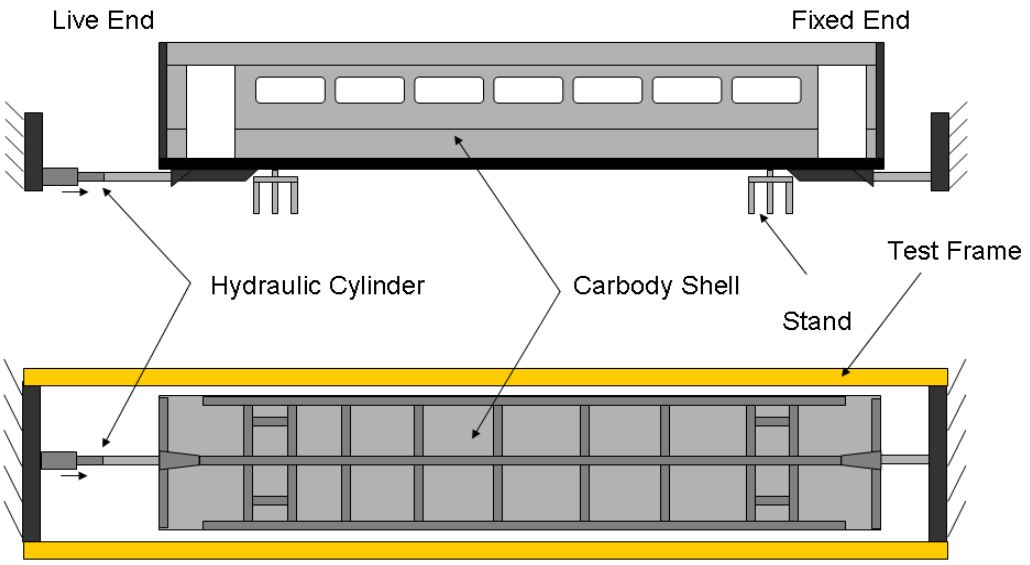


**Figure 8 - Schematic Representation of Buff Strength Test**

The vehicle is to be supported on trucks, or a fixture that simulates the trucks and allows the vehicle to move longitudinally. Since the truck assembly for a passenger railcar represents a significant portion of the cost of the car, it can be desirable to test the structure of the car for compliance with the buff strength requirement before the manufacturer acquires the trucks. Figure 9 shows a photograph of a passenger railcar being supported by a fixture during a compressive strength test. The supports are typically placed at the locations where the trucks and suspension would be connected to the carbody.

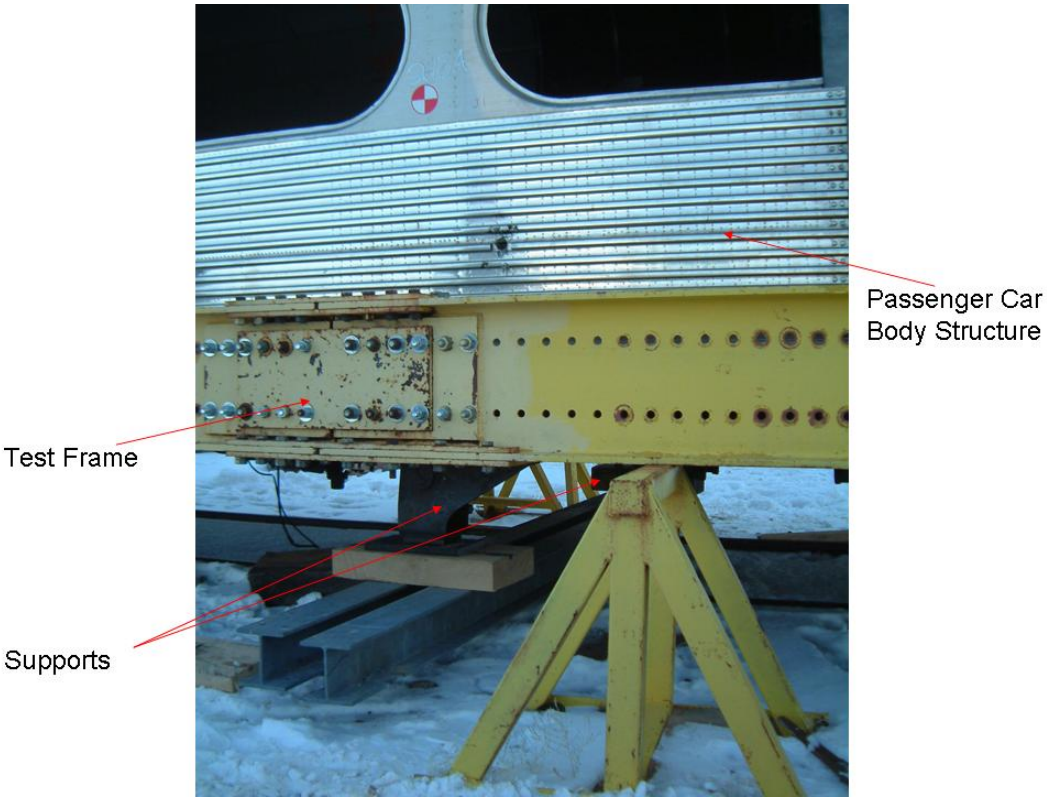


**Figure 9 - Carbody Supports for Compressive Strength Test**

The draft gear is removed from each end of the car, as the loads involved in this test are higher than the draft gear is designed to sustain without permanent deformation. The compression load is applied to the buff stop at the centerline of draft by a controlled ram. The load is to be applied horizontally and quasi-statically. The setup for applying the load to the buff stops during the test can be seen below, in Figure 10.

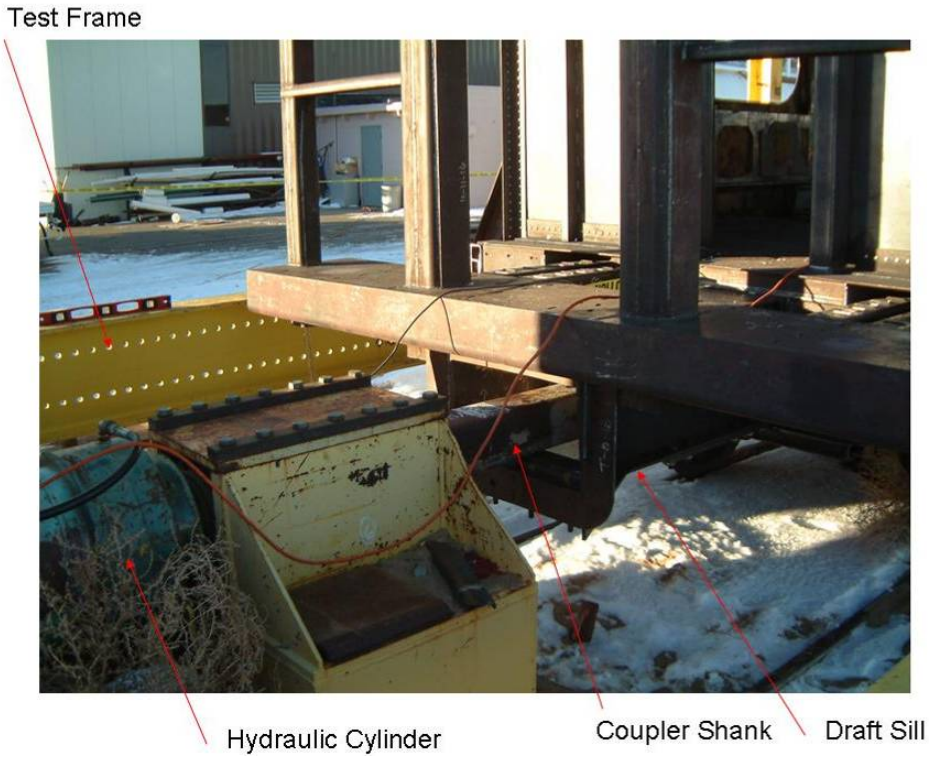


**Figure 10 - Load Application Mechanism for Compressive Strength Test**

The load is applied in gradual increments, with at least one return to a low load (2000 pounds). This gradual loading is done for safety reasons, so that stresses can be extrapolated and the test can be terminated if it appears an area will exceed yield when the full force is applied [18]. The manufacturer can then make appropriate design modifications based on the results of the test to ensure the equipment is compliant.

A load cell is typically used to record the compression loads. Strain gages are placed on key structural members on the car to determine whether these structures yield. The exact placement of strain gages is typically determined by the manufacturer of the car and is based on prior analyses of locations expected to have high stresses. Additionally, the APTA standard states:

> There shall be no visual permanent deformation, fractures, cracks, or separations in the vehicle structure. Broken welds shall be jointly inspected by the Purchaser and Manufacturer to determine if the failure is the result of inadequate weld quality or overstress [18].

This test has become the standard test for determining the longitudinal strength of the car for a number of reasons. The pass or fail criterion is straightforward and easy to measure; by visual inspection of the members and analysis of the strain gage results, it can be established whether the vehicle experiences yielding. The testing setup is reasonably simple, requiring jackstands, a hydraulic cylinder capable of developing the 800 kip compressive load, and load cells capable of measuring the applied loads.

Finally, since a vehicle that passes this test does not experience yielding, this test is a nondestructive one. The importance of this feature of the test cannot be overlooked. In the United States, new passenger railroad equipment orders typically are on the scale of 100 per year. Additionally, there is a significant investment of both time and money in the development of the first production model of a new design [5]. The test article that passes the 800 kip buff strength test is typically not discarded, but has its assembly completed and is then delivered to the customer. Any changes to the testing required to assure longitudinal structural strength must account for these factors if they are to be accepted by the industry.

### 1.4.2 Potential Difficulties Associated with the Current Standards

Because standards have evolved over time in a reactionary way, they

usually are enacted to address a specific concern in existing railroad equipment. The standard shapes the design of the next generation of railroad equipment, which in turn establishes the starting point for the next round of standards. This has resulted in manufacturers developing a design that meets the current standard and modifying it to meet the new standard. Due to a small number of companies engaged in the manufacture of passenger railroad cars, there are a small number of distinct railcar designs being manufactured at the current time. The improved standards have consistently provided an incremental improvement to the performance of existing equipment.

One drawback associated with standards that have evolved in such a way is a difficulty in bringing radical, alternative, or otherwise different designs to the North American passenger railcar market. Any design that wishes to deviate from the conventional, single-level construction that has flourished since the early days of railroading must find itself in compliance with standards that have evolved alongside the single-level equipment.

While both the APTA standard SS-C&S-034-99 and 49CFR238.203 refer to applying the compressive end strength load along the "line of draft," neither document provides a definition of what the line of draft actually is. Historically, the line of draft has been an abstraction, rather than a physical attribute. The line of draft can be thought of as the line of action of the longitudinal forces in the coupler at either end of the car. The line of draft runs from one coupler to the other, although the forces applied to the coupler must travel through the carbody structure to reach the opposite end of the vehicle.

In the case of both the single-level and the multilevel railcars, the line of draft does not correspond with any physical feature of the car. Figure 11 shows the approximate line of draft and underframe height for the single-level car as well as the multilevel car. In the single-level car, the line of draft is located below the underframe for the entire length of the car. For the multilevel car, the line of draft is above the underframe for the region between the two goosenecks.

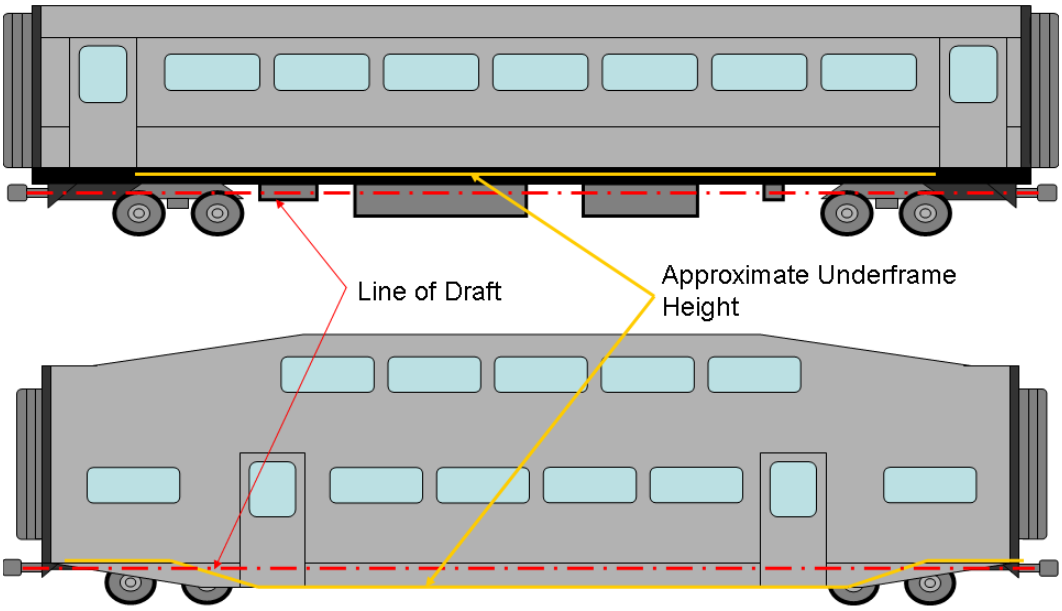


**Figure 11 - Line of Draft and Underframe Height, Single-level and Multilevel Cars**

Both of these vehicles were designed to be put into service on the North American general railroad system, and thus both cars were designed to be compliant with the applicable standards and specifications. While the multilevel railcar design has developed over the latter half of the 20$^{th}$ century, the 800 kip compressive strength requirement had already been established as the longitudinal load requirement to design to. The multilevel equipment was designed with this requirement in mind, so that even with an underframe that transitions from one

height to another the vehicle can meet the requirement.

A challenge arises when the line of draft is not as easily defined for a passenger rail vehicle. While the two examples presented above both feature couplers at the same height, designs do exist where this is not the case. One such example is shown schematically, in Figure 12. This particular design represents a railcar that couples via an articulated connection at one end of the car, as opposed to a tightlock coupler.

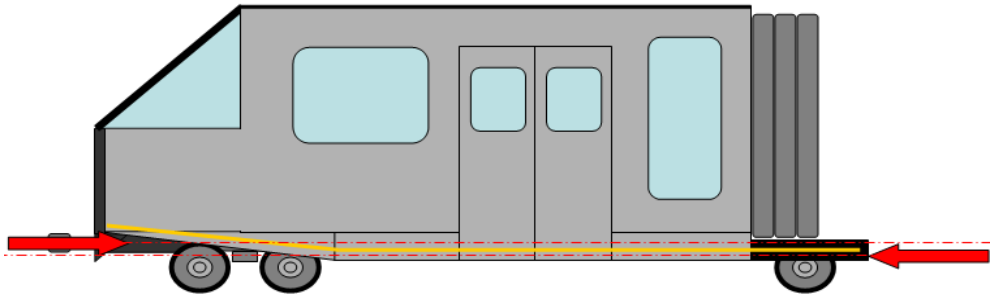

**Figure 12 - Representative Articulated Railcar Design**

Vehicles with an articulation or partial low-floor are currently in service throughout much of Europe, where different structural standards exist [20]. Domestically, articulated vehicles are used on transit systems, where the vehicles are not subject to the same FRA regulation as the general railroad system. These vehicles are typically adapted from the designs being produced for overseas service [21].

As can be seen in Figure 12, one difficulty associated with a vehicle of this type is simply defining the line of draft. Since the vehicle features coupling mechanisms at different heights, applying the 800 kip compressive load at the coupling mechanism at each end of the car induces a pitching moment in the car.

Additionally, since the car may couple without the conventional draft sill and tightlock coupler arrangement, a structure identifiable as the buff stops may not exist. As specified in Section 8.2 of APTA SS-C&S-034-99, Rev. 2, "The compression test load shall be applied to the rear draft stop in the draft gear housing at the centerline of draft by means of a controlled ram," [18]. While this section does make allowances for rail equipment utilizing "shear-back" couplers or drawbars, this type of device may not be included in the design of a particular piece of articulated equipment.

While an articulated design may offer a level of passenger protection equal to that of a conventionally-designed passenger car, there does not exist a domestic standard for evaluating this. It is desirable that a standard for evaluating designs not readily evaluated by the current compressive strength test be established. The new standard would need to ensure that any equipment that passes provides an equal or greater level of passenger and crew protection than a design that qualifies under the existing standards. Additionally, the new standard should be applicable to a broader range of passenger equipment, to prevent the establishment of a new "baseline" articulated design that all future designs will become based off of.

## 1.5 Crashworthiness Research Program

Prior passenger crashworthiness research has been performed by the Volpe National Transportation Systems Center (Volpe Center) on behalf of the FRA. The federal research program has included the crash testing of

conventionally-designed, single-level passenger rail equipment [22, 23, 24]. The full-scale tests were conducted to help understand the manner of failures of conventional passenger rail equipment under known collision scenarios, which can then be applied to computer modeling of such rail collisions [25]. Since full-scale destructive testing of railroad equipment is an expensive undertaking, it is important to have accurate computer models in order to further research attempts.

In each of the full-scale tests, the equipment that was being tested was retired mainline passenger railroad equipment that had been built to the 800 kip buff strength requirement. The cars used also featured underframes similar to the design used on most single-level conventional passenger cars in North America. The first test consisted of a single car running into a wall at approximately 35 MPH. The measurements taken during this test were used to determine the deformation of critical elements, the deceleration-time histories of the car in all three directions, and the displacements of the suspension components [23].

In this test, the railcar crushed by approximately 5 feet after impacting the wall [23]. The car in its pre- and post-collision states can be seen, in Figure 13. During this test, the dominant mode of failure in the draft sill was axial crushing, with material failure in the region of longitudinal welds. This failure mode is different from the mode observed in a number of accident investigations, which is the formation of a plastic hinge at the rear of the draft sill, near the body bolster connection [26].

**Figure 13 - Single-car Impact Test, Before (left) and After (right) Impact**

The second test in this series consisted of two similar cars coupled to one another impacting a wall at 26 MPH. This test was designed to measure the gross motions between two coupled cars, obtain the force-crush characteristics, and to observe the failure modes of major structural components during a collision situation [24]. In this test, the draft sill on the lead car failed by buckling in its tapered region, while the widest part of the draft sill remained relatively intact. In both the single-car and the two-car test, the measured force-crush characteristics on the impacting cars were similar, despite the different failure modes of the draft sills [24]. These characteristics are shown in Figure 14.

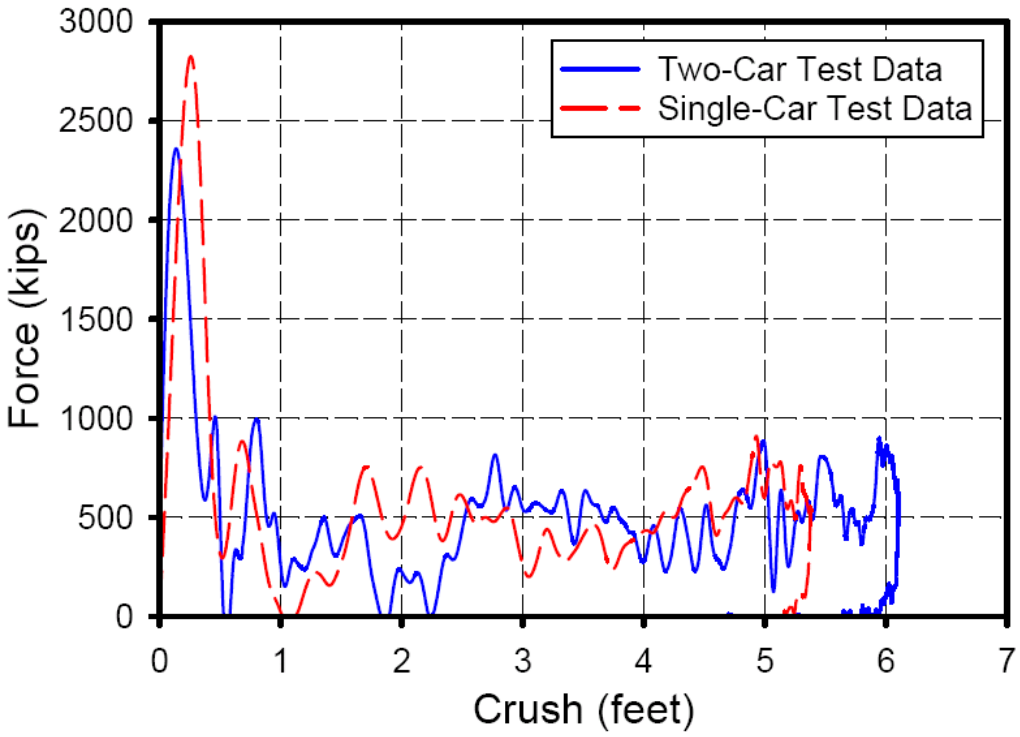


**Figure 14 - Force-crush Characteristics from Single-car and Two-car Impact Tests**

In both tests, the collision force on the vehicle builds to a relatively high level. At a certain point, a critical load is reached and a component of the draft sill fails. The force needed to continue to reduce the length of the railcar drops off to a lower level. In both tests, this level is approximately 500,000 pounds of force.

While the vehicles used in this testing program were designed to the static 800 kip standard, Figure 14 indicates that the dynamic force sustained by the car is well above this level. Since this force is dynamic and applied across a large area of the car, the carbody cannot be expected to sustain the same peak force value if the load application is quasistatic.

## 2 Modeling Approach

Previous research into passenger railcar crashworthiness has included the development of detailed finite element models of conventional-design equipment [27, 28, 29] as well as multilevel equipment [30]. These models have been developed for simulation of full-scale crash testing, are capable of capturing 3-dimensional motion, and include complex material behaviors. A summary of four previously developed finite element models of conventional cars is shown below, in Table 1.

**Table 1 - Summary of Previous Finite Element Models**

| | Passenger Car Type | Number of Elements | Original Purpose |
|---|---|---|---|
| Model 1 | Single-level | 50,000 | Dynamic impact into rigid wall |
| Model 2 | Single-level | 516,000 | Dynamic impact into rigid wall |
| Model 3 | Single-level | 150,000 | Dynamic impact into locomotive |
| Model 4 | Multilevel | 550,000 | Dynamic impact into rigid wall |

While these four models provide a high level of structural fidelity, they are not the most appropriate tools for evaluating static compressive strength. Due to the large number of elements in these models, the associated processing times are rather costly. Structures such as the trucks and suspension will not influence the static end strength. Since each of these models was meant to simulate a collision with large deformations, complex material behaviors are defined for specific components.

A more efficient approach is a finite element model specifically for the purpose of evaluating the static strength test. The draft gear, couplers, suspension, and trucks can be left out of the model without invalidating the results

obtained when simulating the buff strength test. The members making up the skeleton of the car are the primary structure. The wall and roof skins connect the members to one another, causing the entire car to function as a single beam.

The materials used in this new model can be maintained as linear elastic, since equipment that passes the compressive strength test exhibits no permanent deformation. The FE model will calculate all stresses assuming a linear material behavior, regardless of the stress magnitude. The areas of stress that exceed the yield stress can be determined through simple analysis of the results. One method employed in this work involves displaying the contour plot of stress results with the minimum contour level set to the yield stress of the material of interest. This plots areas of stress greater than yield in color, with any stress below yield displayed as a neutral color. This technique is used to generate the contour plots in Appendix D – Stress Contour Plots for Various Load Cases**.**

The structural frame of the railcar is what is being principally evaluated in this test. The finite element models developed in this thesis represent a generic single-level passenger car of conventional design and an exemplar multilevel passenger car. Design drawings, previous FE models, and equipment photographs were utilized as guidelines for the assembly of the models. While exact member geometries were available for specific passenger railcars, they were generalized when designed into the conventional model.

Three finite element models were developed as part of this research. The first model used beam elements to represent the skeletal frame of the railcar with shell elements to model the roof, wall, and floor structures. This model provided

a basic evaluation of the beam-like behavior of the railcar. The beam and shell model featured a processing time of approximately one minute.

This model was useful as a "first cut" approach to simulating the 800 kip compressive strength test, as it provided guidance on the salient features of the railcar's structure that were necessary to generate results. Using this model, it was determined that the structural skin of the railcar was necessary to effectively transfer load through the skeletal structure of the railcar. Additionally, this model was used to evaluate the beam-like behavior of the railcar. It was found that the neutral axis of the railcar is approximately 24.4 inches above the floor of the car. The neutral axis height varied with axial location, particularly near the car ends. Throughout the center of the occupied volume the location was fairly consistent. Additional results using this model are discussed in Appendix E – Beam and Shell Model.

There were a number of drawbacks associated with the beam and shell model. Beam elements are useful for modeling prismatic members, of which there are many in the railcar. However, significant members such as the draft sill and body bolster are not prismatic. Additionally, stress output from beam elements is needed at points throughout the cross-section. Defining these points complicates post-processing, as results may be desired at locations in the cross-section where output was not requested during pre-processing.

These negative aspects of the beam and shell model outweighed the benefits of the quick runtime of the model. A model that captured the geometry in greater fidelity without approaching the complexity of the models developed

for dynamic analyses was desired. A more complex single-level model was constructed using shell elements to model the entire structure of the railcar. This model is discussed in the next section. The same modeling approach was also used to construct a model of an exemplar multilevel railcar. The multilevel model is discussed in Section 4.1.

## 2.1 Shell Model of Single-level Conventional Car

Since conventionally-designed single-level passenger railcars in service today share a number of common design features, an FE model serves as a "generic cousin" to the actual railcars themselves. The overall layout of the FE model resembles the models developed in References 28 and 29. Key structural members, such as the center and side sills, were sized in the FE model to have similar cross-sectional areas and moments of inertia as those used in the actual car construction. Simplifications were made to the cross-sectional shapes of members to increase the minimum element size needed to accurately capture the geometry.

Shell elements can be used to model both the beams that make up the frame of the car and the panels that make up the walls, floor, and roof skins. Shell elements allow more complex geometries to be modeled with greater fidelity than beam elements. With an increase in complexity of the model comes an increased runtime for the quasi-static test. However, the complete simulation of the compressive strength test can be run in minutes, even with the use of shell elements for the entire model.

The shell model's geometry was defined using ABAQUS/CAE [31]. For shells, there are a number of ways of constructing parts. The method employed in this thesis to define the prismatic members consisted of sketching a 2-dimensional cross-section of the member, dimensioning and constraining this sketch, and extruding the member to its proper length. The mesh was then defined on the part, with partitions made to the part as necessary to ensure nodal alignment between mating parts. The material properties and thickness of the plate used in a given area are defined separately from the geometry and applied to the individual shell elements. Figure 15 shows the cross-sectional sketch, the extruded geometry, and the final mesh for a portion of the center sill used in the conventional car model.

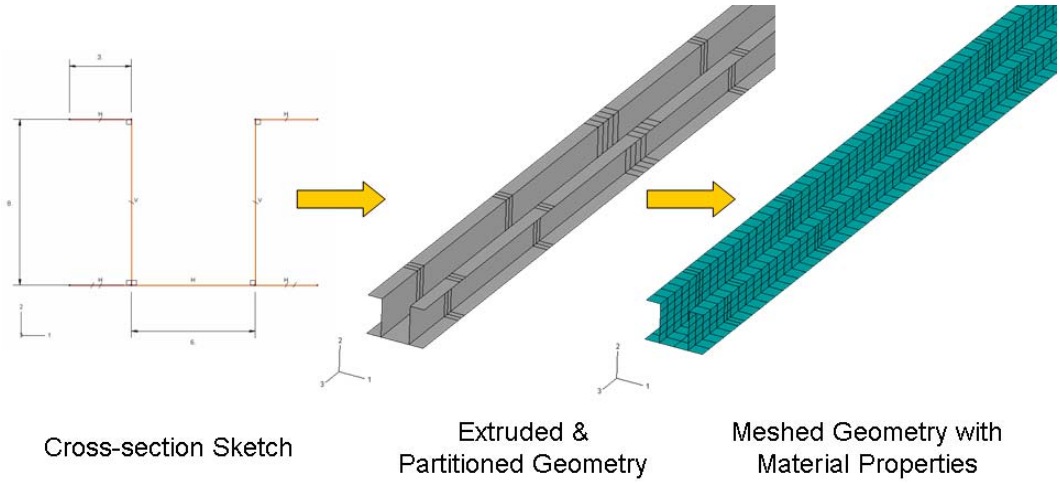


**Figure 15 - Progression of Shell Mesh for Prismatic Longitudinal Center Sill**

Tied constraints were employed to connect the various parts to one another to form the assembled railcar. These constraints were used to simulate perfectly welded joints between members by restricting the motion of a set of nodes on one part to that of the corresponding nodes on the mating part. The

mesh on individual parts was designed in such a way that the nodes on the master part and slave part would occupy the same location in space once the parts were aligned with one another to form an assembly. By aligning the nodes on constrained parts, the resulting deflections and stresses at the interface of the two parts will be the same as if a single part had been meshed to incorporate both geometries. This point is further elaborated in Appendix A – Tied Constraints versus Single Parts.

The shell element model included a number of details not captured by the beam and shell model. Members with varying cross-sections, such as the draft sill and body bolsters, can be modeled with greater fidelity using shell elements. Additionally, it was anticipated during the development of the shell element model that the endframe should be included, as it could provide a number of locations to apply an alternative evaluation load. The endframe chosen for the model car is the SOA endframe, as described in Reference 8. This endframe was chosen for its compliance with the most recent industry standards.

### 2.1.1 Mesh

The assembled railcar measures 83’-5” from buffer beam to buffer beam. The endframe, at the buffer beam and anti-telescoping (AT) plate, measures 10’-4” across. The occupied volume measures 7’-4” from the top of the floor supports to the bottom of the roof supports. The railcar resembles a beam, with a length-to-height ratio greater than 10 and a repeating cross-section throughout the center of the occupant volume. Front, side, and isometric views of the assembled,

unmeshed railcar geometry are shown in Figure 16. The sizes and shapes of the individual members, as well as the overall railcar, are typical of a number of models of single-level passenger car. Because the FE model combines features from multiple designs, it is referred to as a "generic" single-level passenger railcar.

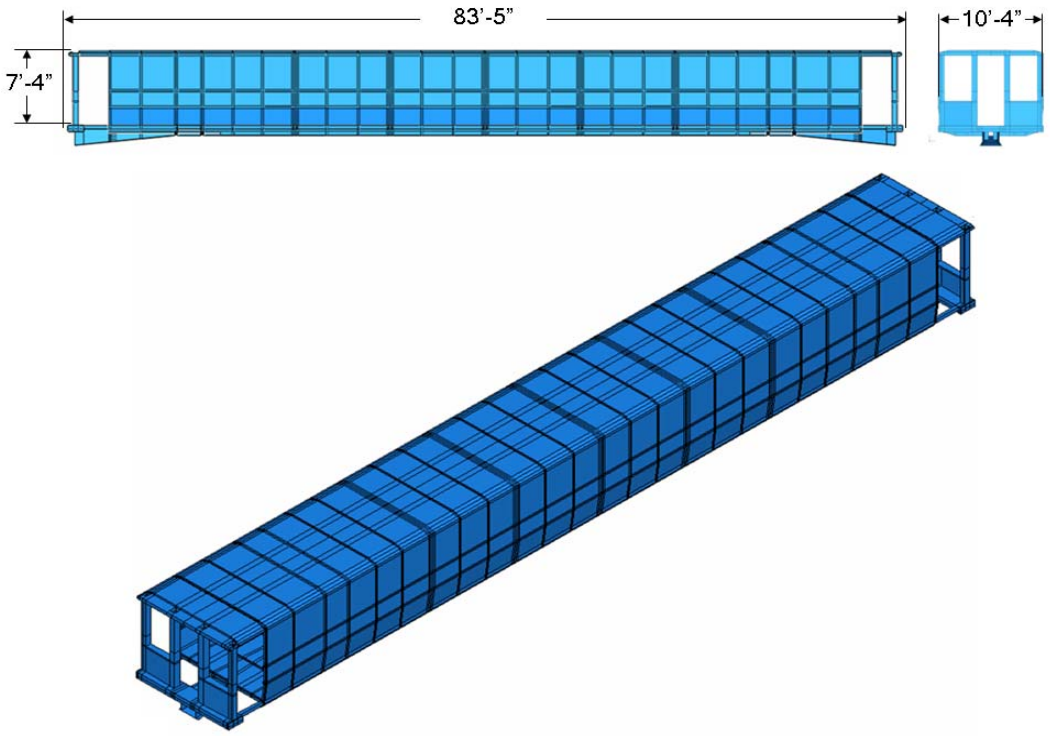


**Figure 16 - Single-level Car Model Geometry**

The longitudinal members making up the underframe include the draft and center sills and the side sills. In the superstructure of the car, the longerans include the belt rail, the upper window rail, the roof rail, and the purlin. A profile view of the railcar, with the skin removed, is shown in Figure 17 as a means of identifying the longerans that will be further discussed in subsequent sections.

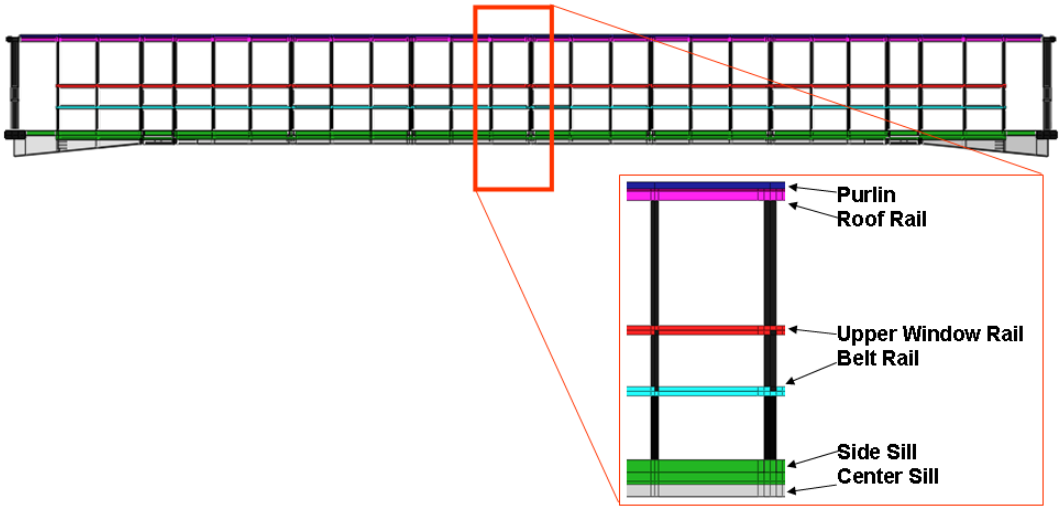


**Figure 17 - Single-level Car Longitudinal Members**

The railcar was meshed using S4 shell elements to represent the frame structure as well as the floor, roof, and wall skins. This element type is a four-node, linear quadrilateral shell element [31]. The model utilizes Spring1 elements to characterize the suspension. One end of the spring is connected to a node in the structure while the other end of the spring is grounded. The spring elements all act in the vertical direction in this model.

A total of 79,796 elements are used in this model, 16 of which are Spring1 type. The characteristic element length is 2.73 inches. The meshed railcar is shown in Figure 18. Processing time for a simulation consisting of a gravity load and a single, static compressive load was less than five minutes for this model. This time includes generation of an input file, processing the model, and generating the necessary output files. This time represents the runtime of the model on a high-end desktop PC using a single processor.

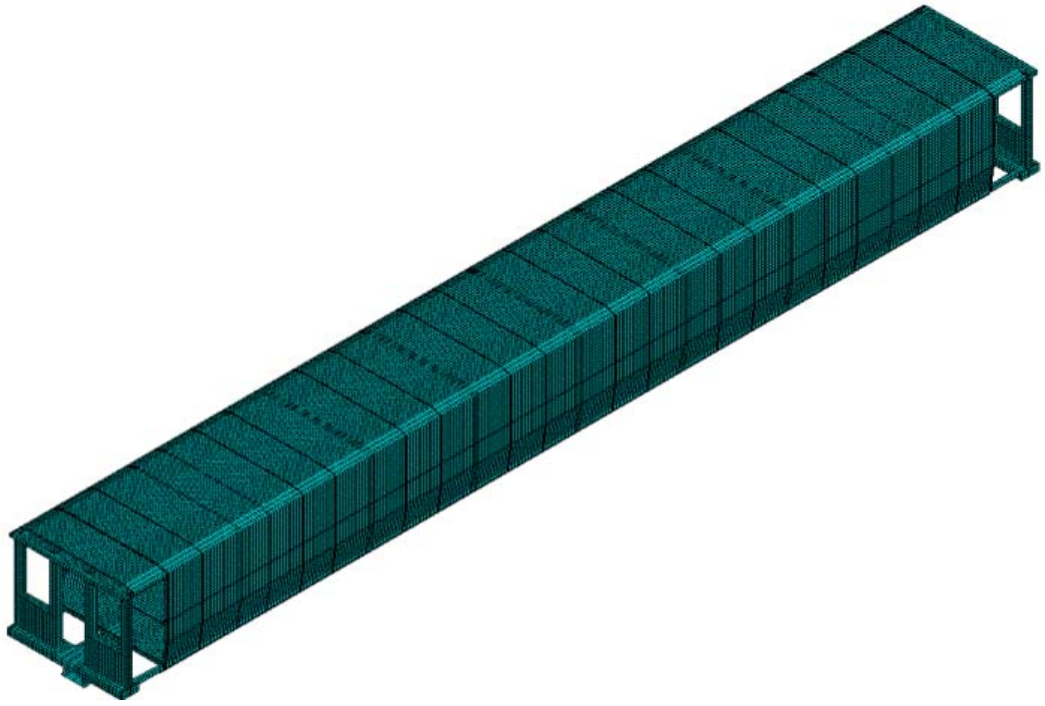

**Figure 18 - Mesh of Single-level Railcar**

### 2.1.2 Weights

While still a simplified representation of the geometry of a passenger railcar, the shell model has a greater level of detail than the model in Appendix E – Beam and Shell Model. The shell model incorporates SOA endframes, as well as a more realistic approximation of the suspension supporting the car.

The weights of the structural components of the carbody, the trucks, and the car loaded to AW0 are provided in Table 2 for the finite element model. For comparison purposes, the corresponding weights from conventional, single-level passenger railcar data are also provided. The weight of the structural carbody in the model compares favorably with the structural material in one (actual) railcar. While only the secondary suspension from the trucks is included in the finite

element model, it is assumed that the trucks would weigh the same as on a typical railcar of similar construction.

**Table 2 - Single-level Railcar Weights**

| | **FE Model Weight (lbf)** | **Actual Railcar Weight (lbf)** |
|---|---|---|
| Structural Carbody | 21,290 | 24,000 [6] |
| Trucks (each) | 13,700 | 13,700 [5] |
| AW0 | 102,380 | 100,000 [6] |
| AW0, no trucks | 74,980 | 72,600 |

The AW0, no trucks case is the weight the carbody is to be loaded to in running the current 800,000 pound static end strength test [18]. This value represents the carbody structure with all of the interior fittings, electrical, and mechanical equipment installed. This loading case was implemented in the FE model by setting the gravitational acceleration to approximately 3.5 times the normal gravitational acceleration. The value of acceleration used is 1,361 in/sec$^2$.

### 2.1.3 Material Used

The mechanical properties of the structural members of the carbody are taken from manufacturer reports and previous FE models. The structural members of the carbody, as well as the outer skin, were all steel. The properties of the steel are shown below, in Table 3.

**Table 3 - Material Properties Used for Steel**

| Property | Value | |
|---|---|---|
| Young's Modulus (E) | 2.9E+07<br>200 | psi<br>GPa |
| Weight Density | 0.284<br>7.8 | $lb/in^3$<br>$g/cm^3$ |
| Poisson's Ratio | 0.3 | |

In this FE model, the endframe design is taken from Reference 32. The endframe includes the buffer beam, corner and collision posts, anti-telescoping (AT) plate, and side sill extensions. In order to determine whether a member was close to the yield stress, typical yield stresses for the classes of steel in use in the structural members were compared to the values of stress obtained from the quasistatic simulation. The yield stresses for the structural members in the shell model are listed below, in Table 4.

**Table 4 - Yield Stresses for Structural Members, Shell Model**

| Member | Yield Stress (ksi) | Yield Stress (MPa) |
|---|---|---|
| Belt Rail, Roof Rail, Upper Window Rail | 110 | 760 |
| Body Bolster | 65 | 450 |
| Center Sill | 100 | 690 |
| Cross Bearer | 75 | 520 |
| Draft Sill | 100 | 690 |
| Endframe | 75 | 520 |
| Floor Stiffeners | 110 | 760 |
| Floor Pans | 32 | 220 |
| Outer Skin | 50 | 345 |
| Roof Stiffeners | 110 | 760 |
| Side Sills | 75 | 520 |
| Wall Stiffeners | 110 | 760 |

# 3 Results for Conventional Car

The first compression test performed on the conventional car was the static end strength test, consisting of 800 kips applied statically on the buff stops. The railcar is sitting on simulated trucks and is allowed to move in the longitudinal direction. The applied force is resisted at the opposite buff stops. Additional compression loads are then investigated for their effects on the multilevel railcar. These loads were examined to determine what loading conditions could be applied to a different region of the car but produce similar behavior as the conventional 800 kip load. These locations include loads at the buffer beam and AT plate. A detailed look at the implementation of these tests on the conventional shell model car is described in the following sections.

## 3.1 Loading Conditions

The analysis was performed in two static load steps. The chronological first step is the application of the gravity load. The gravity field applies to all elements that have mass, which only the 16 suspension elements do not.

During the conventional static compressive strength test, the 800 kip compressive load is applied to the car already loaded by gravity. To approximate the physical loading, a pressure load was calculated, based on the area of the buff stops in the model. This pressure load acts entirely in the longitudinal direction in the model. The buff stops, with applied load, are shown in Figure 19. A portion of the draft sill has been cut away to provide this view.

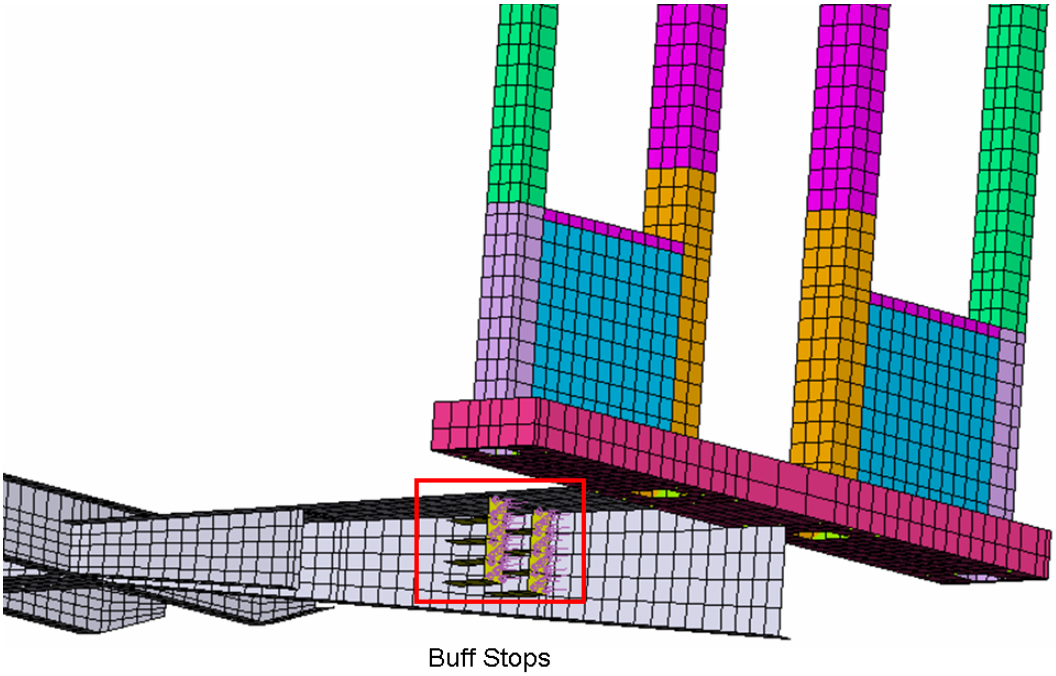


**Figure 19 - Location of Buff Stops in Single-level FE Model**

## 3.2 Boundary Conditions

During the gravity step, the model simulates the railcar sitting at rest. In an actual railcar, motion in the lateral direction is prevented by the flange of the wheel contacting the rail. If the brakes are set, motion in the longitudinal direction is prevented. Vertical support to the car is provided by the trucks, with the secondary suspension as the connection between the body bolster and the truck bolster.

A series of boundary conditions are applied to the body bolsters during the gravity step. The bolsters are meshed such that single element in the center of the bolster plate approximates the location where the secondary suspension attaches to the bolster on the physical railcar. This location is indicated in Figure 20 for

one body bolster. The corresponding elements are allowed only vertical translation during the gravity step.

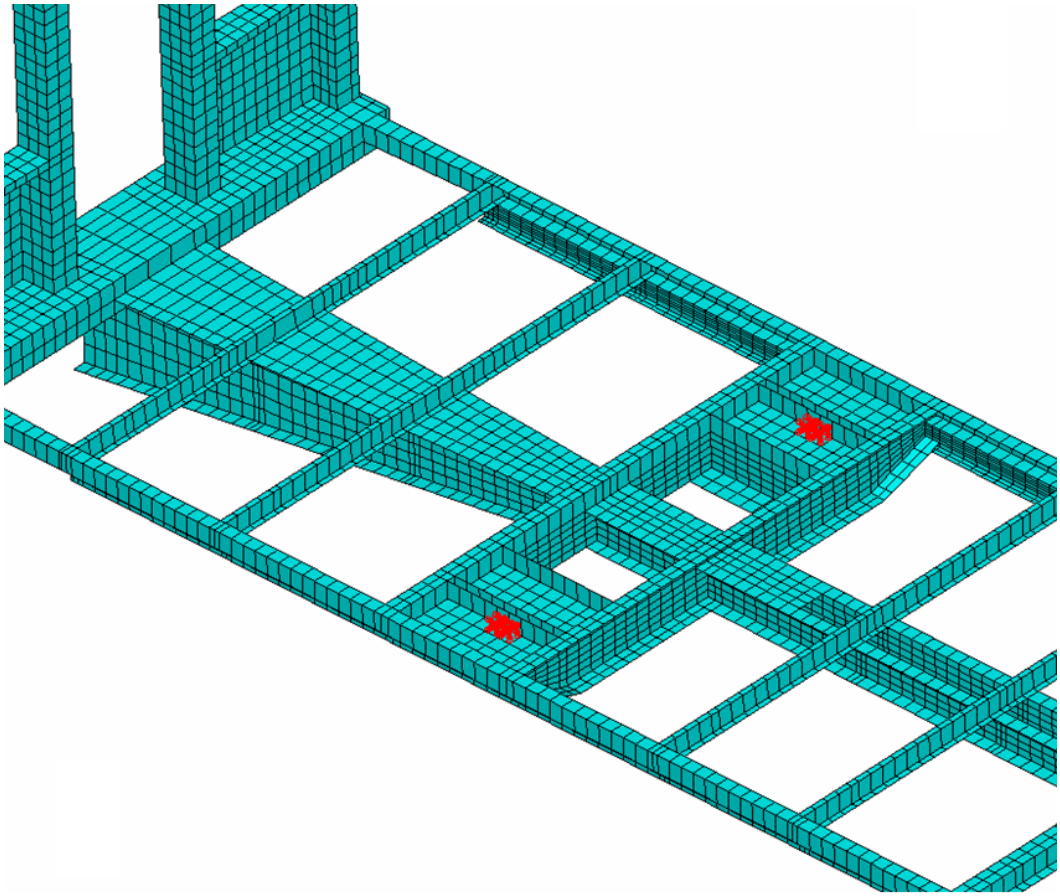

**Figure 20 - Boundary Conditions Applied to Body Bolster**

To approximate the secondary suspension's attachment to the body bolster, a linear spring is attached to the node at each corner of the center element. Each of these sixteen springs has its other end grounded. This allows the railcar to rest on the springs during the gravity step. The spring constant used in each spring is 442 lbf/in, for an effective spring stiffness of 1,768 lbf/in at each bolster element. The calculations used to obtain this value of suspension stiffness are provided in Appendix B – Calculation of Suspension Spring Stiffness.

During the application of the 800 kip load, the boundary conditions are modified to more closely match the conditions applied to the railcar during an actual compressive strength test. The bolster is now allowed motion in the longitudinal direction, with the boundary conditions in the other axes propagated from the gravity step. Additionally, longitudinal motion of the railcar is restricted at the rear buff stops. The use of springs to model the suspension allows the body of the railcar to lift upward in response to the moment induced in the carbody during the application of the compression load. A summary of the boundary conditions applied during each step, as well as the location of the applied boundary conditions, is provided in Table 5.

**Table 5 - Summary of Boundary Conditions, Single-level Model**

| Step | Degree-of-Freedom | Location of Boundary Condition |
|---|---|---|
| Gravity Load | Lateral Translation (x) | Bolster-truck Attachment |
| | Vertical Translation (y) | Bolster Springs |
| | Longitudinal Translation (z) | Bolster-truck Attachment |
| | Rotation about x | Bolster-truck Attachment |
| | Rotation about y | Bolster-truck Attachment |
| | Rotation about z | Bolster-truck Attachment |
| Buff Load | Lateral Translation (x) | Bolster-truck Attachment |
| | Vertical Translation (y) | Bolster Springs |
| | Longitudinal Translation (z) | Fixed End Buff Stops |
| | Rotation about x | Bolster-truck Attachment |
| | Rotation about y | Bolster-truck Attachment |
| | Rotation about z | Bolster-truck Attachment |

## 3.3 Carbody Neutral Axis

Before analyzing the carbody for its response to simulated compressive

tests, the neutral axis location was sought. The simplest method of finding this location was similar to the approach used in Appendix E – Beam and Shell Model; cantilevering the carbody and determining the location where longitudinal stress transitioned from tensile to compressive. In the case of the single-level conventional railcar, the railcar was loaded by its own weight during the cantilever load, which is an approximation of a uniformly distributed transverse load on a beam.

A contour plot of the cantilevered railcar is shown in Figure 21. The contour levels have been set to show positive displacement as black and negative displacement as gray. The neutral axis location is the vertical height where the displacement changes from positive to negative. Because the boundary condition is applied at the left endframe of the car, there is some influence on the results at this end of the car. However, moving further from this end of the car provides a more consistent neutral axis location.

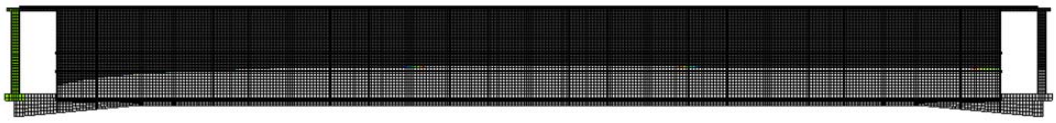

**Figure 21 - Contour Plot of Longitudinal Displacement, Cantilevered Conventional Railcar**

The longitudinal displacement is investigated along the height of the vertical wall support members. The height above the floor where the positive-to-negative displacement transition occurs in each vertical member examined is shown in Figure 22. The average value for the neutral axis is found to be

approximately 26.6 inches above the top of the floor. This value compares favorably with the value obtained from the beam and shell model, which determined the neutral axis to be approximately 24.4 inches above the top of the floor in the occupant volume of the railcar. More details on the beam and shell model can be found in Appendix E – Beam and Shell Model.

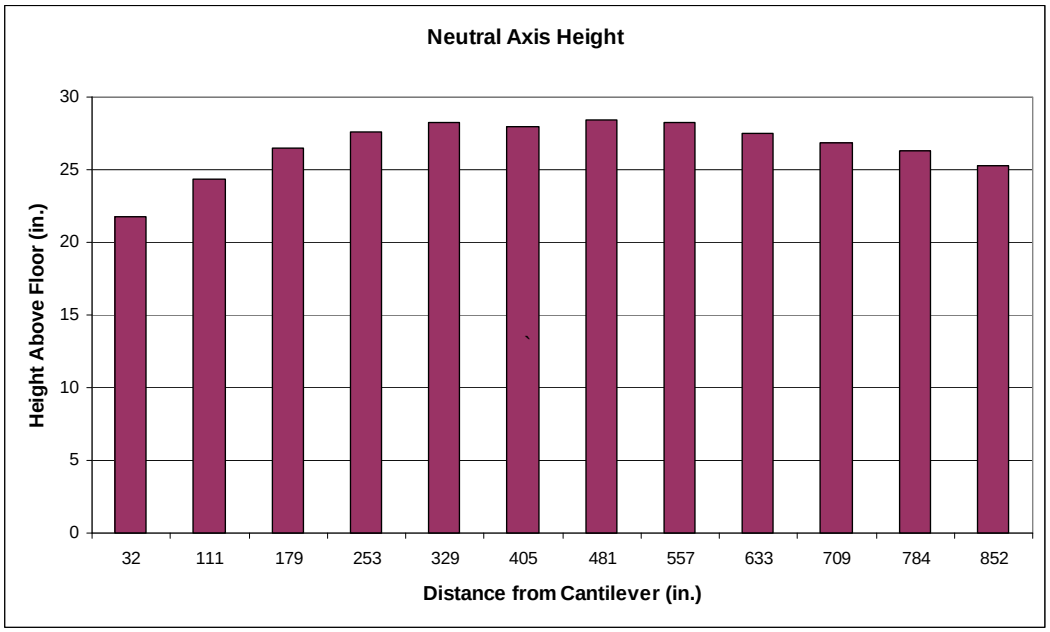


**Figure 22 - Neutral Axis Height for Varied Cross-section Locations**

## 3.4 Standing Car Results

The first loading case examined is the railcar standing on simulated trucks, loaded by its own weight. The AW0 standing car can be thought of as a simply-supported beam overhanging both of its supports, where those supports are represented by springs in the FE model.

The undeformed car and the deformed car, with superstructure and floor suppressed for visual clarity, are both shown in Figure 23. Under AW0 loading

conditions, the centerline of the center sill deflects downward by 0.2 in. The deflection is scaled by a multiple of 100 in this figure to emphasize the deformed shape of the railcar. The body bolster springs are denoted by red squares on both the undeformed and the deformed figures.

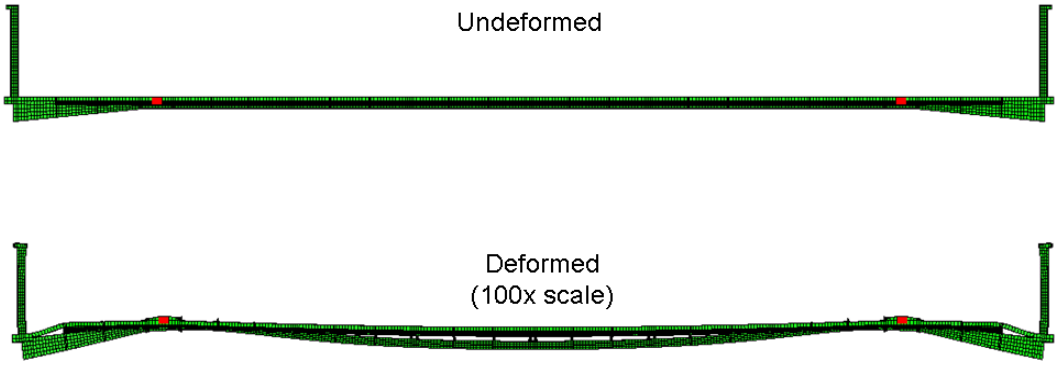


**Figure 23 - Undeformed and Deformed Profiles, AW0 Railcar**

The longitudinal stress was examined at various locations within the center sill, side sill, belt rail, upper window rail, roof rail and purlin. For each member, stress was recorded along the entire length of the member to determine the variation of stress throughout the entire occupied volume of the car. Because the FE model is symmetric about the plane bisecting the center sill longitudinally, the stress values could be analyzed in the longitudinal members on only one side of the railcar. This symmetry was verified for the model, and the results recorded in Appendix C – Symmetry of Results. The value of stress is reported at the top surface of each element. In the following plots, the horizontal axis has its origin at the outer edge of the buffer beam at one end of the model railcar.

The plot in Figure 24 displays the stress in the center sill along its entire length. The stress was evaluated at six heights in one of the vertical webs of the

sill, with Row 1 representing the very bottom of the web and Row 6 representing the top.

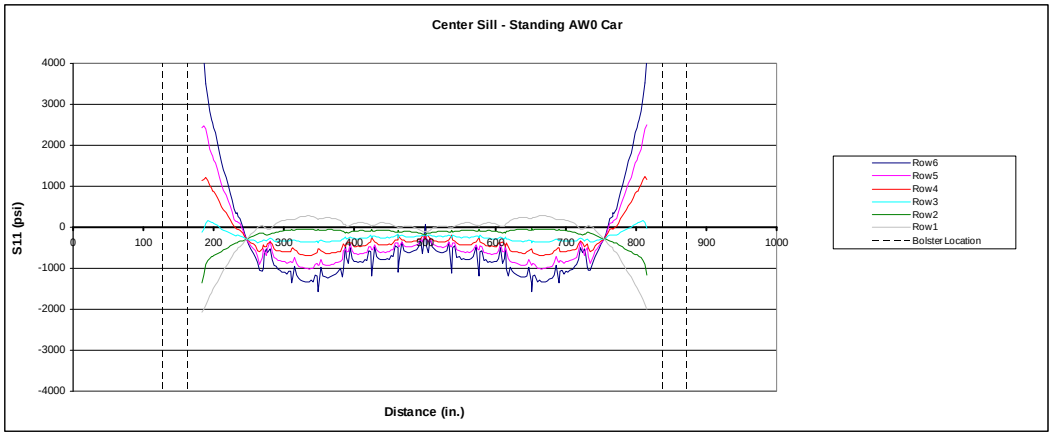


**Figure 24 - Stress Distribution in Center Sill, Standing AW0 Railcar**

The center sill is in a state of tension at the bottom of the web and in a state of compression at the top of the web. The periodic peaks correspond to the locations of the lateral members' (cross bearers and floor stiffeners) attachments to the center sill. The perturbations in the stress levels in the center sill are more pronounced in the top row of elements than in the bottom, as the lateral members are connected directly to the top flange of the center sill.

In the FE model, the side sills run from just inboard of one buffer beam to the buffer beam at the opposite end of the car. There is a change in the cross-section shape of the side sill that occurs at the inboard side of the doorframe. The stress results presented in Figure 25 are for the portion of side sill that runs from inboard of one doorframe to the inboard side of the doorframe at the other end of the car.

The stress distribution along the length of one side sill is presented in

Figure 25. The stress was investigated for four rows of elements at different heights within the side sill: at the bottom of the web, 1" above the bottom of the web, 4" below the top of the web, and at the top of the web. These locations were chosen to take advantage of rows of elements spanning the length of the side sill.

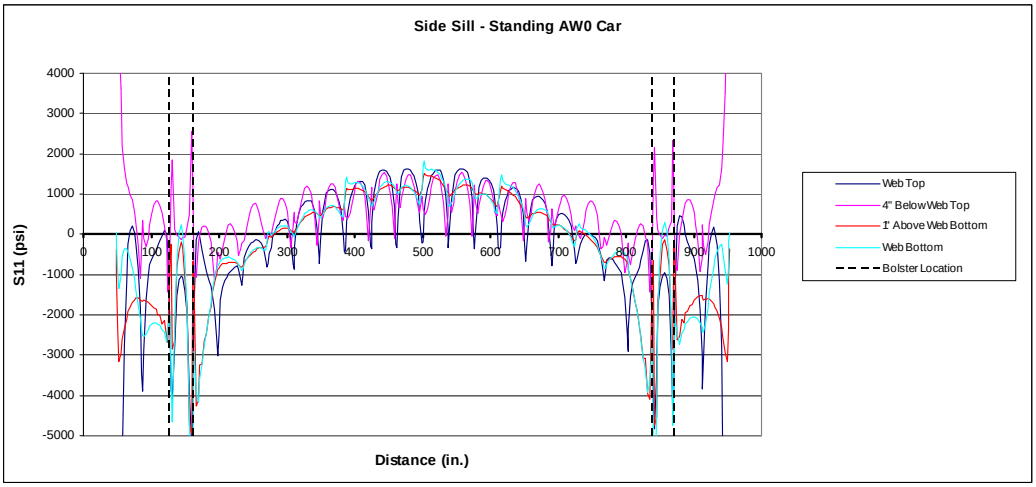


**Figure 25 - Stress Distribution in Side Sill, AW0 Railcar**

Toward the center of the occupied volume of the car the side sill is under tension at all row heights investigated. This gradually shifts to the side sill being under compression in the region around the body bolsters. The periodic spikes in stress levels correspond to the lateral members, which attach to the upper web of the side sill. Under AW0 loading conditions, the stress levels are low at all locations throughout the side sill. Additionally, the stress levels are comparable at all heights investigated.

The stress distribution in the belt rail is shown in Figure 26. The centroid of the belt rail's cross-section is located 22.5 inches above the top of the side sill. The stress was measured along the row of elements toward the outside of the

carbody, corresponding with the wall skin's attachment to the belt rail. The belt rail in the FE model runs continuously from inboard of one doorframe to inboard of the opposite doorframe with no change in cross-section.

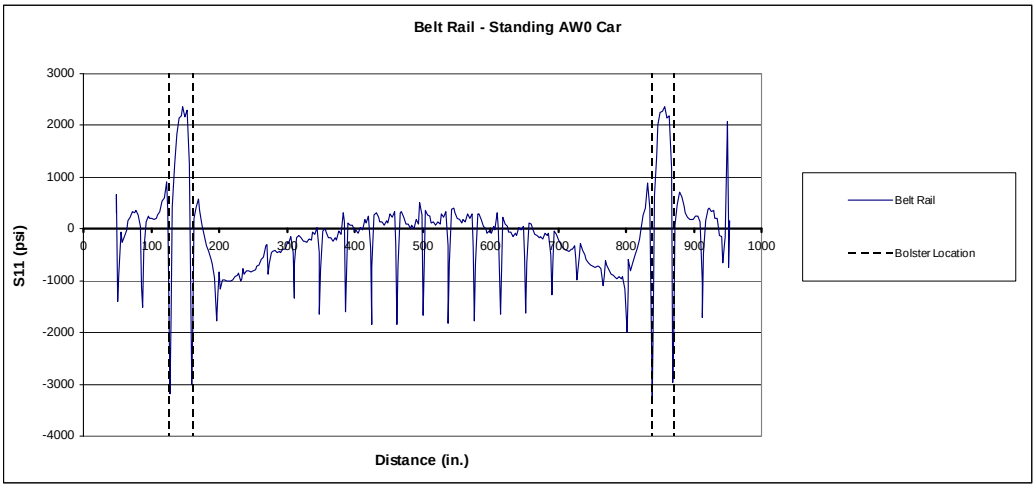


**Figure 26 - Stress Distribution in Belt Rail, AW0 Railcar**

The belt rail is under tension at the center of the occupant volume and under compression at the ends of the occupant volume. Compared to the side sill under the same loading condition, the stress levels in the belt rail are of smaller magnitude at the same longitudinal location. The periodic spikes in the belt rail stress levels correspond to the locations of the wall stiffening beams within the railcar.

The stress distribution in the upper window rail is shown in Figure 27. The centroid of the upper window rail's cross-section is located 42.5 inches above the top of the side sill. The stress was measured along the row of elements toward the outside of the carbody, corresponding with the wall skin's attachment to the rail. The upper window rail's cross-section is a mirror image of the belt rail, and

also runs continuously from inboard of one doorframe to inboard of the opposite doorframe with no change in cross-section.

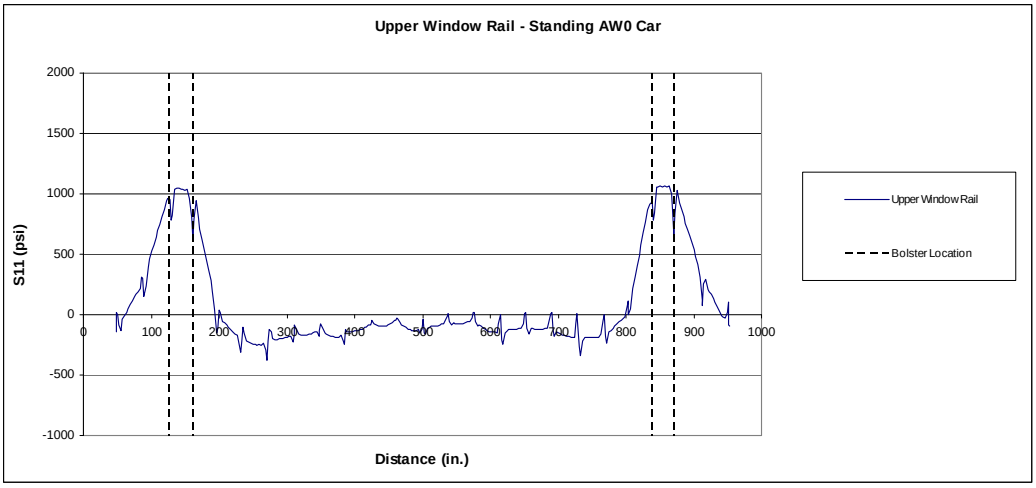


**Figure 27 - Stress Distribution in Upper Window Rail, AW0 Railcar**

In the upper window rail, the stress is tensile toward the outboard ends of the occupant volume and compressive toward the center of the car. The belt rail and side sill both demonstrate tensile stresses toward the center of the occupant volume. This change in stress from positive at the center to negative at the center indicates that the vertical location being investigated has crossed the neutral axis of the carbody. The stress levels throughout the upper window rail are also consistently low, with the highest magnitude being approximately 1,000 psi, seen in the same cross-section as the body bolsters.

The roof rails in the FE model run continuously from the AT plate at one end of the car to the AT plate at the opposite end of the car. The cross-section of the roof rail does not change over the length of the railcar. The stress distribution of the roof rail along the length of the car is shown below, in Figure 28. The

stress values are taken at the outer surface of the outer web of the rail. This location is where the wall skin attaches to the roof rail.

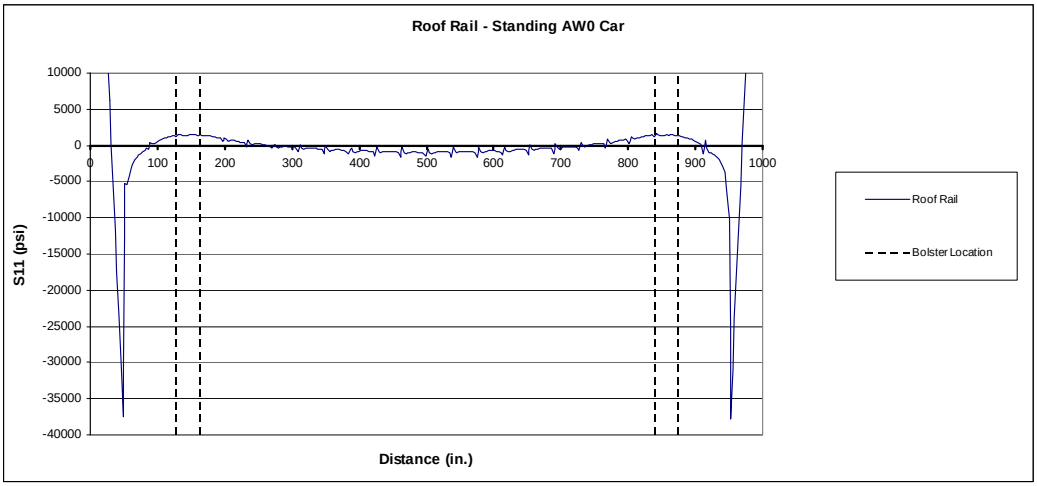


**Figure 28 - Stress Distribution in Roof Rail, AW0 Railcar**

The roof rail features high stress levels at the ends, near the attachment to the AT plate. This stress concentration can be attributed to a sudden change in geometry, when the open section roof rail attaches at a right angle to the stiff AT plate. The stress contour plot, indicating this region of high stress, can be found in Appendix D – Stress Contour Plots for Various Load Cases. In the region of the body bolsters, the roof rails are under tension. The stress gradually moves to a compressive state as the location examined moves further away from the body bolsters. The stress distribution of the roof rail between the body bolsters is similar to the stress distribution at the top of a double-overhanging beam subject to a uniform transverse load.

The longitudinal members located at the greatest height are the purlins. These relatively thin members span the length of the car from inboard of one AT

plate to inboard of the opposite one. The purlins attach directly to the underside of the roof skin, providing additional stiffness to the thin sheet of the roof. The stress distribution along the length of the purlin is shown in Figure 29.

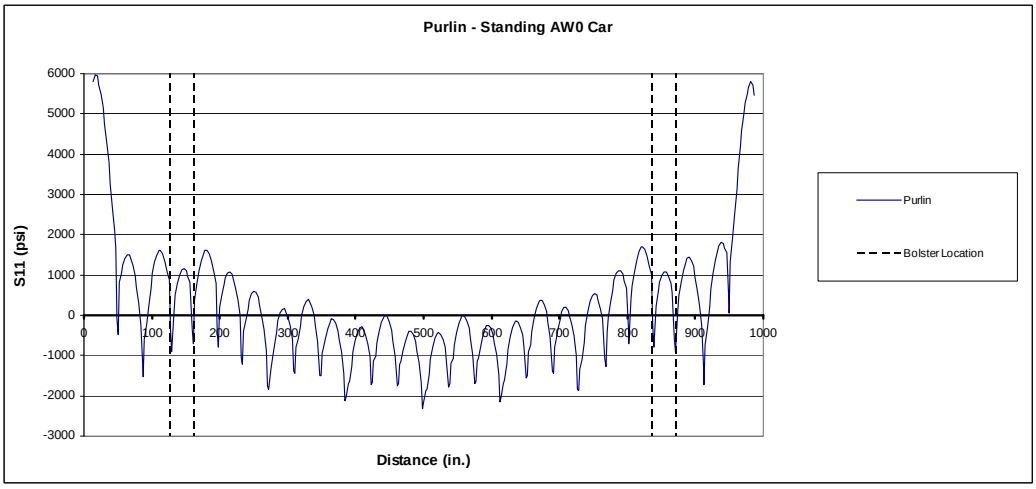


**Figure 29 - Stress Distribution in Purlin, AW0 Railcar**

The purlin experiences tensile loading in the area around the body bolster's cross section, but moves into a compressive state toward the center of the occupant volume. The large, periodic peaks can be attributed to the geometry of the roof structure. The purlins are the same height as the lateral roof supports and cross them at right angles. However, the general trend of the stress data indicates a compressive stress with maximum magnitude at the center of the occupant volume. Like in the roof rail data, this behavior is consistent with the stress situation at the top of a double-overhanging beam.

The stress distribution in each of the longitudinal members discussed above is plotted in Figure 30. The longitudinal stresses are shown only for the occupant volume inboard of both body bolsters.

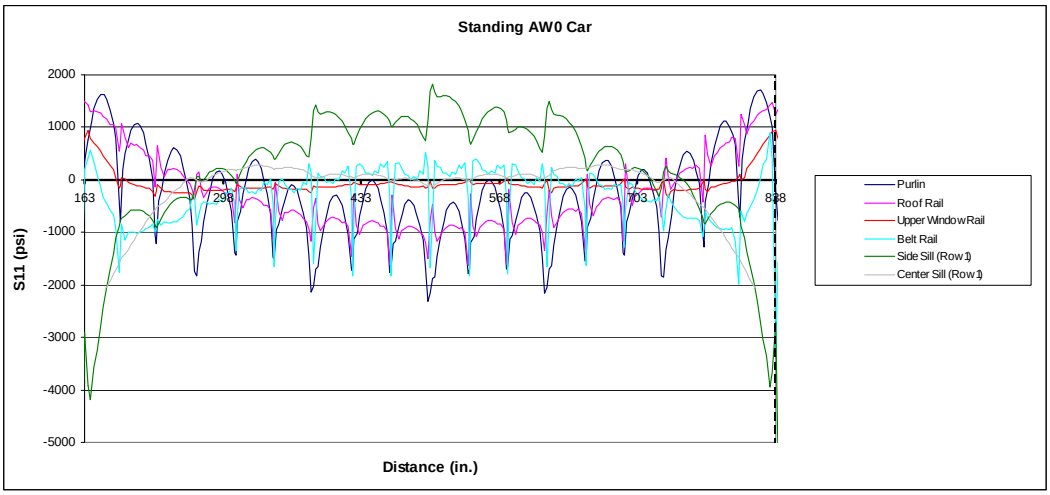


**Figure 30 - Stress Distribution in Longitudinal Members Over Occupant Volume, AW0 Railcar**

## 3.5 Buff Stop Loading Results

The second load case simulated was the railcar loaded to AW0 and subjected to an 800 kip compressive load, applied at the buff stops. The load was modeled by a pressure applied across the surface of the buff stops at one end of the car. The buff stops at the other end of the railcar were restricted from motion in the longitudinal direction during the compressive load test.

Since the buff stops are located below the neutral axis of the railcar, applying a compressive load to them induces a bending moment within the carbody as well as a compressive load. In addition to inducing stresses in the railcar from the compressive load, significant bending stresses will be generated in the railcar. The stresses generated from bending will add to the compressive stress below the neutral axis but act in opposite direction above the neutral axis. The stress distribution in a member subject to a combined axial compression and

bending is shown in Figure 31.

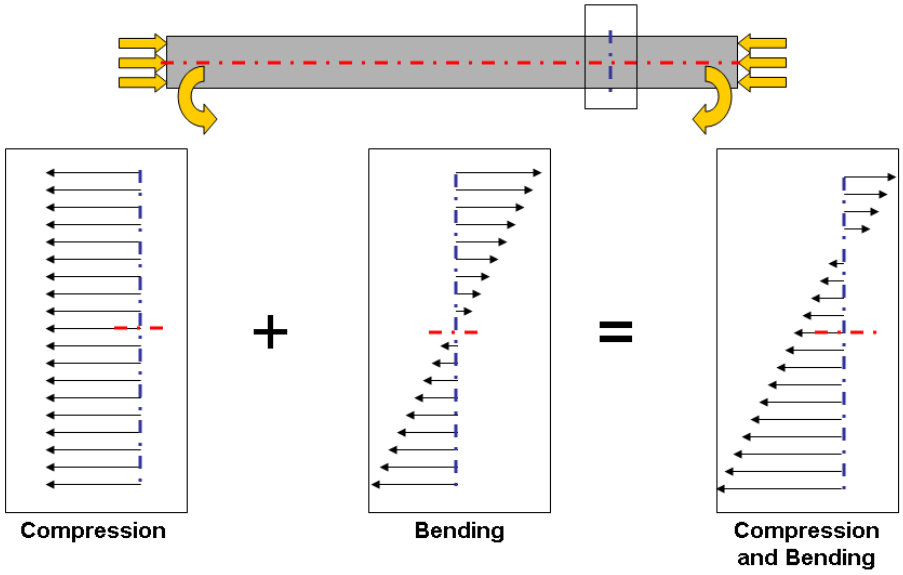


**Figure 31 - Schematic of Stresses from Compression and Bending**

In the center of the car, the bending moment acts in the opposite direction of the bending caused by gravity acting on the car. Where gravity causes the car to deflect downward, the bending moment tends to lift the center of the car. This behavior is illustrated schematically in Figure 32, which is an exaggeration of the deflection mode the carbody undergoes.

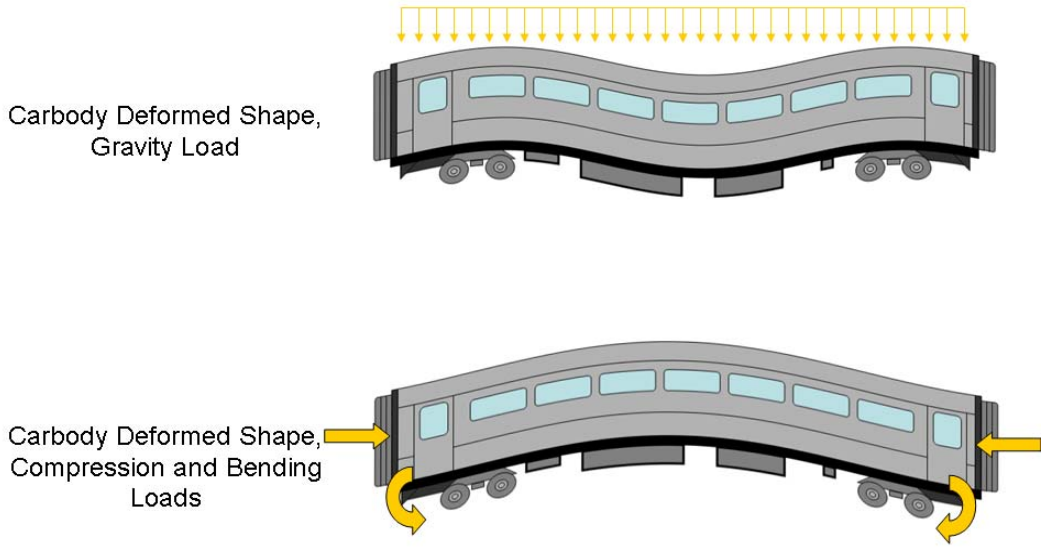


**Figure 32 - Shapes of Deformed Carbody under Gravity and 800 kip Loads**

The stress distributions in the longitudinal structural members of the railcar are presented in this section. The stress was analyzed in the same manner as for the standing car: stress values were recorded for rows of elements along the length of a given longitudinal member and plotted against distance along the carbody. In the plots presented below, the horizontal axis begins at the outer edge of the buffer beam at the fixed end of the model railcar.

Longitudinal stress along the length of the center sill is presented in Figure 33. The stress levels were examined at different heights within the center sill web, with Row 1 being the very bottom of the web and Row 6 being the very top.


**Figure 33 - Stress Distribution in Center Sill, 800 kip Load**

The center sill is in compression along its entire length, at all heights examined. The bottom row is under a larger magnitude compressive state than the top row of the center sill. This is expected, as the line of draft connecting the two sets of buff stops is vertically lower than the center sill. As seen in Figure 32, the entire railcar deflects vertically upward at the center. This places the bottom of the railcar into compression and the top of the railcar in a state of tension.

The magnitude of compressive stress in the center sill is considerable when compared to the stress levels in the AW0 standing car (Figure 24). Consistent with industry practices of the mid-20$^{th}$ century, the center sill was designed to be the main longitudinal load bearing member in the railcar [7]. As seen in previous stress distribution plots, the peaks in this figure correspond to the locations of the lateral members. The magnitude of the peaks becomes larger as the area examined becomes closer to the top of the web, where the lateral members are attached to the center sill.

The side sills were also examined for their stress distribution at a number of heights within the cross-section. The heights examined were at the bottom of the web, 1” above the bottom of the web, 4” below the top of the web, and the top of the web. The longitudinal stress distribution in the side sill is show below, in Figure 34.

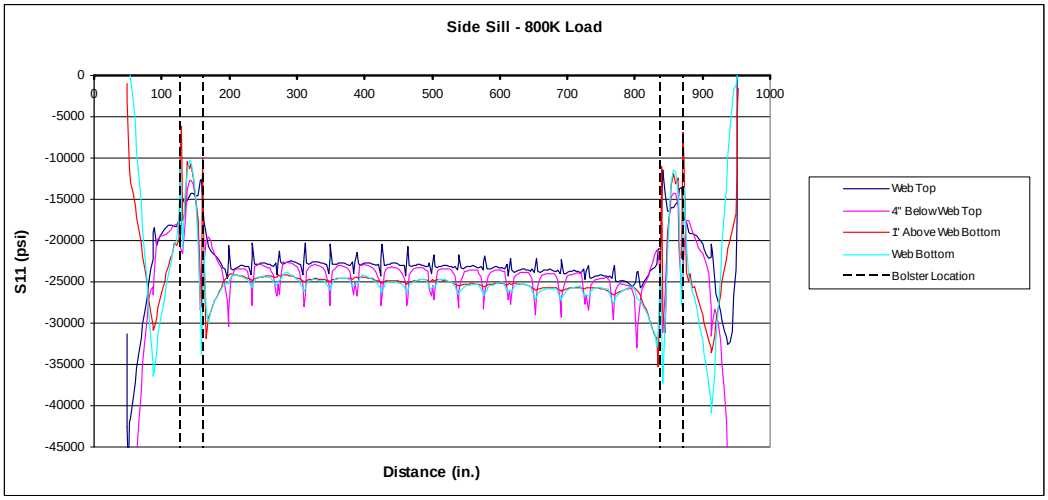


**Figure 34 - Stress Distribution in Side Sill, 800 kip Load**

The side sill remains in compression throughout the occupant volume. The stress levels increase in magnitude toward the ends of the side sill. At both ends of the member, the side sill has been extended across the space for the stepwells, connecting to the buffer beams at both ends of the car. The cross-section of the side sill in the extensions is different from the cross-section throughout the rest of the car. While the data in Figure 34 does not include the stress levels in the extensions, the change in cross section contributes to the large magnitude stresses seen at the extreme ends of the continuous side sill. The stress contour plots showing this concentration of stress can be found in Appendix D –

Stress Contour Plots for Various Load Cases.

The stress levels in the side sill are higher at the bottom of the web and gradually decrease toward the top for a given longitudinal distance. This behavior is similar to the stress distribution in the center sill in the railcar subject to the same 800 kip load (Figure 33). The stress magnitudes in the side sill are roughly half of the stress levels in the center sill.

The belt rail's stress distribution is shown in Figure 35. Between the two body bolsters, the belt rail is entirely loaded in compression. The stress levels between the bolsters are, on average, of smaller magnitude than the stress levels recorded in the side sills. This distribution is consistent with the stress behavior seen in a beam in bending, where the material below the neutral axis is being compressed while the material above the neutral axis is under tension.

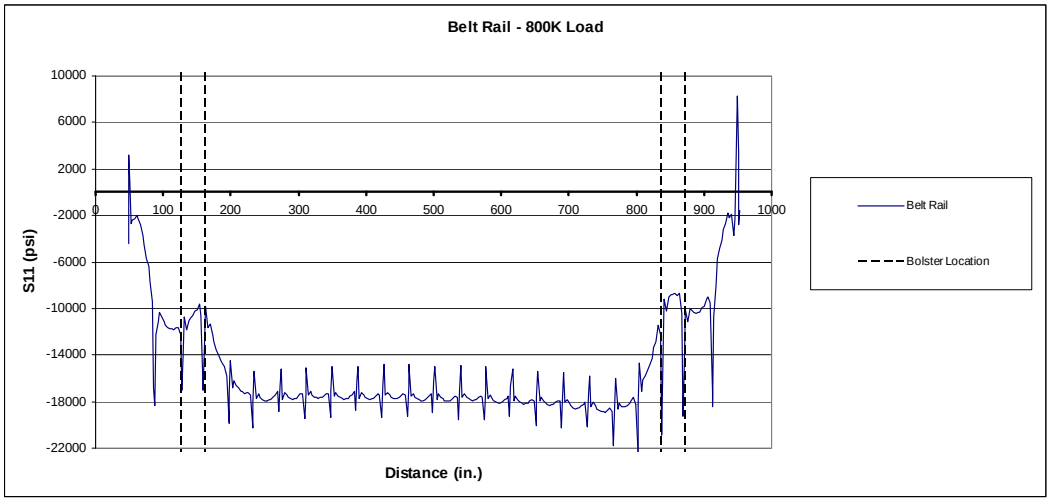


**Figure 35 - Stress Distribution in Belt Rail, 800 kip Load**

The stress distribution along the length of the upper window rail is presented below, in Figure 36. The stress levels between the body bolsters are

compressive and smaller in magnitude than the stress levels in the previously discussed longitudinal members.

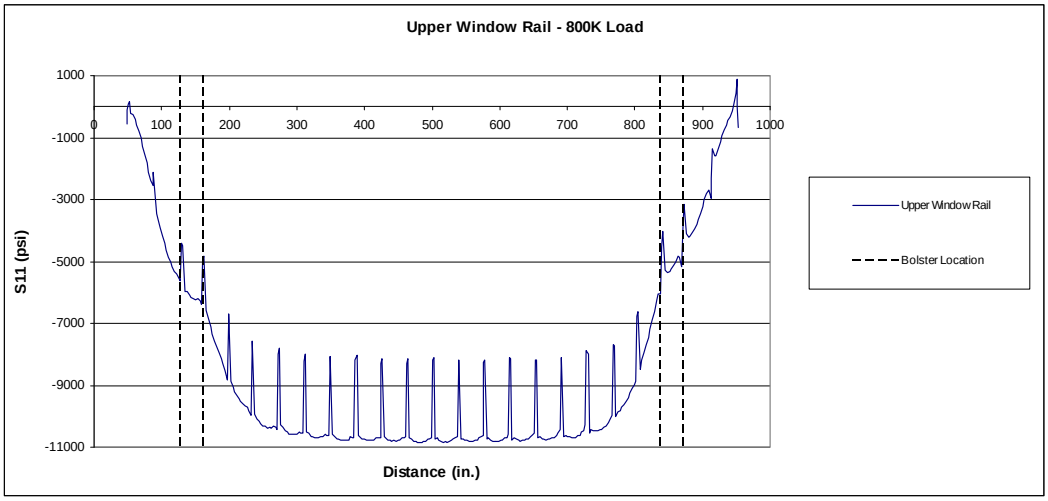


**Figure 36 - Stress Distribution in Upper Window Rail, 800 kip Load**

At the top of the sidewall structure is the roof rail. The stress distribution in the roof rail, from AT plate to AT plate, is shown in Figure 37 for the 800 kip load applied at the buff stops. The roof rail is in a tensile state from body bolster to body bolster. The moment component of the 800 kip load results in enough tensile stress at the top of the carbody that the compressive stress in the roof rail from the weight loading (Figure 28) is overcome. This stress state can be expected from a location above the neutral axis in a beam in positive bending, such as a double-overhanging beam.

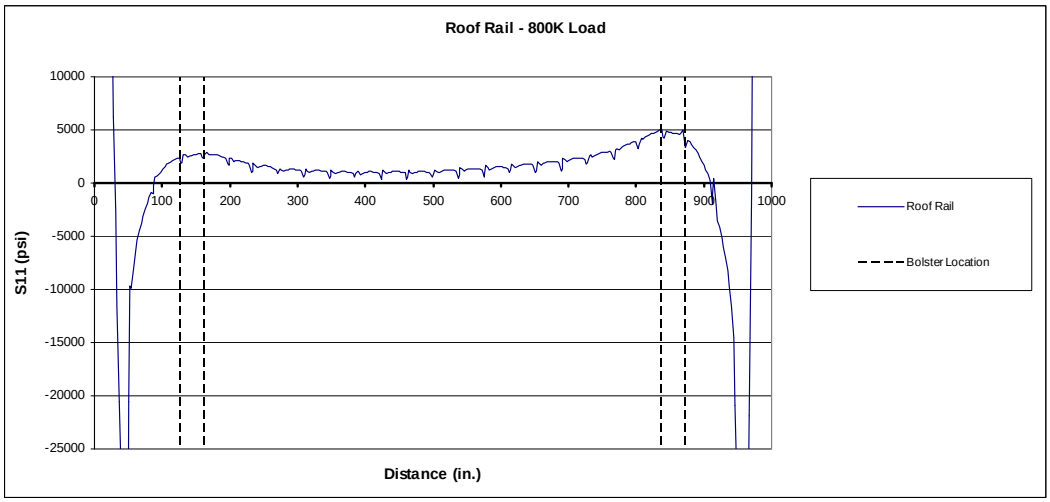


**Figure 37 - Stress Distribution in Roof Rail, 800 kip Load**

The stress distribution in the purlin is displayed in Figure 38. Similar to the distribution in the roof rail, the purlin is also under tension in the region between the two body bolsters. The stress values are slightly higher in the purlin than in the roof rail, on average.

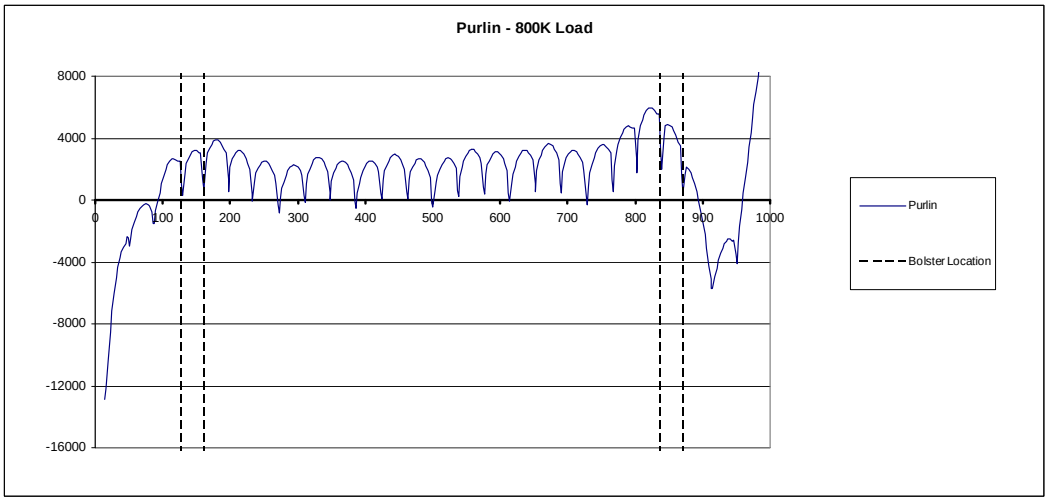


**Figure 38 - Stress Distribution in Purlin, 800 kip Load**

Figure 39 plots the stress distribution for the center sill, side sill, belt rail, upper window rail, roof rail, and purlin in the car subjected to the 800 kip

compressive load. In this plot, the distance scale has been adjusted to show only the region inboard of both bolsters. The relative levels of stress in each member are apparent, with the bottom of the railcar experiencing a state of compression and transitioning to a state of tension at a location between the upper window rail and the roof rail.

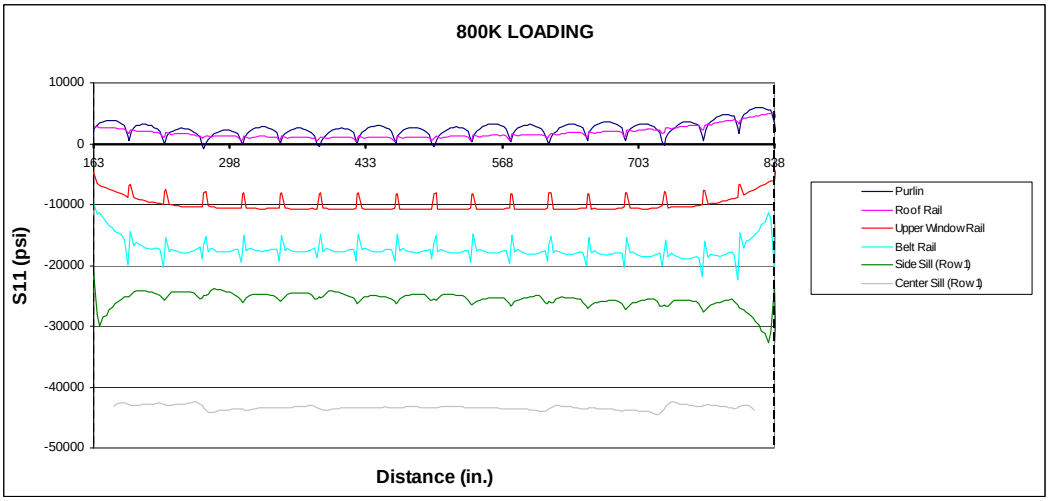


**Figure 39 - Stress Distribution in Longitudinal Members, 800 kip Load**

The average value of stress between both body bolsters is shown in Figure 40 for each of the longitudinal members discussed. This figure indicates the beam-like behavior of the carbody during the 800 kip compressive test. The lowest longitudinal member, the center sill, experiences the largest compressive stress. As the stress level is analyzed at higher members in the car, the compressive stress steadily decreases. At the roof of the car, the roof rail and purlin experience tensile stresses due to the bending moment generated by the application of the 800 kip load at the buff stops. Because the carbody is being loaded simultaneously in bending and compression, the transition between

positive and negative average stress occurs above the measured carbody neutral axis.

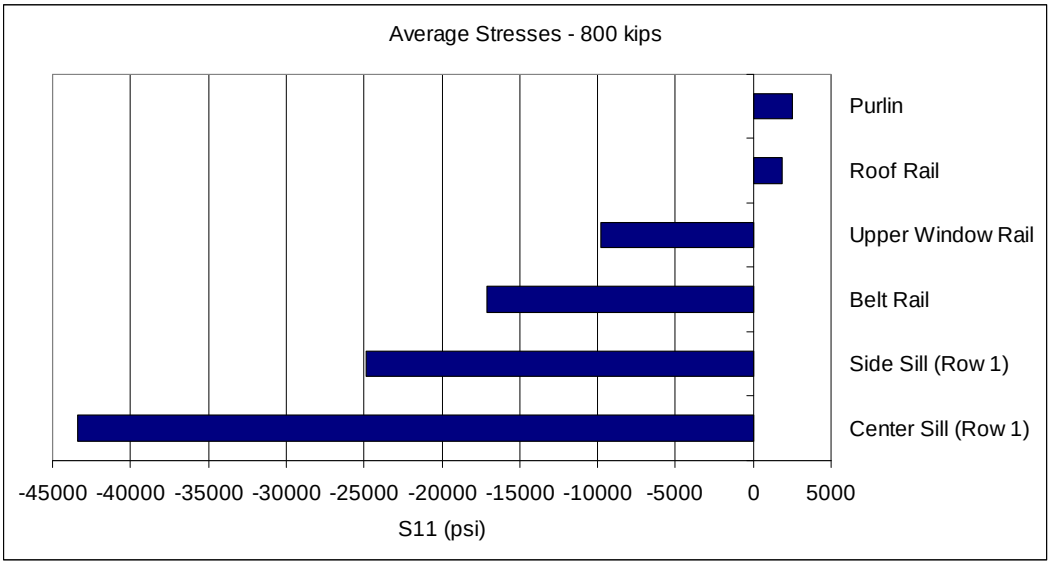


**Figure 40 - Average Occupant Volume Stresses, 800 kip Load**

## 3.6 Alternative Proof Load

An alternate loading condition is desired that places the occupied volume of the car under stress comparable to that resulting from the 800 kip proof load. It is also desirable that the alternate load be applicable to a wider range of equipment than the current 800 kip load. This implies that any alternate load be applicable to a greater variety of structure on the railcar than the existing load.

Consistent with past domestic practice and current international practice, the buffer beam was chosen as a preliminary location for further investigation. Since the buffer beam is located at the extreme end of the railcar, it will always be outboard of the occupant volume. Additionally, the beam is located above the centerline of draft but below the neutral axis in a single-level railcar of

conventional construction. This implies that the bending condition of the railcar will be similar to the bending condition experienced by the railcar when subjected to the current 800 kip loading at the buff stops.

As an evaluation case of any proposed alternative proof load, it is desirable to compare the stress states in an exemplar railcar under this new load to the same car subject to the 800 kip load. The results of this comparison will be useful in determining the equivalence of the two tests, as well as demonstrating that the occupant volume is assured an equal level of protection regardless of the method used to evaluate the structural strength.

Where previous U.S. practice has placed 500,000 pounds across the center of the buffer beam of the car, a proposed alternative proof load examined is 1,000,000 pounds distributed across the entire face of the buffer beam. Because the area of load application is closer to the neutral axis of the single-level car than the location of the 800 kip load, the resulting bending moment would be reduced for a load of the same magnitude. Hence, a larger load was chosen to maintain the static strength test as one of both compressive and bending components.

While current railroad equipment is based on the conventional design of a stiff underframe with a less structurally-significant superstructure, it is important to realize that this is not the only possible design for a load path into the vehicle. For example, a number of prototypical railcars incorporating crash energy management (CEM) have been designed, built, and tested [4]. This particular design features pushback couplers that retract into the draft sill, enabling the buffer beams and AT plates of the coupled railcar to come together during a

collision. If the collision forces are large enough, a set of energy absorbers are activated and crush an unoccupied area of the railcar. These energy absorbers are located below the floor level of the car as well as at the level of the roof rails. Two CEM railcars coupled to one another are shown in Figure 41.

**Figure 41 - Coupled CEM Railcars**

This arrangement of endframe and energy absorbers causes this railcar to load differently during a collision event. While conventional railcars react the majority of the collision load through the buff stops and into the underframe, the CEM car is loaded at the buffer beam and the AT plate simultaneously. A static strength test that evaluates the railcar for its reaction under this type of loading may be desirable if equipment designed to be loaded in this manner is to enter revenue service in the future.

As an evaluation of cars loaded over a greater area of the endframe than

just the underframe, a third load case is evaluated. This case retains the 1,000 kip load across the buffer beam, and adds a 200 kip load across the AT plate. This 200 kip load was first evaluated as a single load, and then when applied in parallel with the 1,000 kip load discussed earlier. Because the AT plate is above the neutral axis of the single-level car, the 200 kip compressive load deforms the carbody in the same way as the car under its own weight. The moment generated by the 200 kip load will be opposite in direction as the load from the 1,000 kip load at the buffer beam. However, the total compressive force will be 1,200 kip that must be resisted by the structure of the railcar.

### 3.6.1 Buffer Beam Loading Results

As in the 800 kip loading case, the standing railcar was loaded to AW0 using an artificial gravitational constant. Vertical and lateral motions were restricted by appropriate boundary conditions and springs at the body bolsters, as described in Section 3.2. The buffer beam at one end of the car was restricted from motion in the longitudinal direction. At the opposite end of the railcar, a pressure load was applied across the entire outboard face of the buffer beam, such that the longitudinal force was 1,000,000 pounds. The boundary condition and compressive load are illustrated in Figure 42.

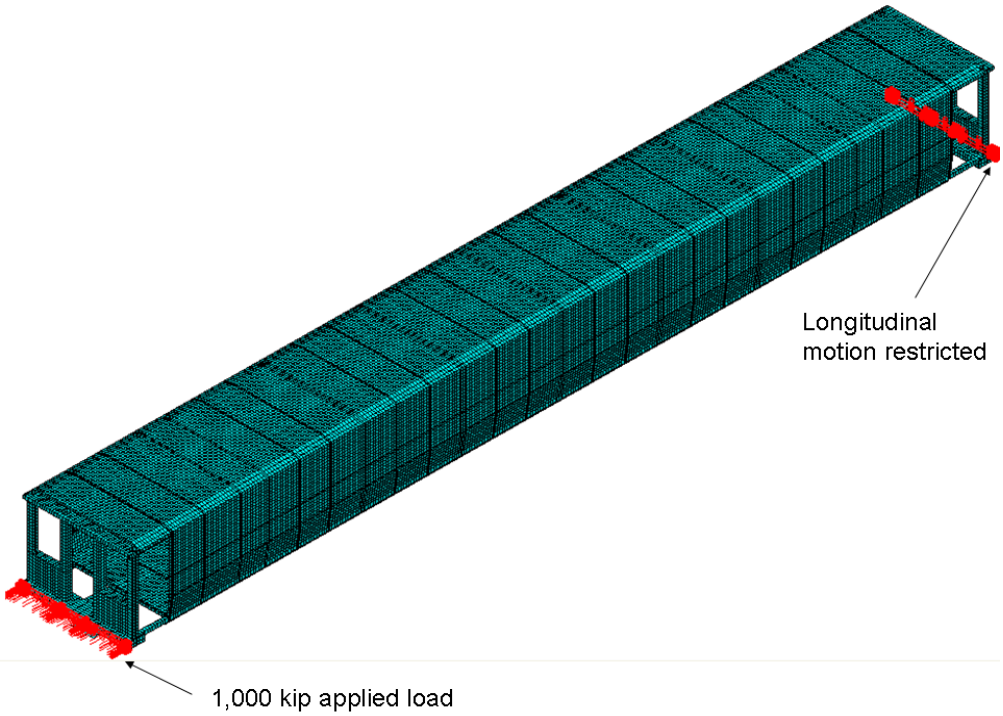


**Figure 42 - Buffer Beam Compressive Test Setup**

Since the buffer beam is below the neutral axis of the railcar, the carbody is expected to deform in a similar manner as the carbody subject to the 800 kip load. The deformed shapes of the carbody under its own weight and under a compressive and bending load are shown schematically in Figure 32.

The stress values along the length of the center sill are measured in the same manner as for the 800 kip load. The stress was recorded along rows of elements at different heights within the center sill. Row 1 represents the lowest row of elements in the web, and Row 6 represents the very top row in the web.

Similarly to the distribution of stress during the 800 kip load (Figure 33), under the 1,000 kip load the center sill experiences the largest compressive stresses at the bottom of the web and steadily decreases in magnitude as the stress

is examined closer to the top of the web. The magnitude of stress is larger in the 1,000 kip load at each cross section examined. The average stress in the center sill is plotted for each row of elements for both the 800 kip load and the 1,000 kip load in Figure 43, and shows the larger magnitude compressive stress state generated in the center sill by the 1,000 kip load. This plot also demonstrates that the difference between the two loads is largest at the bottom of the center sill web and decreases toward the top of the web.

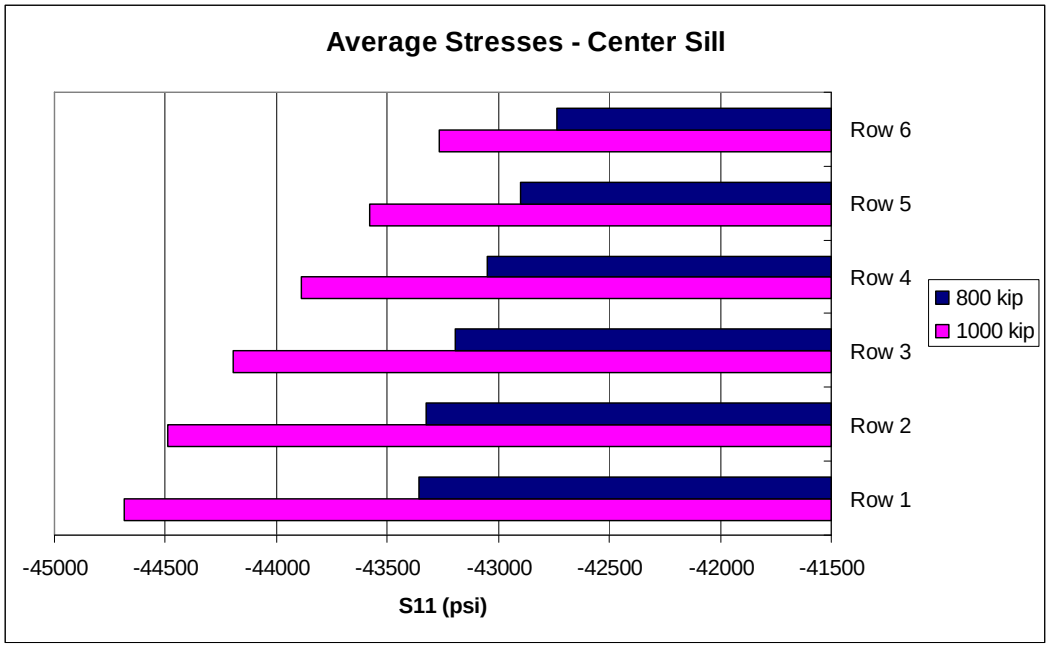


**Figure 43 - Average Stresses in Center Sill, 800 kip and 1,000 kip Loads**

The average value of stress along the length of the side sill is shown in Figure 44 for both the 800 kip load and the 1,000 kip load. At all locations examined, the side sill is under compressive stress during both loading cases. The 1,000 kip load causes a larger magnitude stress at all locations examined. Because the 1,000 kip load is distributed across the entire buffer beam, the load

path to the opposite buffer beam includes a direct connection to the side sills. The 800 kip load must travel through the draft sill and into the lateral members before it is transmitted into the side sills of the car.

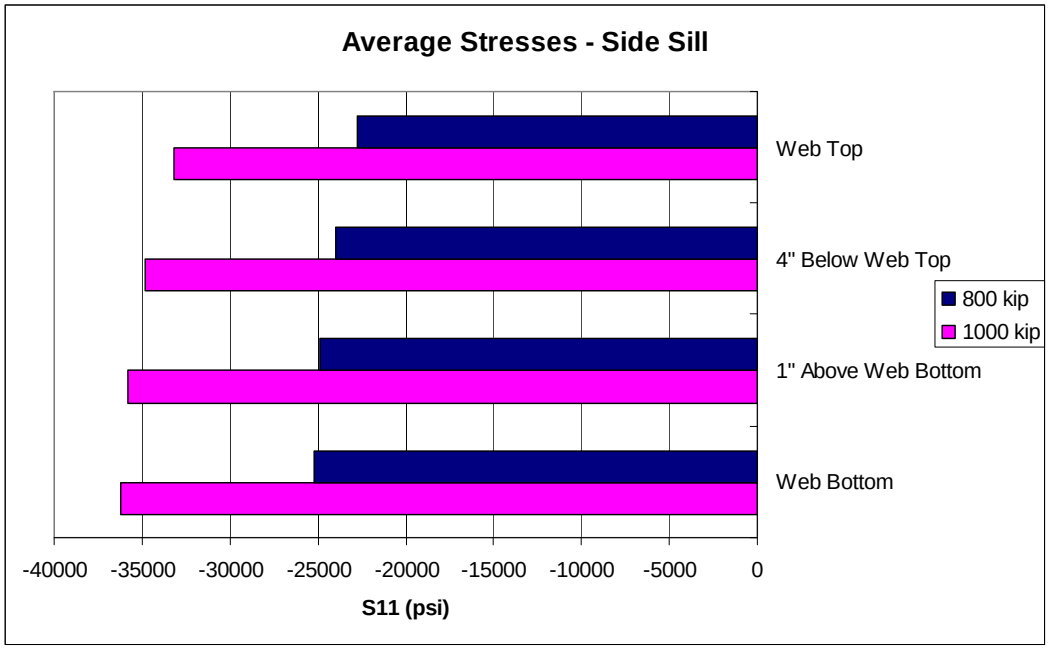


**Figure 44 - Average Stresses in Side Sill, 800 kip and 1,000 kip Loads**

The average occupant volume stresses in all longitudinal members examined are shown for both the 800 kip load and the 1,000 kip load in Figure 45. The stresses in the belt rail and upper window rail are compressive for both loading cases. The roof rail experiences a tensile stress during the 800 kip case, caused by the bending associated with a load below the neutral axis. The roof rail stress is compressive in the 1,000 kip load case, despite the load's application below the neutral axis of the railcar. In both load cases, the purlin experiences tension.

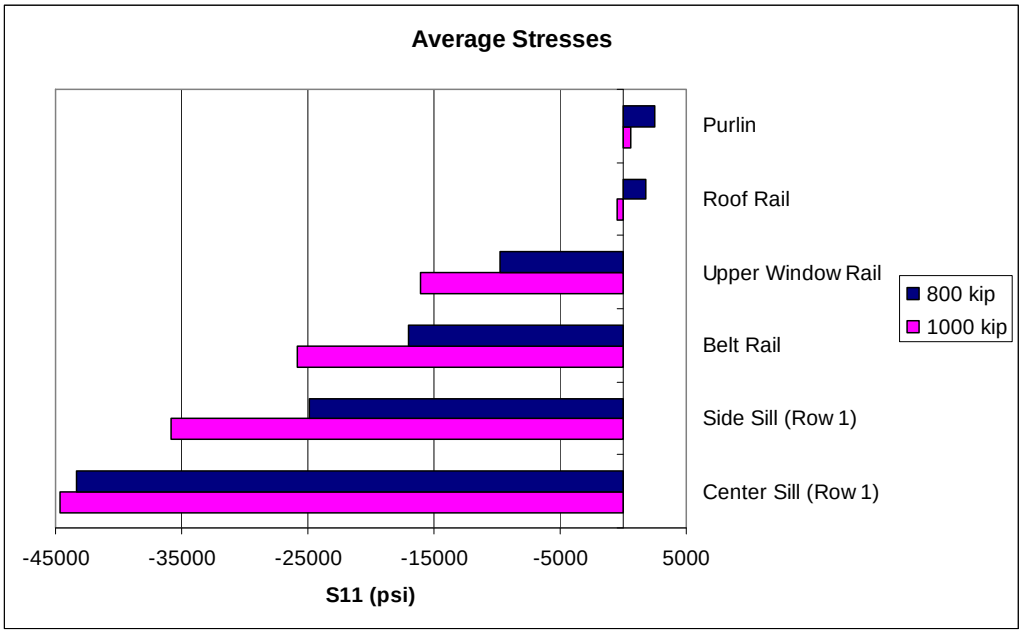


**Figure 45 - Average Occupant Volume Stresses, 800 and 1,000 kip Loads**

The total longitudinal load is a larger compressive load in the 1,000 kip load case than in the 800 kip load case. Since the boundary condition is applied at the opposite end of the railcar, this force must somehow be transmitted through the car. Because the 1,000 kip load is distributed across a portion of the endframe, it is reasonable to expect that the longitudinal members that run from endframe-to-endframe will bear more compressive force in this load case than in the 800 kip case. This is reflected in the stress results seen above. The members below the effective neutral axis of the car are subject to compression from bending and the axial force, while those at the top of the car are subject to tension from bending but pure compression from the longitudinal load.

The distribution of stress for the center sill, side sill, belt rail, upper window rail, roof rail, and purlin from bolster to bolster is shown in Figure 46.

This distribution compares similarly to the plot of the stress distributions in the same members for the 800 kip loading, seen in Figure 39. In both loading cases, the carbody is subject to compression loads as well as bending stress that tends to compress the underframe members and extend the members at the roof level. The 1,000 kip load results in a more severe state of compressive stress in the center and side sills, the belt rail, and upper window rail. The roof rail is under tension in the 800 kip load, but remains in compression for the 1,000 kip load. The purlin is under tension for both load cases, but the 800 kip load results in a larger magnitude stress in this member.

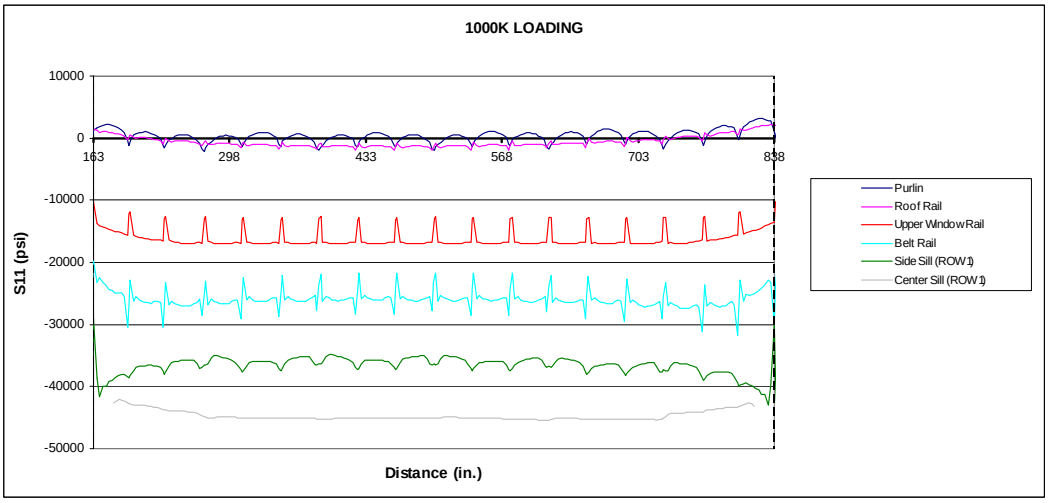


**Figure 46 - Stress Distribution in Longitudinal Members, 1,000 kip Load**

### 3.6.2 AT Plate Loading Results

The largest magnitude load case being investigated as part of this thesis is a 1.2 million pound load distributed across the buffer beam and AT plate of the railcar. As an intermediate loading case, a 200 kip load placed across the surface of the AT plate is investigated. This intermediate load case will aid in the

understanding of the combined 1,000 kip load across the buffer beam and 200 kip load at the AT plate, as the results for just the 1,000 kips across the buffer beam have already been analyzed.

The boundary conditions at the body bolsters were kept the same as in the 800 kip load case and the 1,000 kip load case. The 200 kip load was applied to the outer face of the AT plate at one end of the railcar. This load was simulated using a pressure, distributed across the entire face of the plate. At the opposite end of the railcar, the outer face of the AT plate was restricted from motion in the longitudinal direction. The loading and boundary conditions at the AT plates are shown in Figure 47.

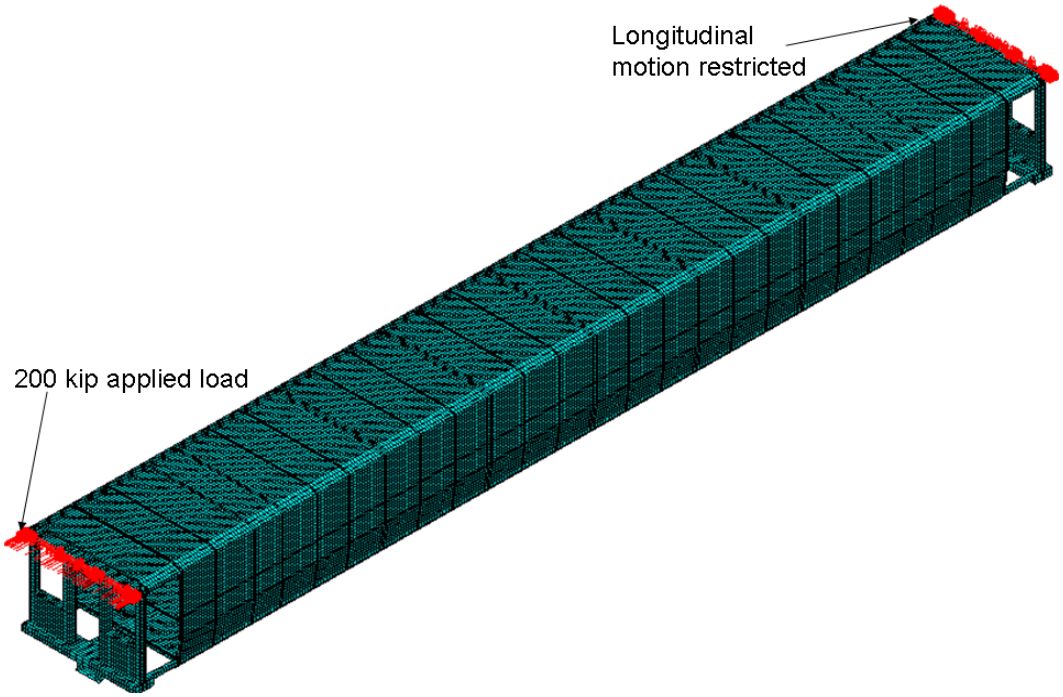


**Figure 47 - AT Plate Compressive Test Setup**

Unlike the 800 kip load and the 1,000 kip load, the 200 kip load is applied at the roof level, above the neutral axis. This loading will cause a different

behavior in the railcar. Where the loads at the buff stops and buffer beam caused bending moments that acted in opposite direction from the moments caused by the gravity loading, the 200 kip load causes moments that act in the same direction as the gravity moments between the body bolsters.

As was done for the 800 kip and 1,000 kip load cases, the stress values are recorded for the longitudinal members making up the underframe and superstructure of the car. The stress levels in the center sill are recorded at a number of heights throughout the web of the member. Row 1 represents the lowest row of elements in the web, and Row 6 represents the very top row in the web. The stress distribution along the entire length of the center sill is shown below, in Figure 48. Additionally, the average value of the stress in the center sill along each row of elements investigated is shown in Figure 49 for the 200 kip load as well as the AW0 railcar loaded solely by its own weight.

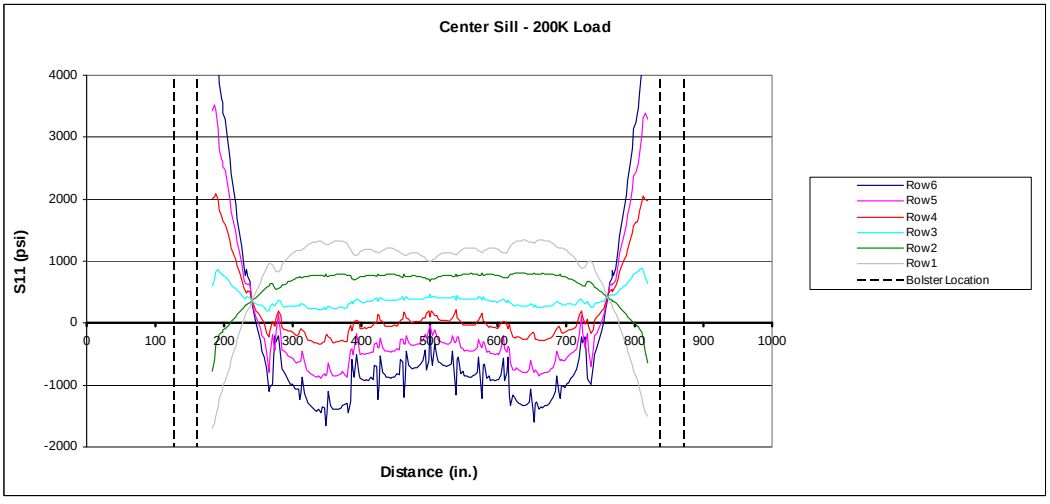


**Figure 48 - Stress Distribution in Center Sill, 200 kip Load**

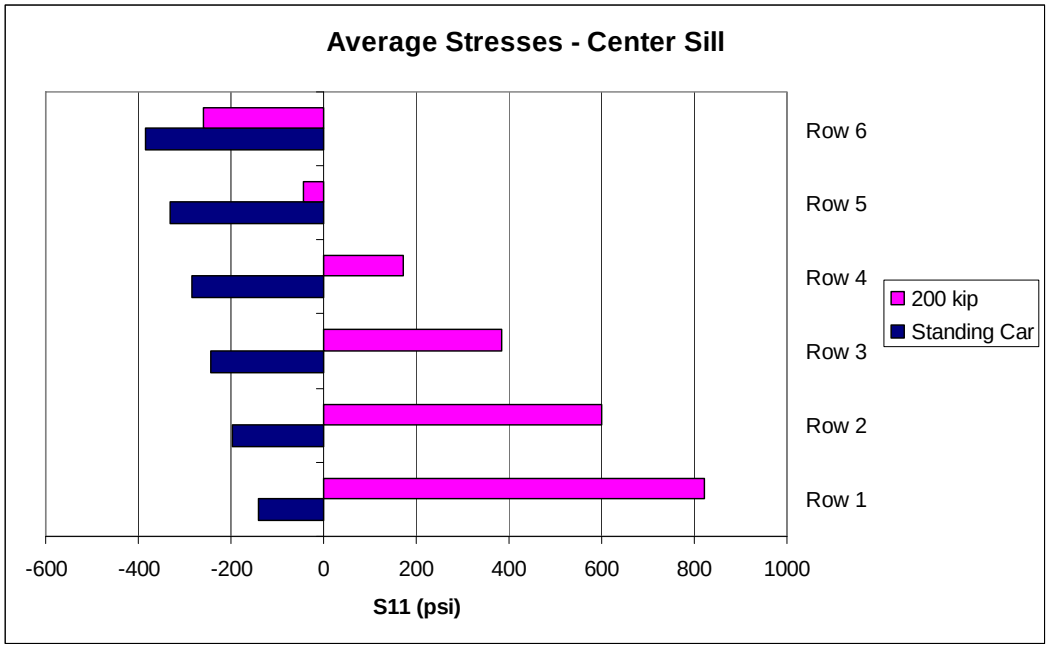


**Figure 49 - Average Stresses in Center Sill, 200 kip and AW0 Loads**

The stress values in the center sill gradually transition from compressive at the top of the web to tensile at the bottom of the web during the 200 kip loading. When the car is loaded under its own weight, the center sill is under an average compressive stress at all web heights examined. The difference between the two cases can be attributed to the bending component of the 200 kip load. The load is being applied at the extreme height of the car, while the center sill is at the extreme low end of the car. Since these two locations are on opposite sides of the neutral axis of the carbody, the bending moment generated by the compressive load will result in tensile stresses in the center sill. As the location in the center sill moves further away from the neutral axis, the tensile stresses become greater.

The stress distribution along the length of the side sill is shown below in Figure 50. The general trend in the side sill is a tensile stress at all locations

examined. This behavior is clearly seen in the plot of average stress in the side sill between the bolsters, shown in Figure 51.

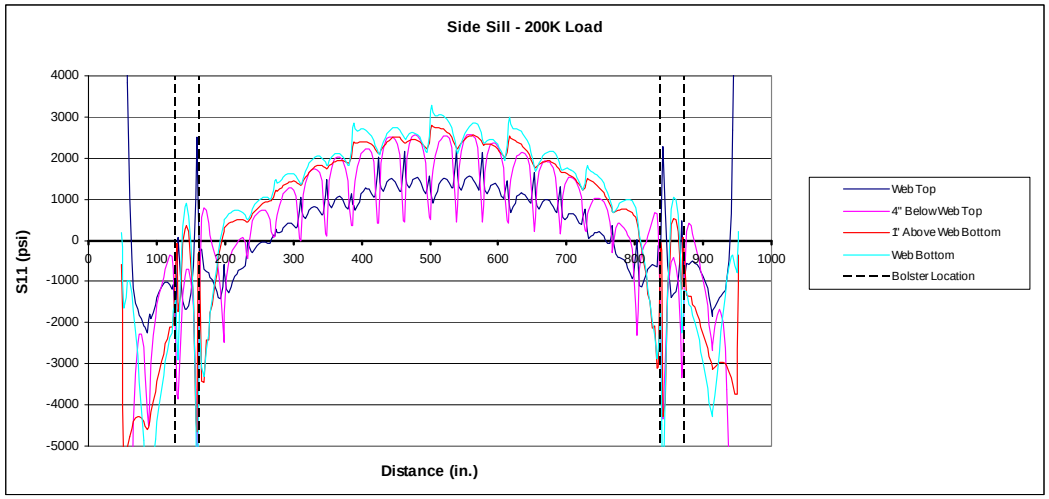


**Figure 50 - Stress Distribution in Side Sill, 200 kip Load**

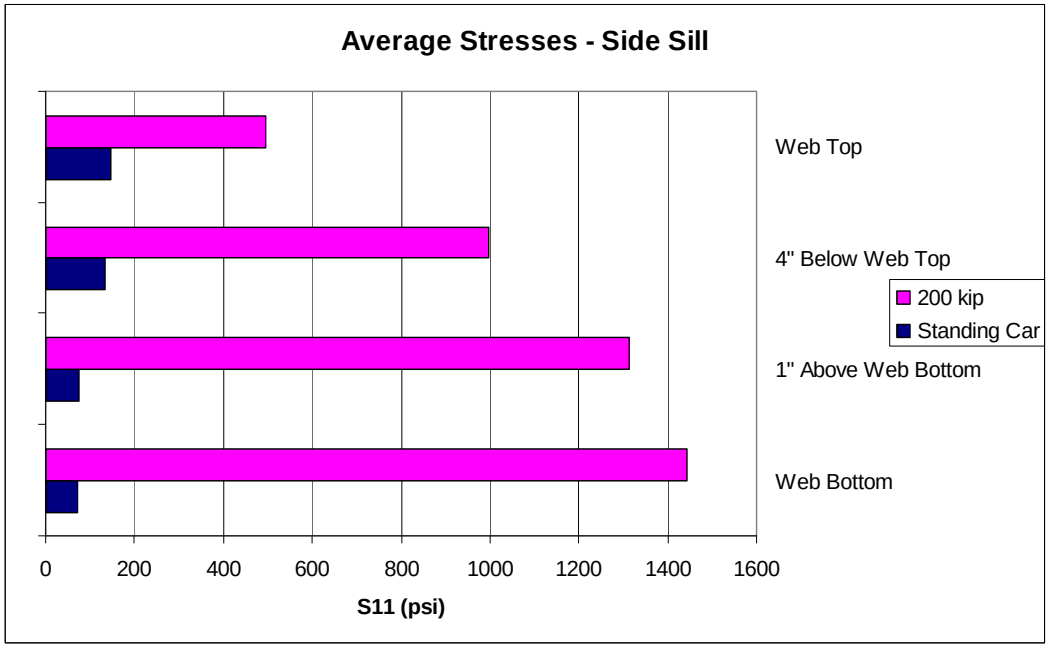


**Figure 51 - Average Stresses in Side Sill, 200 kip and AW0 Loads**

Figure 51 also shows the average value of stress for the same locations in the railcar subject to its own weight loading. Under its own weight, the side sill is

subject to tensile stresses at all heights examined. This trend is the same for the 200 kip load, with the magnitude of stress being larger at all heights examined. The tensile stresses experienced by the side sill during the 200 kip load are a sum of the stresses from the gravity load as well as the moment generated by the 200 kip load.

The average values of bolster-to-bolster stresses are reported for each member in the superstructure of the railcar under both the 200 kip load and the railcar's own weight in Figure 52. In both loading cases, the average stress is tensile for all the members. In the 200 kip loading case, the stresses are of larger magnitude in each member. In particular, the roof rail and purlin experience stress levels dramatically higher than those present in the standing car. This is attributed to the load being applied at the roof level in the 200 kip case, which places the purlin and roof rail in the immediate load path between the AT plates at either end of the car.

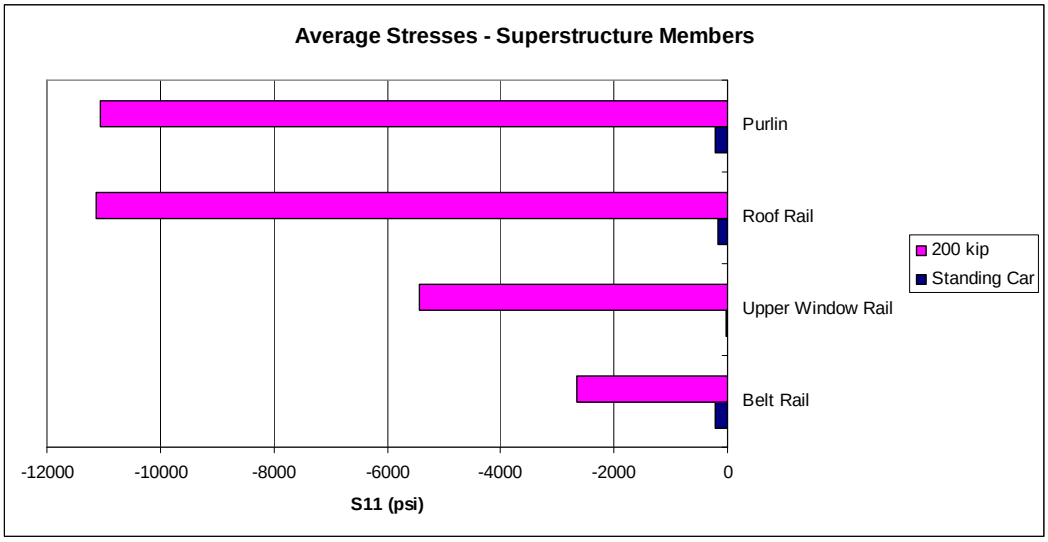


**Figure 52 - Average Stresses in Superstructure Members, 200 kip and AW0 Loads**

Figure 53 shows the stress distribution in the center sill, side sill, belt rail, upper window rail, roof rail, and purlin for the carbody under 200 kip loading at the AT plate. The horizontal axis has been chosen to show only the stress distribution from body bolster to body bolster. The stresses are tensile in the side and center sills, but compressive for the other superstructure members.

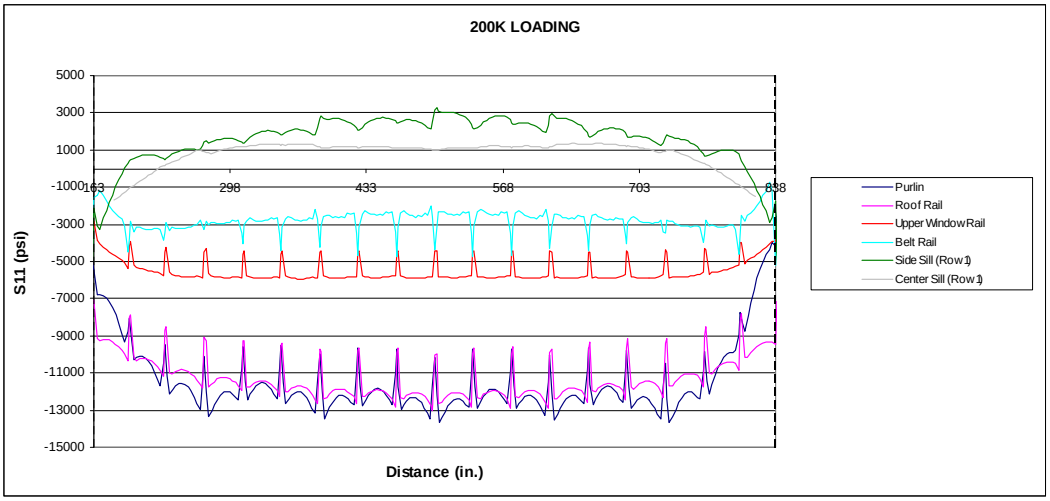


**Figure 53 - Stress Distribution in Longitudinal Members, 200 kip Load**

Despite being located below the side sills in a cross-section of the railcar (Figure A32), the center sill experiences a lower tensile stress than the side sill. While the analogy of the railcar acting as a single beam is generally useful for describing its behavior, this is one instance of the complexity of the car's geometry not being adequately described by the beam simplification.

The center sill, being designed to bear the majority of the longitudinal loads of the train, has a cross sectional area of approximately 9.4 square inches. It is made from 0.25" thick steel sections. The side sill is considerably less massive, having a cross-section of less than 2 square inches. This member is made of

0.125” thick sections. Because the center sill is much larger than the other longitudinal members, the stress levels would be less than in the other members for a similar load.

### 3.6.3 Combined Endframe Loading Results

The final load case investigated on the single-level car is a 1.2 million pound load distributed across the buffer beam and AT plate of the railcar. This load is made up of 1,000 kips applied across the buffer beam and 200 kips applied across the AT plate. The load is reacted at the opposite end of the railcar by restricting the outer faces of both the buffer beam and the AT plate from longitudinal motion. The longitudinal boundary conditions and loads are shown in Figure 54. The vertical and lateral motions of the railcar are taken out at the body bolsters, as described in Section 3.2.

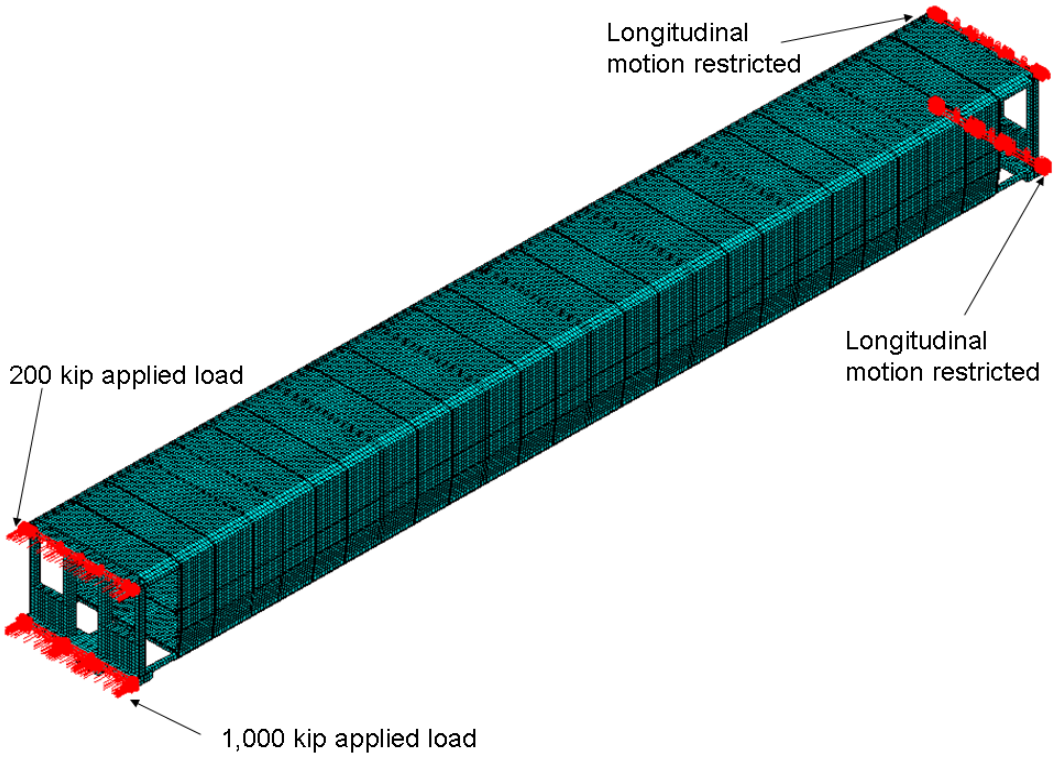


**Figure 54 - Combined AT Plate and Buffer Beam Compressive Test Setup**

This loading case places the largest magnitude compressive force on the endframe of the railcar of any of the previously-analyzed compressive strength tests. The bending component, however, is less severe than that of the 1,000 kip load alone. Because the 200 kip load is applied in the same direction as the 1,000 kip load but on the opposite side of the neutral axis, some portion of the two moments generated by these forces cancel one another out.

The stress distribution in the center sill is shown in Figure 55. The stress is measured along six rows of elements in the web of the center sill. Row 1 is located at the bottom of the web, while Row 6 is located at the top. The general trend in stress levels seen in this figure shows compression at all of the locations examined. The compressive stress has a decreasing magnitude as the location

examined is closer to the top of the web and thus, the neutral axis of the railcar.

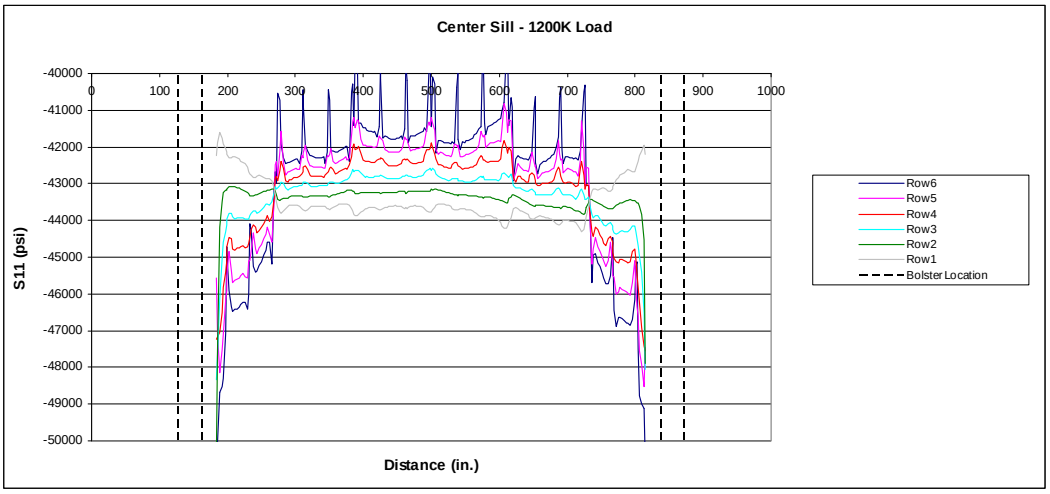


**Figure 55 - Stress Distribution in Center Sill, 1,200 kip Load**

The average value of stress measured inboard of the two body bolsters is plotted for each row of elements during the 800, 1,000, and 1,200 kip loading cases in Figure 56. At all locations within the center sill, the 800 kip load causes the least severe compression stress. The 1,000 kip load causes the largest magnitude of compressive stress at each location, and the 1,200 kip load is between the 1,000 kip and 800 kip loads. While the 1,200 kip load has a larger total force applied to the railcar, the bending stress is less than the 1,000 kip load's due to the presence of the 200 kip load at the top of the car. The greatest difference in stress occurs in Row 1, where the difference between the stress from the 800 kip load and the 1,000 kip load is approximately 1,330 psi.

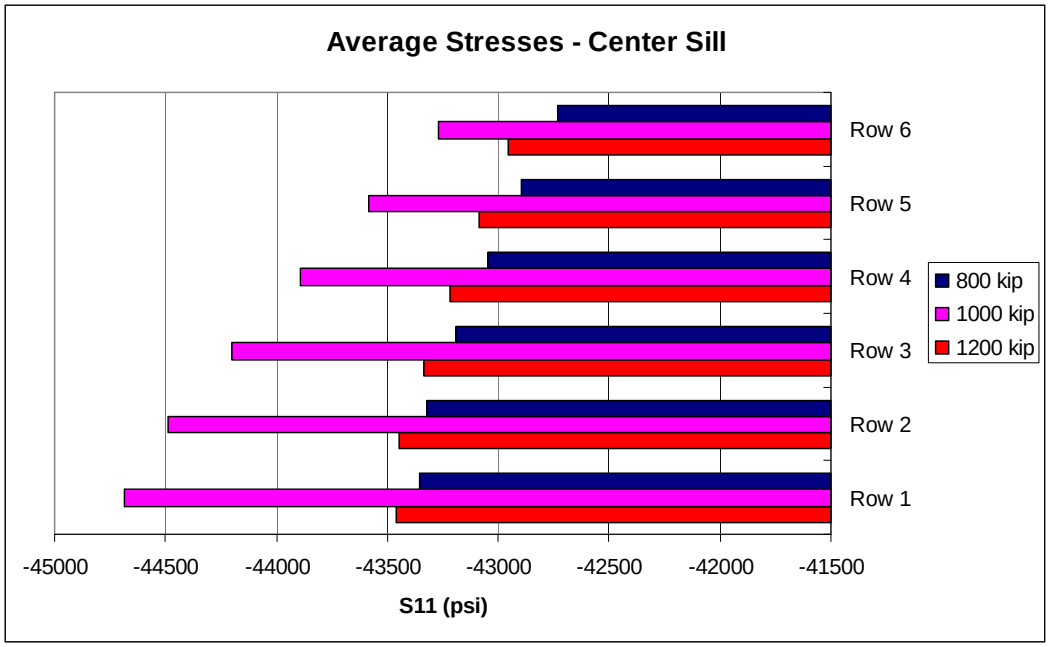


**Figure 56 - Average Stresses in Center Sill, 800, 1,000, 1,200 kip Loads**

The stress distribution in the side sill is plotted below, in Figure 57. As in previous side sill results, the stresses are examined at four horizontal rows of elements: the top of the web, 4" below the top of the web, 1" above the bottom of the web, and the bottom of the web. The stress levels throughout the occupant volume are compressive at all location examined. The stress levels are also consistent from one row of elements to the next.

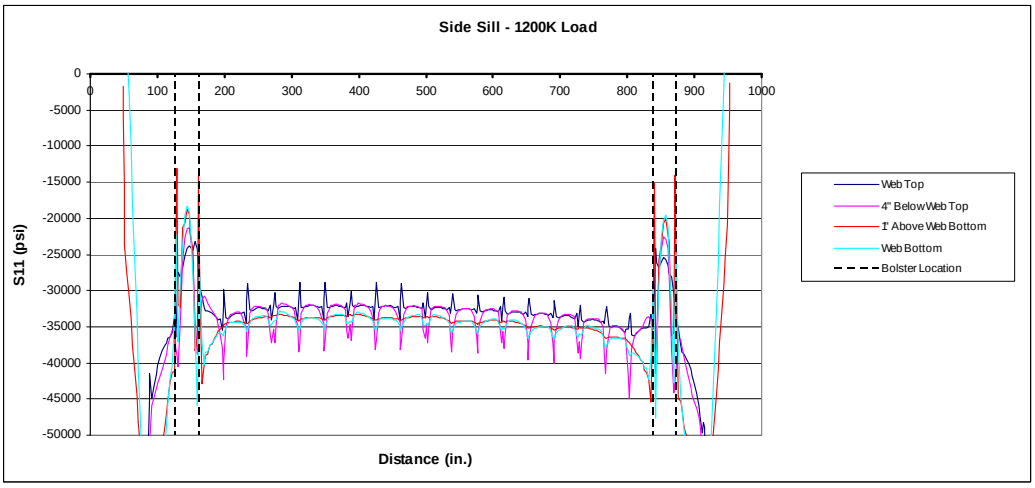


**Figure 57 - Stress Distribution in Side Sill, 1,200 kip Load**

The average value of stress in the side sill from bolster-to-bolster is plotted in Figure 58 for the 800 kip load, the 1,000 kip load, and the 1,200 kip load. In all cases, the average value of stress is compressive. At all locations examined the 800 kip load results in the smallest magnitude of compressive. The 1,000 kip load is the most severe at all locations, with the 1,200 kip load being slightly less than the 1,000 kip load at each location. Because the 1,000 kip load is applied across the full width of the buffer beam, the side sill transmits more load than in the 800 kip case, where the load must travel through the body bolsters and the cross members to get into the side sills.

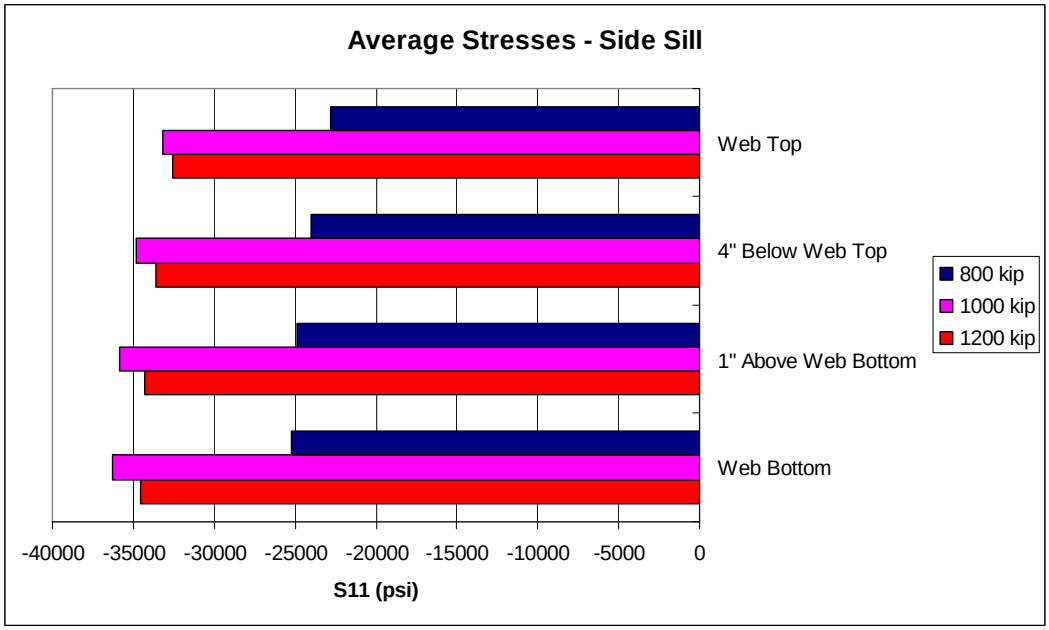


**Figure 58 - Average Stresses in Side Sill, 800, 1,000, 1,200 kip Loads**

The average stress levels between the bolsters are plotted for each of the longitudinal members in Figure 59. The stress levels from the 800 kip load, the 1,000 kip load, and the 1,200 kip load are plotted in this figure. While the 800 kip load as well as the 1,000 kip load both result in tensile stress in the roof rail and/or purlin, the 1,200 kip load places every member in the superstructure into a compressive state. The tensile loading in the roof-level members are principally caused by the moment generated by the compressive loads at either the buffer beam or buff stops. While the 1,200 kip load has a significant (1,000 kip) load located at the buffer beam, the 200 kip load at the AT plate loads the roof rails and purlins directly in compression.

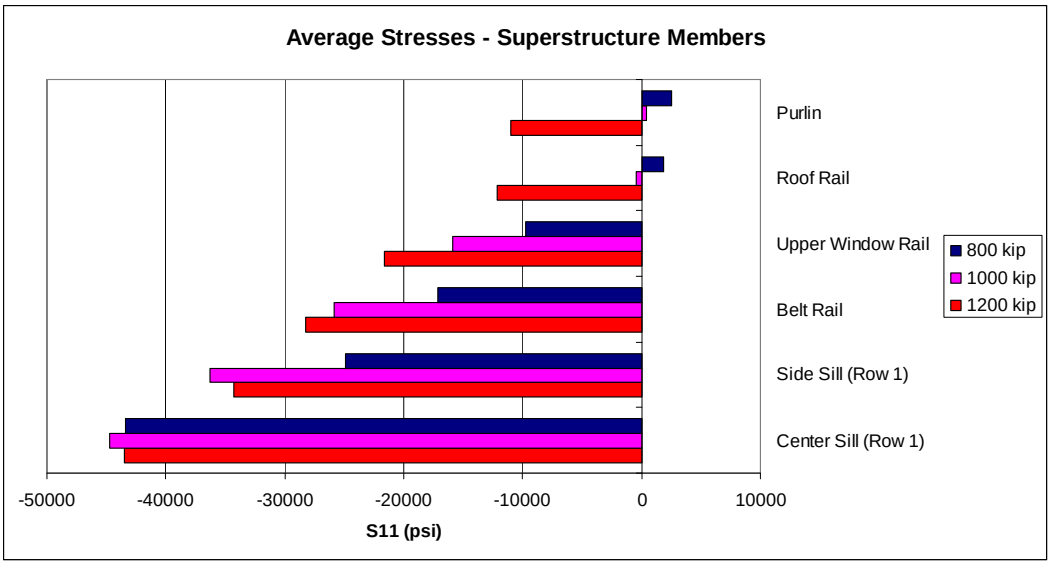


**Figure 59 - Average Occupant Volume Stresses, 800, 1,000, 1,200 kip Loads**

In the belt rail and upper window rail, all three loading cases result in a compressive stress. The 800 kip load causes the smallest compressive stress, and the 1,200 kip load causes the largest stress levels. The combination of bending and compressive stresses is such that the members in the superstructure are all loaded to a higher degree of compression in the 1,200 kip load than in the 800 kip load or the 1,000 kip load.

The stress distributions in the center sill, side sill, belt rail, upper window rail, roof rail, and purlin under the 1,200 kip load are shown in Figure 60. This figure has a horizontal scale adjusted to show only the stress levels inboard of both bolsters. With the exception of the peak values corresponding to vertical or lateral support members, the stress level in a given longitudinal member is fairly consistent throughout the occupant volume. The stress results show the least compressive stress at the roof level, with an increase in compressive stress with

each successively lower member.

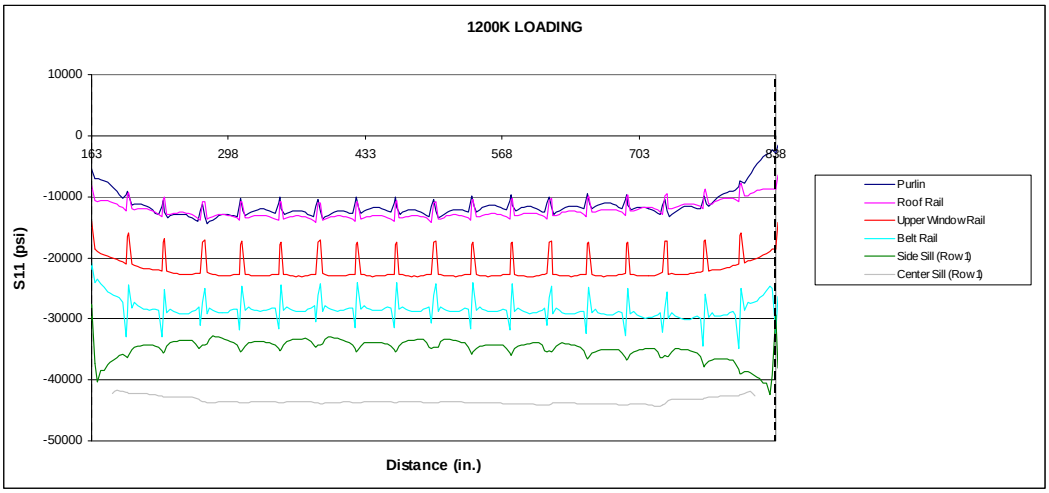


**Figure 60 - Stress Distribution in Longitudinal Members, 1,200 kip Load**

# 4 Results for Multilevel Car

As an extension of the work performed on the single-level car, the same loading cases were applied to a partial low-floor railcar. The goal of this was to establish that the 1,000 kip, 200 kip, and 1,200 kip loads, when applied to equipment other than a single-level railcar, produced similar behavior in the car.

## 4.1 Model Description

A second shell finite-element model has been created as part of this research. It is desirable to understand the load path through equipment that does not have a continuous floor level, both for the current 800 kip load case and for any prescribed alternative loading scenarios. The second model was constructed entirely of shell elements, with spring elements used to model the secondary suspension of both trucks. A similar methodology was employed in the shell model of the single-level car, where detailed connections are not modeled as part of this research.

Both the single and multilevel railcars have similar construction features. The underframe of both vehicles consists of a large center sill and two side sills (Figure A32), with the side sills designed to bear less load than the center sill. In the multilevel car, the side sills and center sill are located at the same height. The three longitudinal underframe members are connected via a series of lateral cross members and floor stiffeners (Figure 1). The body bolster in both cars is similar, with two structurally significant cross members connected by a series of plates and reinforcement webs. The endframes both employ corner and collision posts

connected to one another by shear plates, with a lateral buffer beam at the bottom and an AT plate at the top.

The most significant difference between the single-level car and the multi-level car is the discontinuous floor level in the second car. While this car features a draft sill at each end of the car, these members are not in line with the center sill. In order to allow clearance for the trucks, the body bolster and draft sill are higher at the ends of the car than the center sill in the middle of the occupied volume of the car. A transition zone is provided between the high-floor at the end of the car and the low-floor in the middle of the car. Additionally, a second seating level is provided in the middle section, which consists of a series of cross members and another flooring surface throughout the middle section of the car.

### 4.1.1 Mesh

The multilevel railcar measures 83’-5” from buffer beam to buffer beam. The car has a width of 9’-6” along its entire length. The railcar height ranges from 9’-9” at either endframe to an overall height of 13’-4” within the center section of the occupied volume, measured from the top of the lower floor supports to the bottom of the upper roof supports. The geometry of the multilevel car does not appear beam-like, as the car has a non-prismatic cross section and a length-to-height ratio of 6.25. Front, side, and isometric views of the assembled, unmeshed railcar are shown in Figure 61.

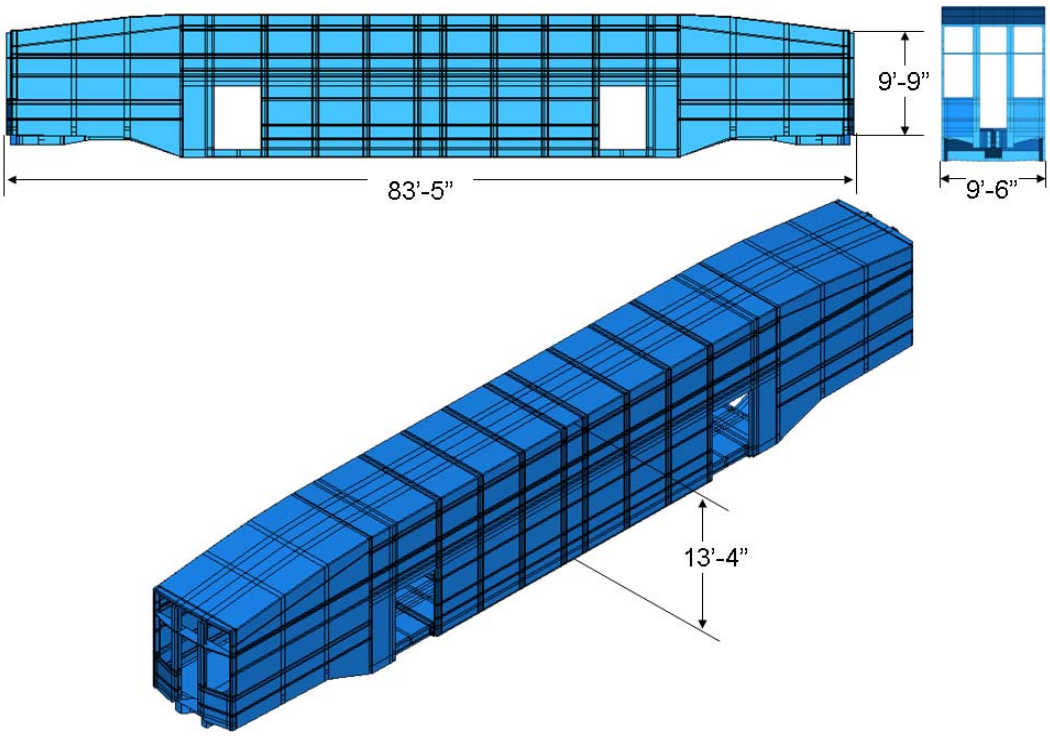


**Figure 61 - Multilevel Railcar Geometry**

The multilevel railcar's structural frame is generally similar to the frame that makes up the single-level car. The multilevel car features draft, center, and side sills making up the underframe, with the obvious difference between the two vehicles being the gooseneck transition on the multilevel vehicle. The superstructure of the multilevel car features a number of longitudinal members that are similar in shape to those in the single-level car. However, these longerans do not all span the entire length of the car. A number of members span the center region of the railcar but do not line up with the longitudinal members in the mezzanine regions.

A cross-section of the multilevel railcar, with the wall skin removed, is shown in Figure 62. The longitudinal members that are discussed further in this

thesis are indicated in this figure using the nomenclature used in this thesis. This figure shows the railcar from the centerline to the endframe for graphical clarity; the car is symmetric about this transverse centerline.

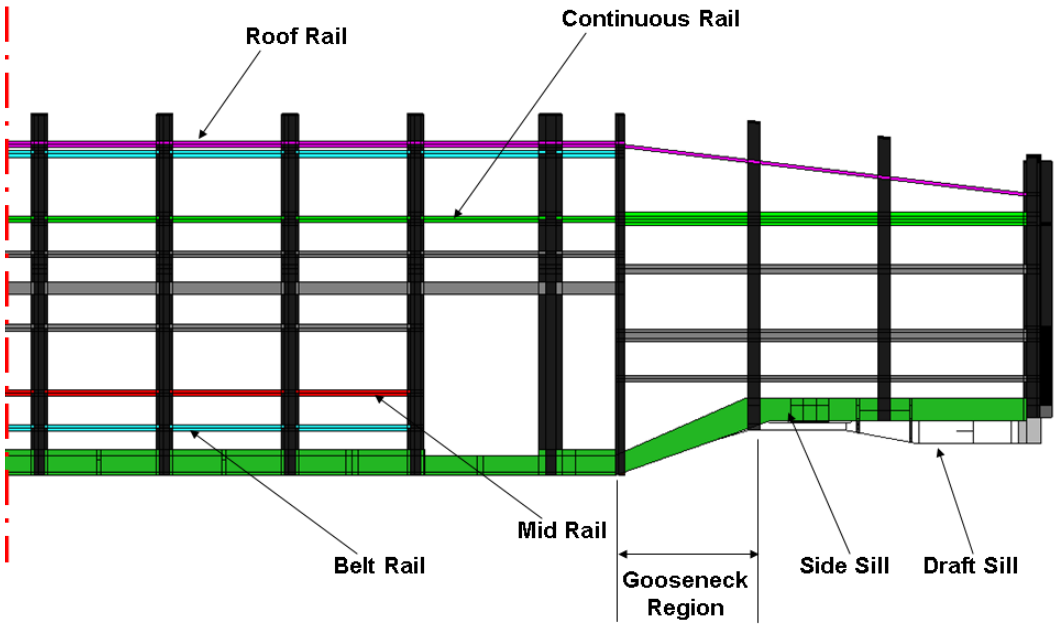


**Figure 62 - Profile of Multilevel Railcar Structure**

The railcar was meshed using S4 and S3R shell elements to model the frame structure as well as the floor, roof, and wall skins. The model also uses Spring1 elements to model the suspension. The spring elements all act in the vertical direction in this model.

A total of 72,716 elements are used in this model. Of these, 72,696 are S4, 16 are S3R, and 4 are Spring1 type. The 3-node shell elements are used in the gooseneck region, in both the wall skin and the side sill. The finite element model has a characteristic element length of 3.4 inches. The meshed railcar is shown in Figure 63. Runtime for a static compressive load applied to the railcar in a gravity field was approximately five minutes on a high-end desktop PC using

one processor.

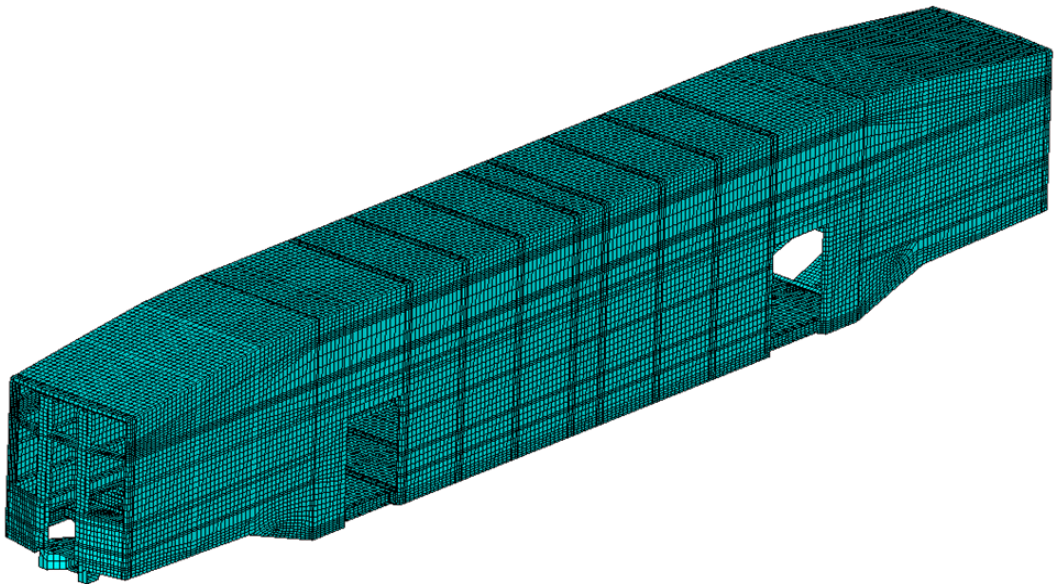

**Figure 63 - Mesh of Multilevel Railcar**

### 4.1.2 Weights

The weights of the assumed trucks and the entire car loaded to AW0 condition are provided in Table 6. The weights of the corresponding materials in an exemplar multilevel railcar are also provided. The AW0 loading case was implemented in the FE model by increasing the value of gravitational acceleration to 3.9 times its normal value, to 1495.5 in/sec$^2$. This was done to bring the weight of the car into line with the AW0 weight of an exemplar multilevel railcar.

**Table 6 - Multilevel Railcar Weights**

| | **FE Model Weight (lbf)** | **Actual Railcar Weight (lbf)** |
|---|---|---|
| Trucks (each) | 12,000 | 12,000 [33] |
| AW0 | 137,103 | 137,000 [33] |
| AW0, no trucks | 113,103 | 113,000 |

### 4.1.3 Material Used

The multilevel railcar utilizes both structural steel and aluminum as part of its construction. The majority of the superstructure, including the wall stiffeners, longitudinal rails, and wall and roof skin is made from aluminum alloy. The draft sills, body bolsters, center sill, and cross members of the underframe are steel. A list of the materials used for the members making up the multilevel railcar model is shown in Table 7.

**Table 7 - Material Properties, Multilevel Railcar Model**

| Member | Material Type | Young's Modulus psi [GPa] | Yield Stress ksi [MPa] |
|---|---|---|---|
| AT Plate | Steel | 3.00E+07 [207] | 50 [345] |
| Belt Rail | Aluminum | 1.04E+07 [72] | 40 [276] |
| Body Bolster | Steel | 3.00E+07 [207] | 50 [345] |
| Buffer Beam | Steel | 3.00E+07 [207] | 50 [345] |
| Center Sill | Steel | 3.00E+07 [207] | 50 [345] |
| Collision Post | Steel | 3.00E+07 [207] | 50 [345] |
| Corner Post | Aluminum | 1.04E+07 [72] | 30 [207] |
| Cross Bearer - Lower Level | Steel | 3.00E+07 [207] | 50 [345] |
| Cross Bearer - Upper Level | Aluminum | 1.04E+07 [72] | 40 [276] |
| Draft Sill | Steel | 3.00E+07 [207] | 50 [345] |
| Floor - Lower Level | Aluminum | 1.04E+07 [72] | 23 [156] |
| Floor Longerans - Upper Level | Steel | 3.00E+07 [207] | 44 [303] |
| Roof Panel | Aluminum | 1.04E+07 [72] | 23 [156] |
| Shear Panel | Aluminum | 1.04E+07 [72] | 30 [207] |
| Side Sill - Center | Aluminum | 1.04E+07 [72] | 38 [262] |
| Side Sill - Mezzanine | Steel | 3.00E+07 [207] | 50 [345] |
| Wall Skin | Aluminum | 1.04E+07 [72] | 29 [200] |
| Wall Stiffeners | Aluminum | 1.04E+07 [72] | 40 [276] |

## 4.2 Boundary Conditions

This railcar model has a similar set of boundary conditions applied to it as the conventional, single-level car. While the car is sitting at rest, motion in both the lateral and longitudinal directions is restricted at the location where the trucks would attach to the body bolsters. This location is indicated in Figure 64 in red. Also at this location, linear springs are used to represent the secondary suspension of the truck. The springs have one end attached to the underside of the body bolster, with the other end grounded. Each acts in the vertical direction with a spring constant of 2,886 lbf/in. The calculations used to obtain the spring constant used can be found in Appendix B – Calculation of Suspension Spring Stiffness.

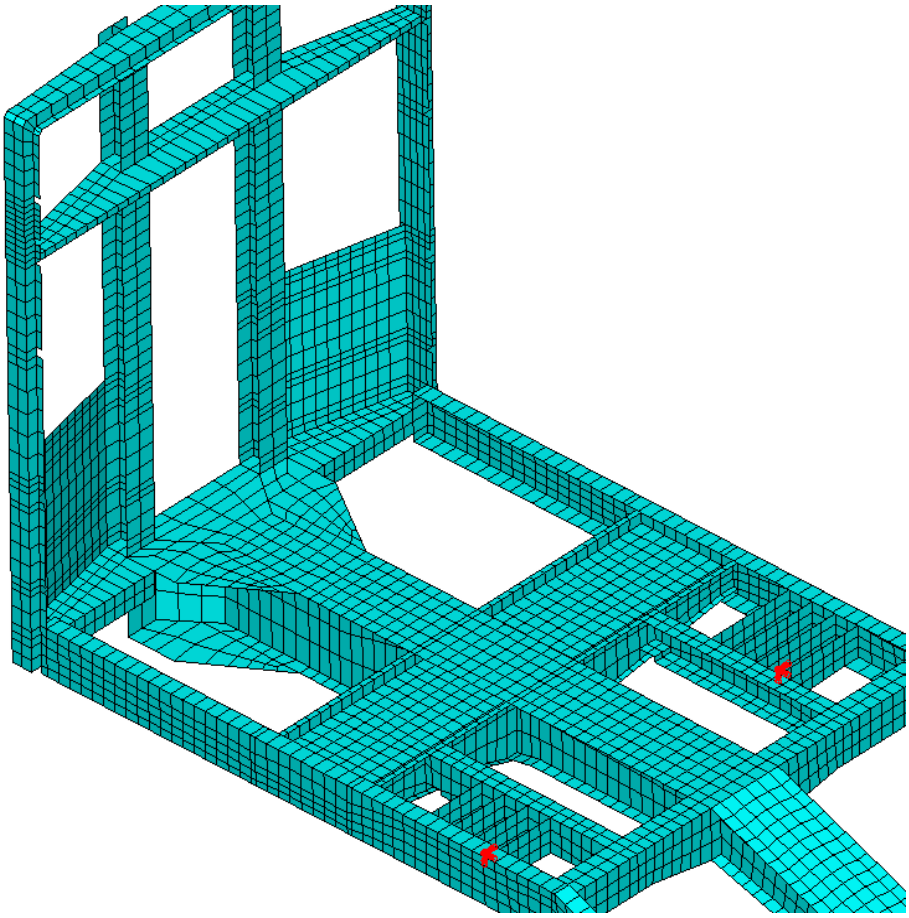

**Figure 64 - Boundary Condition Applied to Multilevel Body Bolster**

During each of the compressive load cases evaluated using this model, the boundary conditions are slightly modified. The longitudinal motion boundary condition that is applied at each body bolster is removed. Depending on the compressive load test being run, the longitudinal motion of the railcar will be restricted at a different location. These locations are the buff stops, the buffer beam, or the AT plate of the railcar. The appropriate boundary condition is applied based on the structure at the opposite end of the car that is being loaded compressively.

## 4.3 Standing Car Load

In all compressive load analyses performed on the multilevel car, the vehicle is first loaded to a simulated AW0 weight. To accomplish this, an artificially high gravitational acceleration of 1,495.5 in/s$^2$ is applied to the entire model. The carbody, subject only to this loading condition, is analyzed first for its behavior. The stress distribution for the center sill, side sills, belt rail, mid rail, continuous rail, and roof rail is plotted in Figure 65. This figure indicates a relatively low level of stress in each of these longitudinal members when the carbody is loaded under gravity. This figure also indicates a trend of tensile stress in the lower members of the underframe and superstructure and a compressive stress in the upper members.

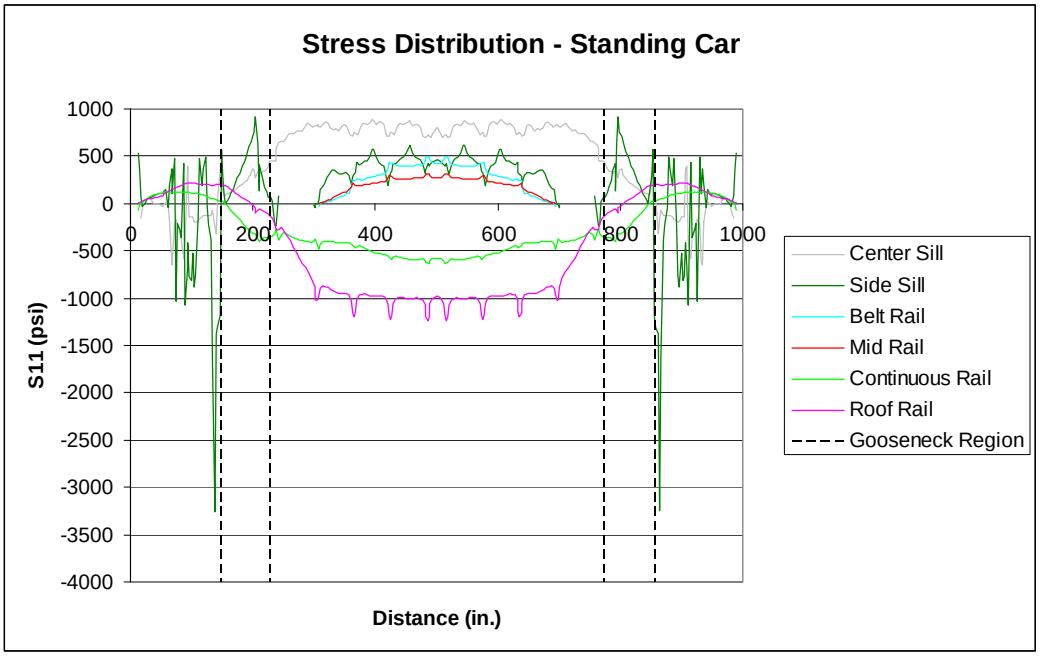


**Figure 65 - Stress Distribution for Multilevel Car, AW0 Load**

The average value of stress, calculated over the center section of the

carbody, is plotted in Figure 66 for each member examined. This plot indicates that the average stress value is tensile in the members of the underframe and the lower members of the superstructure and transitions to a compressive stress somewhere between the mid rail and the continuous rail. This state of stress is consistent with a simply-supported beam being uniformly loaded transversely, where the bottom fiber of the beam is under tension and the top fiber is in compression.

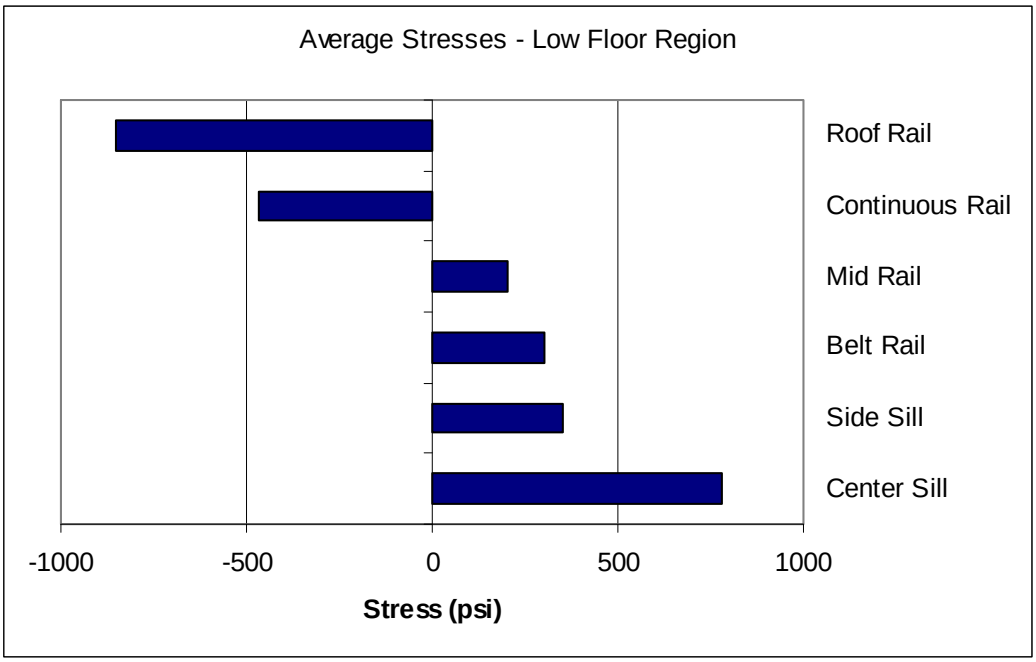


**Figure 66 - Average Stresses in Center Section of Multilevel Car, AW0 Load**

## 4.4 Baseline 800 kip Load

The 800 kip load is applied to the buff stops of the railcar in the same manner as for the conventional single-level car. The longitudinal distance along the length of the railcar is measured from the buffer beam at the fixed end of the car in the plots that follow.

Figure 67 plots the stress distribution in the lowest row of elements through the draft and center sills of the multilevel car during the 800 kip load application. The large spike seen at the right hand side of the graph corresponds to the location of the buff stops in the draft sill.

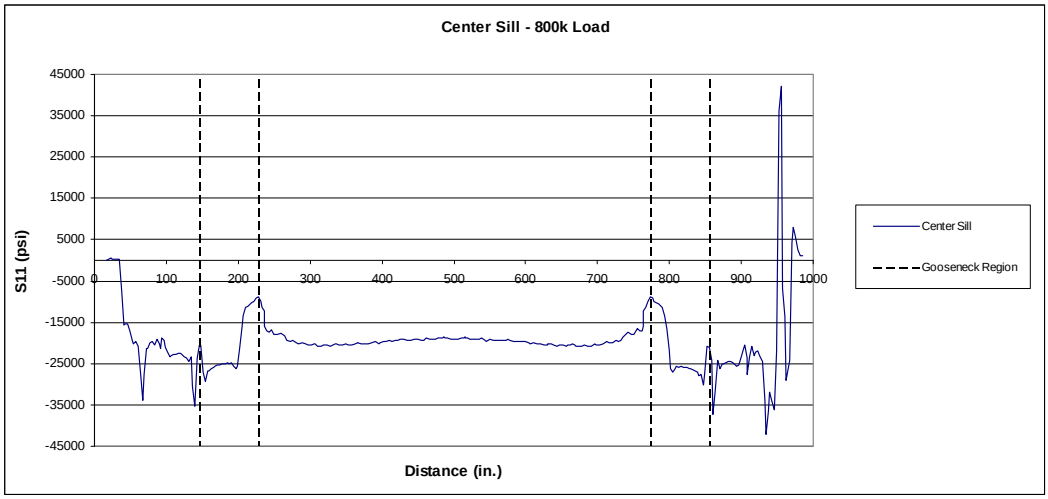


**Figure 67 - Stress Distribution in Center Sill of Multilevel Car, 800 kip Load**

Figure 68 shows the stress distribution in the side sill of the multilevel railcar. This plot begins at the fixed end's mezzanine level and follows the side sill through the transition zone and into the low-floor center section of the railcar before rising to the mezzanine level at the opposite end of the railcar. The stress in the side sill is typically compressive along the entire length of the car, with the

exceptions occurring in the mezzanine level, near the end of the member. The side sill experiences a break in continuity just inboard of both gooseneck regions, at the doorframes.

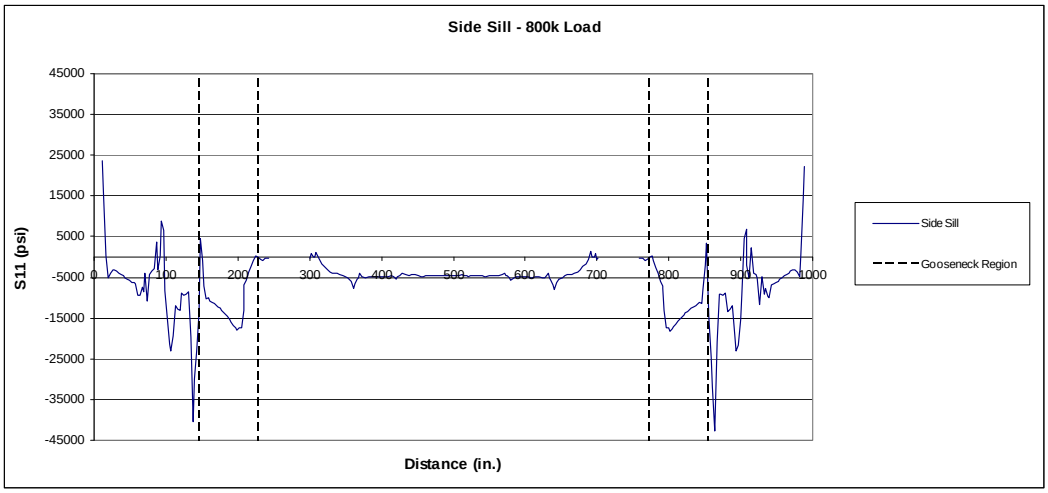


**Figure 68 - Stress Distribution in Side Sill of Multilevel Car, 800 kip Load**

Figure 69 shows the stress distribution in the center sill, side sill, belt rail, mid rail, continuous rail, and roof rail along the length of the railcar. This plot indicates the center sill's role in reacting the majority of the longitudinal load during the 800 kip compressive strength test. The stress levels in a given member are relatively constant along the length of the center section of the railcar.

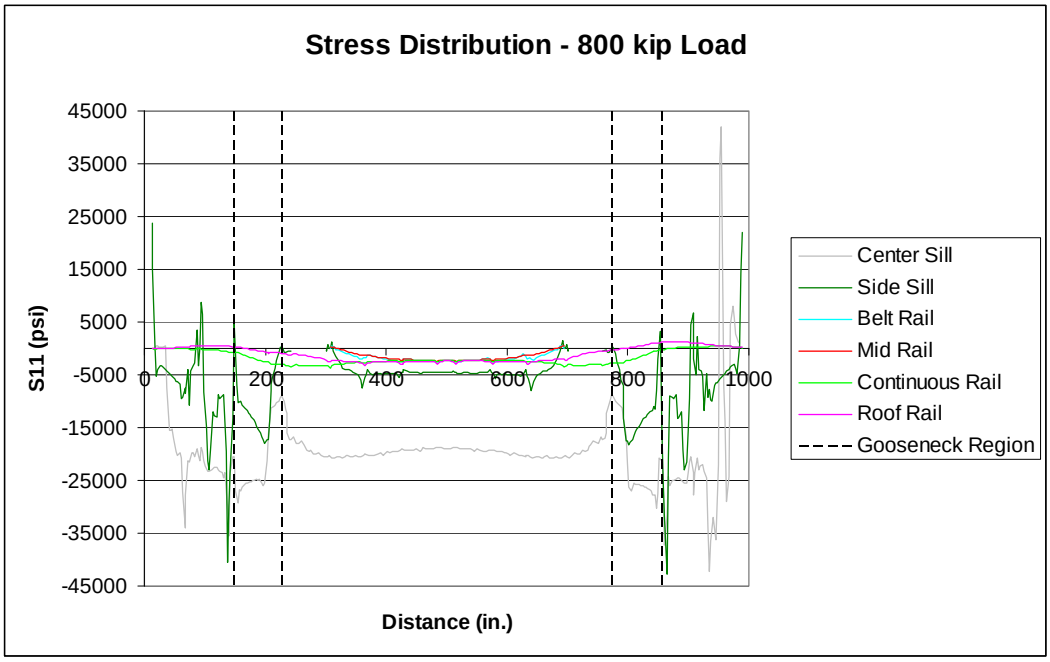


**Figure 69 - Stress Distribution in Multilevel Railcar, 800 kip Load**

Figure 70 shows the average stress value calculated for each of the longitudinal members presented above when loaded under the 800 kip load case. For the multilevel car, the average value for each member was calculated over the center, low-floor region of the railcar body. This figure indicates that the longitudinal members are under a state of compression throughout the height of the center section. The general trend indicates an increased magnitude of compressive stress as the member analyzed gets lower. Additionally, the center

sill experiences a much more severe stress state than the other members analyzed.

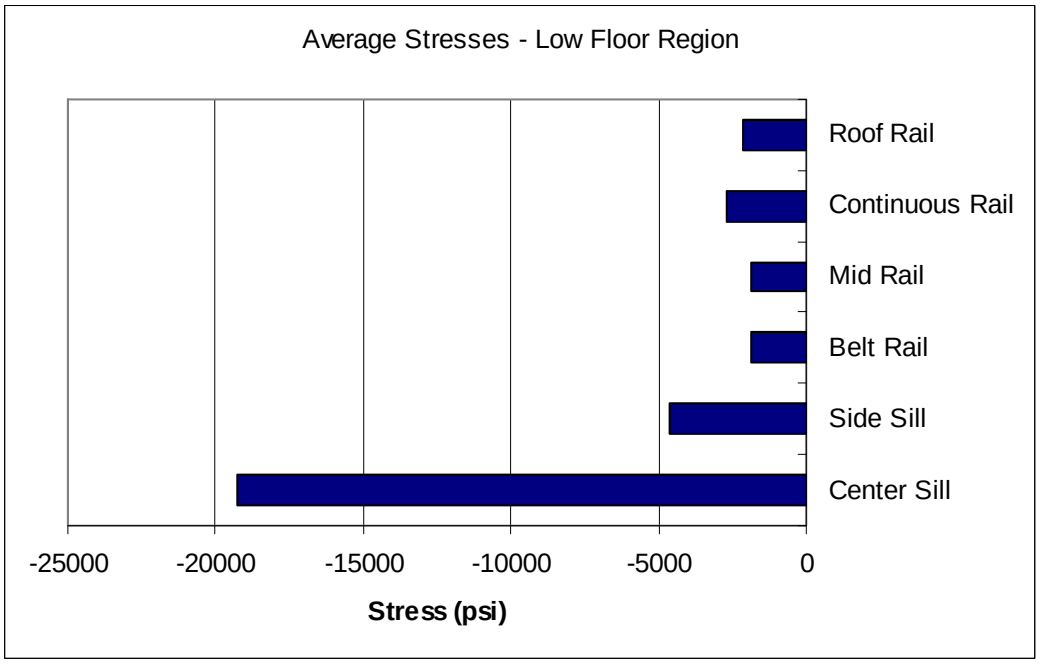


**Figure 70 - Average Stresses in Center Section of Multilevel Car, 800 kip Load**

## 4.5 Alternative Loads

The alternative loads applied to the multilevel car are similar to those applied to the single-level car. These loads consist of 1,000 kips applied across the buffer beam, 200 kips applied across the AT plate, and the two loads reacted at the same time. As in the single-level car model, the loads are being applied as pressures distributed across the outboard face of the members. Figure 71 shows the buffer beam and AT plate locations loaded on the multilevel railcar.

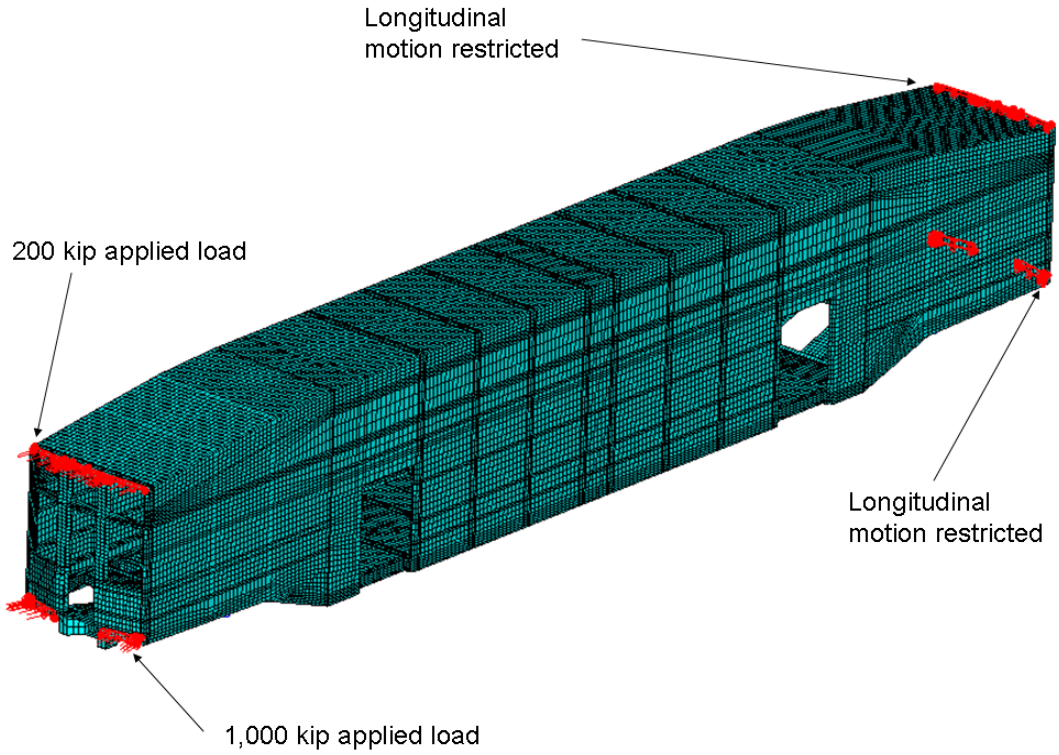


**Figure 71 - Alternative Load Setup for Multilevel Railcar**

The average stresses in the longitudinal members through the center section of the car are plotted in Figure 72 for both the 800 kip buff stop loading case and the 1,000 kip buffer beam loading case. As seen in this figure, the

overall behavior of the railcar is similar under both loading conditions. The carbody experiences a compressive stress state at each member. The 1,000 kip load also causes a larger magnitude stress to occur in each member than is experienced during the 800 kip load.

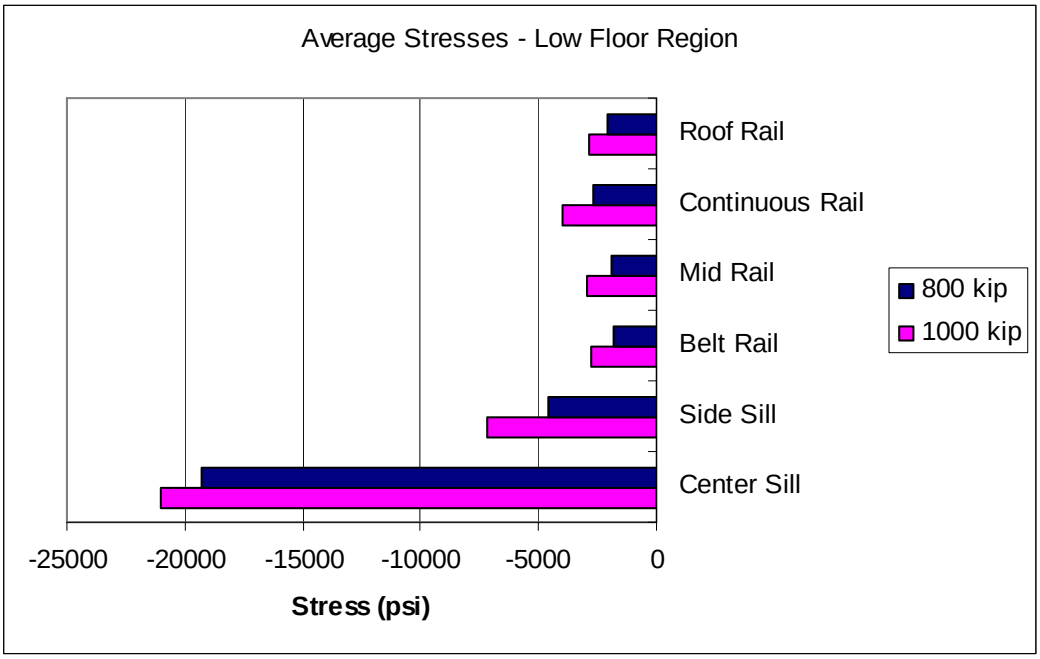


**Figure 72 - Average Stresses in Center Section of Multilevel Car, 800 and 1,000 kip Loads**

The longitudinal stress distribution along the entire length of the railcar is shown below, in Figure 73. This figure indicates a relatively constant stress level for each longitudinal member in the region inboard of both goosenecks. This figure also emphasizes the center sill's role as transmitting the significant longitudinal load from one end of the railcar to the opposite end.

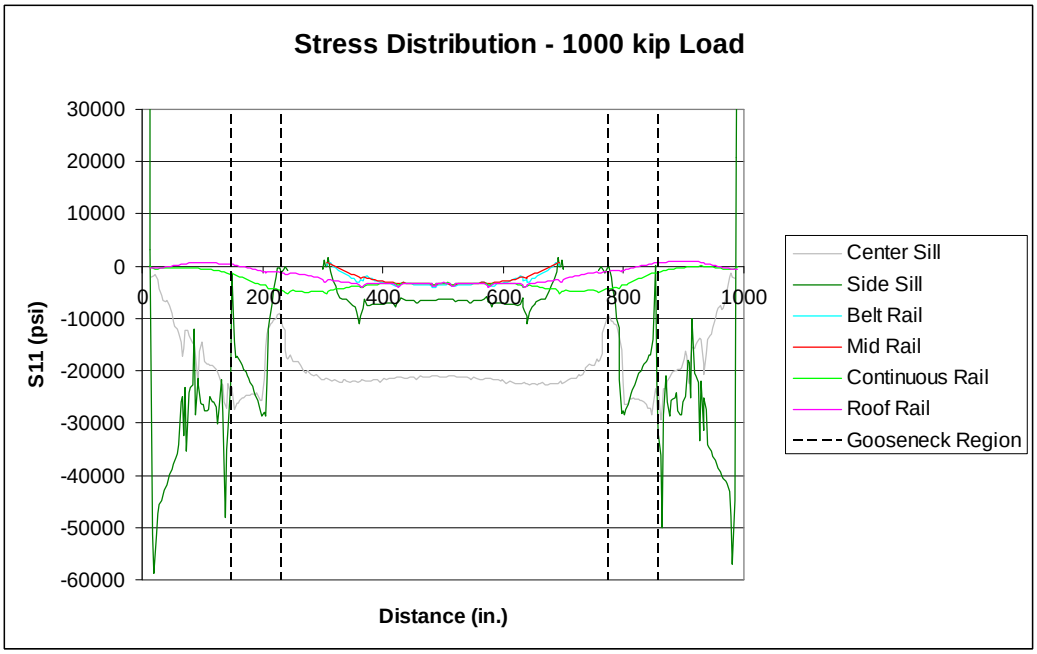


**Figure 73 - Stress Distributions in Multilevel Railcar, 1,000 kip Load**

The next compressive load case analyzed is 200 kips applied across the AT plate at the endframe. This load results in the average stress values seen below, in Figure 74. This figure plots the average stresses from the 200 kip load as well as the average stresses from the AW0 standing car load.

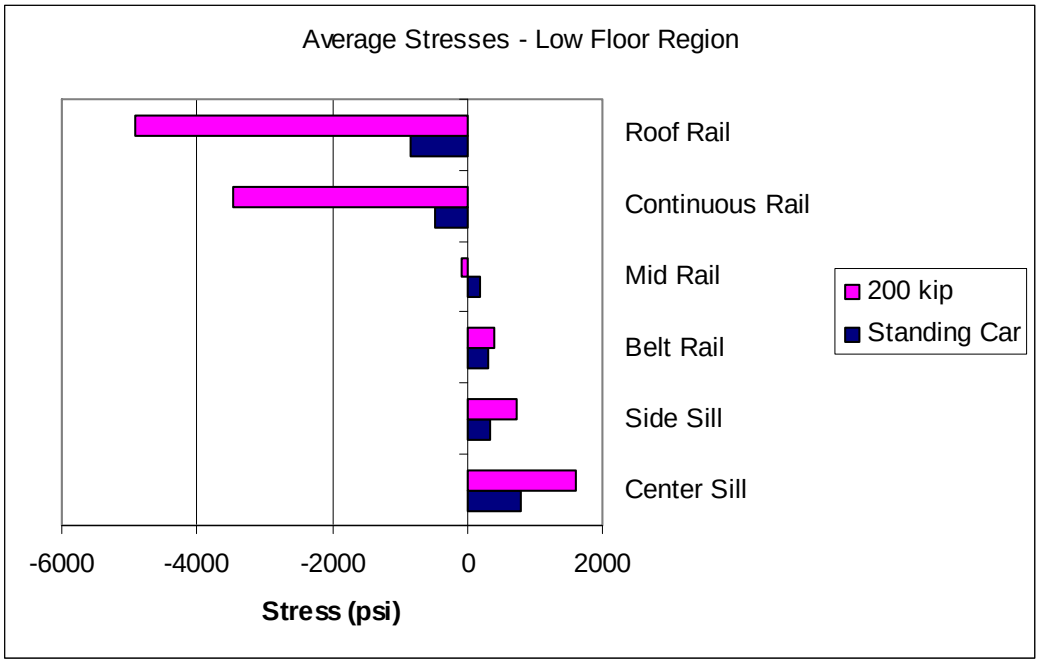


**Figure 74 - Average Stresses in Center Section of Multilevel Car, 200 kip and AW0 Loads**

The 200 kip load results in an increased magnitude compressive stress in the upper members of the superstructure and an increased tensile stress in the lower superstructure and underframe members. This indicates that the 200 kip load is causing a bending moment in the same direction as the bending generated by gravity. The increased compressive loads in the roof rail and continuous rail are likely caused by a combination of compression and bending that occurs in this region. The stress levels are still of relatively low magnitude in each of the members during this loading case. The distribution of stress along the entire

length of the railcar is shown in Figure 75.

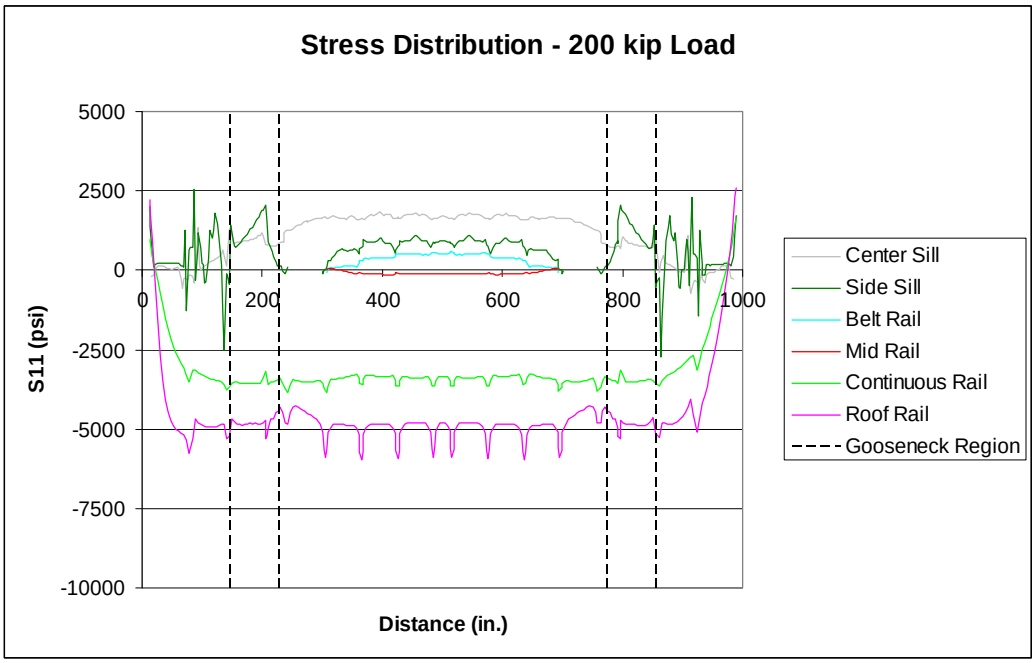


**Figure 75 - Stress Distributions in Multilevel Car, 200 kip Load**

When the 200 kip load and the 1,000 kip load are both applied at the same time, the carbody experiences average stress values as seen in Figure 76. In this case, the stresses are plotted alongside the average stresses obtained from the 800 kip load and the 1,000 kip load, for comparison.

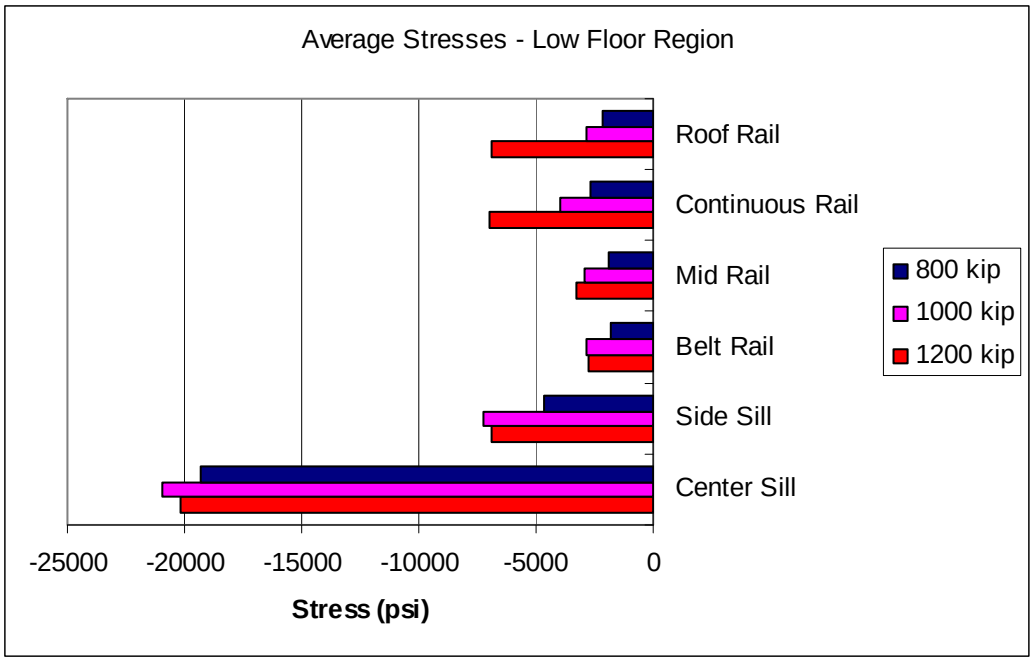


**Figure 76 - Average Stresses in Center Section of Multilevel Car, 800, 1,000, and 1,200 kip Loads**

At each longitudinal member examined, the 800 kip load results in the least severe average stress. Within the underframe members, the 1,000 kip load causes a slightly larger average stress level. In the superstructure members, the 1,200 kip load causes a larger magnitude average stress. While the total force being applied to the endframe is the largest in the 1,200 kip load case, if the 200 and 1,000 kip loads are being applied on opposite sides of the neutral axis some portion of the bending moments generated will cancel one another. This behavior is the likely cause of the decreased stress levels seen in the center and side sills during application of the 1,200 kip load when compared to the 1,000 kip load. Due to the presence of 200 kips applied at the AT plate, the roof and continuous rails experience greater stresses, as they play a more critical role in the load path

through the car. The stress distribution for each of the longitudinal members along the entire length of the railcar is shown below, in Figure 77.

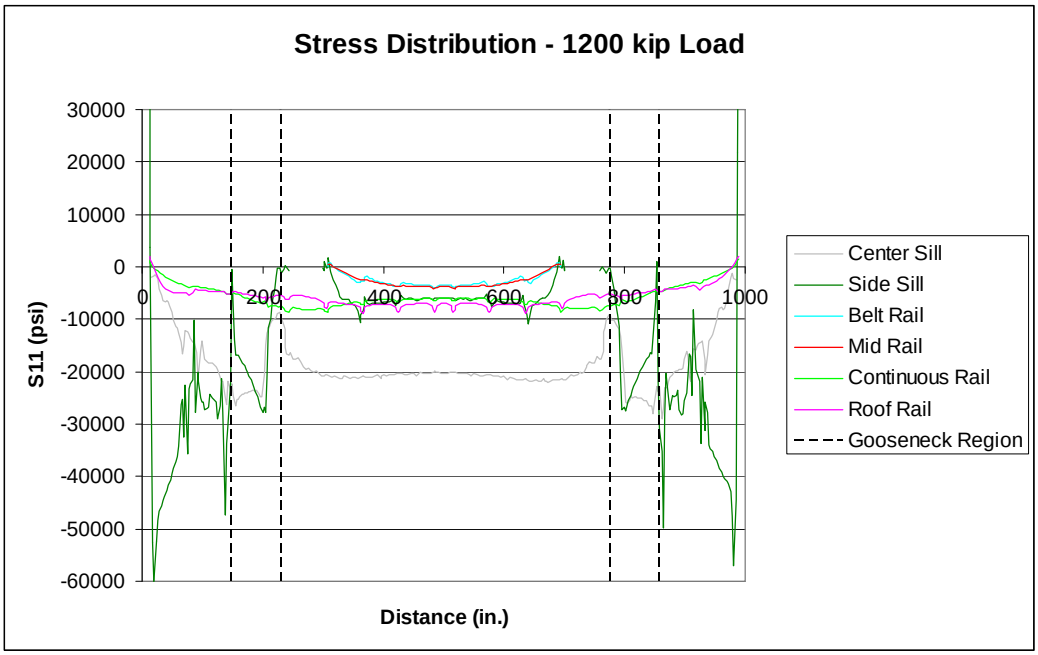


**Figure 77 - Stress Distributions in Multilevel Railcar, 1,200 kip Load**

# 5 Summary

Railroad passenger equipment operating in the United States is subject to both industry standards and federal regulations. These standards and regulations include a minimum compressive strength that all railcars must meet in order to enter passenger service in the U.S. The federal regulations and industry standards both prescribe an 800,000 pound load applied on the centerline of draft that the railcar must resist without permanent deformation. For railcars with a conventional underframe and coupler arrangement, the load is applied to the buff stops at the rear of the draft gear.

The historical development of the specifications and regulations governing compressive strength testing in North American equipment has been reviewed. The standard of applying 800 kips of compressive force along the centerline of draft has evolved over the course of the 20$^{th}$ century, and can trace its roots back to a Railway Mail Specification from 1912. This recommendation has since gone on to be incorporated into the CFR as a legal requirement for all passenger-carrying railcars to be able to resist 800 kips applied on the line of draft in order to be operated on the general railroad system in the United States.

A difficulty arises when a piece of equipment with a non-conventional structure is undergoing qualification tests. If the vehicle does not have an easily defined line of draft or a set of conventional buff stops, the 800 kip strength test cannot be readily applied. An alternative loading condition, designed to be applicable to a wider variety of equipment types, is desirable if alternative railcar

designs are to be evaluated for their compressive strength. This alternative load should not be dependant upon a specific railcar structure, but should ensure an equivalent level of occupant volume protection as the current 800 kip load.

A series of finite element models have been constructed to evaluate the 800,000 pound compressive strength test. The finite element models have used simplified geometry and simplified member-to-member attachments to allow rapid runtimes. The models include a beam and shell model of a single-level railcar, a shell model of a single-level railcar, and a shell model of a multilevel railcar.

The beam and shell model was a first attempt at modeling the beam-like behavior of a passenger railcar of conventional construction. Once it had been determined that simplified modeling efforts would allow the salient beam-like behavior of the railcar to be established, modeling efforts were focused on generating models composed of shell elements. Two models resulted from this effort: a generic single-level railcar and an exemplar multilevel railcar model. All of the models featured less than 80,000 elements in an effort to further limit the runtime of the models on a desktop computer.

The beam and shell model was used as a preliminary estimate of the railcar's behavior. This model was used to determine the neutral axis location of the railcar. The neutral axis was found to be approximately 24.4" above the floor in the single-level conventional railcar using the beam and shell model, and 26.6" above the finished floor in the shell model of the conventional railcar.

The shell models were used to evaluate specific load cases: ready-to-run

standing car, 800 kips applied at the buff stops, 1,000 kips across the buffer beam, 200 kips across the AT plate, and a combined force of 1.2 million pounds shared between the buffer beam and AT plate. The symmetry of the railcar was verified early in the results stage, which allowed the stress distribution in one member in a left/right pair to be reported. This verification was performed for both the single and multilevel models.

For each load case run using the shell models, the stress distribution in different longitudinal members was plotted. Theses members included the center sill, the side sill, and different longerans throughout the height of the superstructure of both railcar models. The average value of stress in the occupant volume of the car was determined for each stress distribution.

# 6 Conclusions

Using simplified geometry and material behavior, FE models of a generic single-level passenger car and an exemplar multilevel car were created. Both models sufficiently captured the general behavior of the railcars during a series of simulated compressive strength tests. The single-level model captured the behavior of the railcar as a single beam, with an easily-defined neutral axis. The multilevel model behaved similarly, although its beam-like properties were less readily apparent, owing to the dramatic change in cross-section geometry on either side of the gooseneck region.

A series of compressive loads are applied to each carbody, with each load magnitude applied to a different component of the railcar structure. The 800 kip load, applied at the buff stops, is the baseline loading case. The application of this load causes a compressive load as well as a bending load in the railcar. Because the neutral axis of the railcar is located well above the underframe of the single-level railcar, the bending moment is a positive one. The compressive load below the neutral axis causes the car to both compress and bend. This bending causes a compressive stress in the underframe members and a tensile stress in the upper members of the superstructure, in addition to the compressive stresses from the longitudinal load.

A 1,000 kip load, applied across the buffer beam of the railcar, results in a similar loading condition to the 800 kip load. The magnitude of the compressive load is larger, but the loading location is closer to the neutral axis of the railcar.

Additionally, the load is now distributed across the width of the endframe, as opposed to concentrated within the draft sill. The overall results are similar to those seen in the 800 kip loading; the carbody undergoes compressive and bending loads, with comparable stress levels in a number of longerans investigated.

A 200 kip load, applied across the AT plate of the railcar results in a bending moment in the opposite direction of that from the 800 or 1,000 kip loads. The railcar is still undergoing both compression and bending, but under this load the upper members are placed into a state of compression and the underframe members are loaded in tension.

When a combination of 1,000 kips across the buffer beam and 200 kips at the AT plate are placed on the single-level railcar, the car is again loaded under both compression and bending. In this case, a portion of the moment from the 1,000 kips below the neutral axis is cancelled by the 200 kips located above the neutral axis. The overall effect of these two loads is to place the longitudinal members of the railcar into compression throughout the occupied volume. The magnitudes of compressive stress in the center sill and side sills are between the magnitudes found for the same members during the 800 and 1,000 kip loads. In the superstructure, the 1,200 kip loading case results in a more severe state of compressive stress in all members than experienced under either the 800 or 1,000 kip loads.

A similar series of compressive loads is then applied to a multilevel railcar model. In the multilevel railcar, the application of the 800 kip load at the buff

stops causes an average compressive stress in each of the longitudinal members examined throughout the center section of the car. This stress is the greatest in the center sill, and decreases in magnitude as the member examined gets higher up in the carbody.

When 1,000 kips are distributed across the buffer beam, the carbody behaves in a similar manner to the 800 kip load case. The stress magnitudes are greater in each member for the 1,000 kip load than for the 800 kip load. The average stress is also compressive in all members examined during the 1,000 kip load.

When the 200 kip load is applied at the AT plate of the car, the carbody deforms in a different manner than in either the 800 kip or 1,000 kip cases. The railcar experiences a state of compression at the top members in the superstructure and gradually transitions to a state of tension in the members of the underframe. This behavior is similar to the measured average stress behavior for the car standing at AW0 weight, with the 200 kip load causing a more severe stress state in nearly all the members examined.

The final loading condition examined on the multilevel car is a combination of 200 kips applied across the AT plate and 1,000 kips applied across the buffer beam. This loading also results in average stresses that are compressive in each member examined. The 1,200 kip load causes a larger magnitude average stress in the roof, continuous, and mid rails, an approximately equal stress in the belt rail, and a less severe stress in the center sill and side sill when compared to the 1,000 kip load. This decrease in stress in the lower members, despite a larger

compressive load, is likely a result of the two loads being located on opposite sides of the neutral axis. This effectively negates a portion of the bending moment that is being transmitted through the railcar.

The simulations run using the simplified shell models of the railcars demonstrate that the current 800 kip compressive strength test places the railcar into a compressive state as well as induces a bending moment in the body of the car. This modeling has also shown that it is possible to induce similar stress states through the use of distributed loads across alternative locations on the car, specifically the buffer beam and the AT plate.

The 1,200 pounds loaded across the endframe causes compressive average stresses within the longitudinal members that make up the single-level and multilevel car. In both cars the 1,200 kip load, despite being 50% larger than the 800 kip load, causes a similar level of compressive stress in the center sills. The center sill also experiences the largest stress level of all the longitudinal members for both cars. In all other members examined, the 1,200 kip load results in a larger compressive stress than the 800 kip load. While the single-level car experiences larger magnitude average stresses than the multilevel car, the stress levels in both cars are below yield stresses. The average stresses for both cars, under the 800 kip and 1,200 kip loads, are shown in Figure 78.

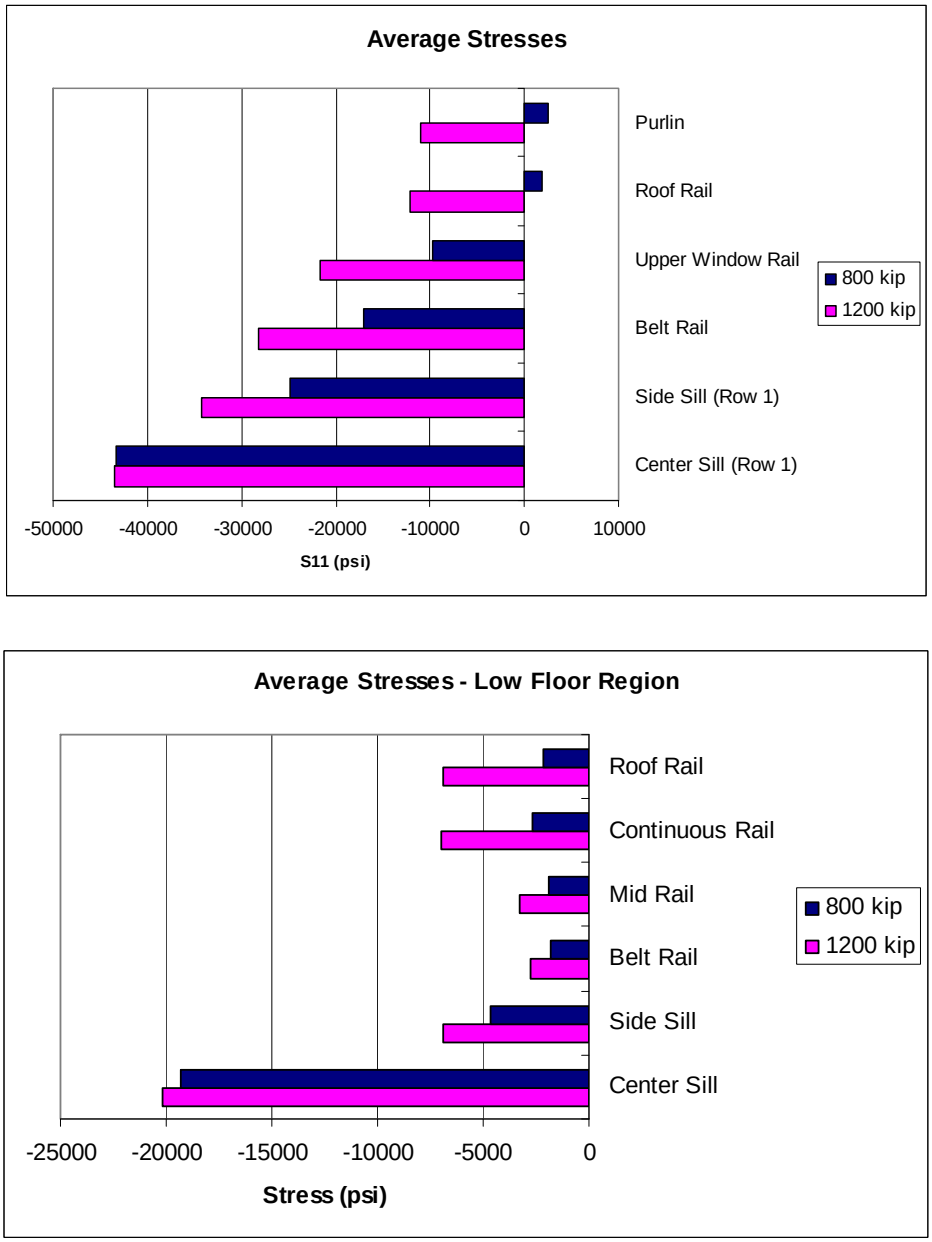


**Figure 78 - Average Stresses in Single-level (top) and Multilevel (bottom) Cars**

The alternative loading cases described in this work demonstrate that it is possible to load the carbody of a passenger railcar to a level greater than the 800 kips currently required if the load location is chosen appropriately. The loads chosen resulted in stress distributions that were similar to the results from the 800

kip loading case.

Evaluating the carbody's structural strength using the alternative loads offers a number of advantages over the existing proof load testing. While the buff stops are located near the end of the railcar, it is possible to design a vehicle with occupant space located outboard of them. Since the alternative loads are applied at the endframe of the vehicle, the entire occupied volume is being evaluated.

Additionally, because the alternative loads are applied over a larger area of the car than the existing 800 kip load, it is possible to design equipment that shifts away from the conventional practice of utilizing the center sill to carry the majority of the longitudinal load. Equipment designed to react service or collision loads through structures other than the conventional coupler may be evaluated for their occupant protection, assuring the same level afforded by equipment qualified under the existing tests.

As with any step away from conventional practice, there are some potential difficulties associated with the alternative tests. The current 800 kip test evaluates the bending and compressive strength of the car in one test. The proposed alternative would evaluate these two aspects separately, requiring two testing setups. Since the proposed alternative allows the load to be distributed over a greater area of the railcar, it is likely that multiple devices would be required to generate such loads. Since there is no facility that currently performs the proposed alternative, there is likely to be some cost associated with developing a test rig capable of performing the test.

Further work can be done on examining the detailed load path through the

car. While areas of localized high stress concentration are indicated by the finite element models used in this work, it is important to investigate further whether these concentrations are due to the coarse mesh and simplified member-to-member connections used in this research, or if these concentrations are likely to be locations of yield in an actual carbody.

Additional work can also be performed in developing a finite-element model of a non-conventionally coupled piece of equipment. With the guideline values for load magnitude and loading scenarios that have been developed in this thesis, the potential alternative loads can be applied to a non-conventional piece of equipment. This work will likely result in the adjustment of the load magnitudes, locations, or boundary conditions required to prevent gross motions of the railcar.

## Appendix A – Tied Constraints versus Single Parts

Early in the development of the beam and shell FE model it was decided that constructing and meshing separate parts that were then tied to one another to form an assembly would be a desirable methodology. This would allow the parameters of individual parts, such as the floor or cross bearer, to be varied without requiring a redesign and remeshing of the entire model. Additionally, individual parts could be suppressed from the assembly and would only require the suppression of the corresponding constraints to run the model.

As a verification of using tied constraints to simulate the connection between parts, a test case was run. In this case, five similar beams were constructed using shell elements: one made up of a single part, and four using tied constraints. A cantilever boundary condition was applied on one end of each beam, such that it had zero degrees of freedom at that end. A uniform pressure load was applied transversely along the full length of the beams, causing a downward bending.

ABAQUS/CAE allows the definition of tied regions in two ways: tying node-to-surface and tying node-to-node on the mating parts. Each case was investigated. Additionally, each constraint definition was investigated for two purposes: either holding two half-length beams together at the longitudinal midplane, or attaching the flanges to the webs of the full-length beams. The four test cases, along with the single part, are shown in Figure A1. The regions of applied constraint are highlighted in red.

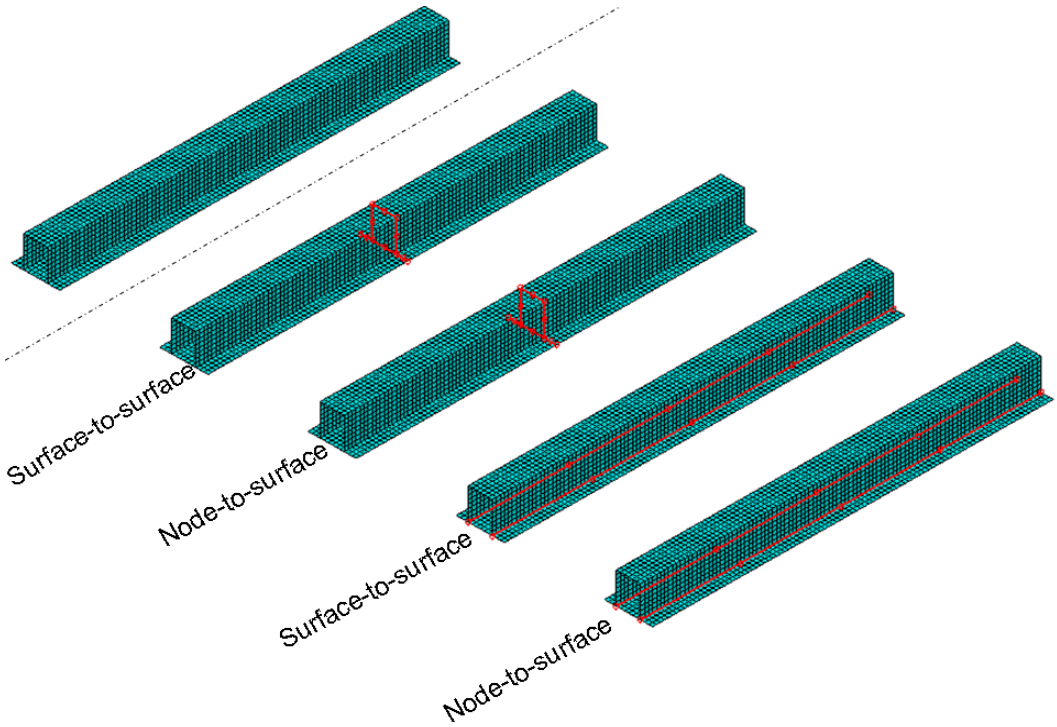


**Figure A1 – Tied Constraint Test Cases**

In all the beams, the mesh was the same. In the cases of the tied constraints, this meant that the nodes on the master part had corresponding nodes on the slave part in the same location. The tied constraints tied the motion in all three translational directions as well as all three rotational directions, forming a perfect bond between the discrete parts.

In order to assure identical behavior between the different models, stress results as well as displacement results were analyzed for all of the beams. A plot of the five beams in a deformed condition is shown in Figure A2. The contour variable is the longitudinal stress, S11. Visually, this plot indicates good correlation among the five beams, with similar stress distribution in each.

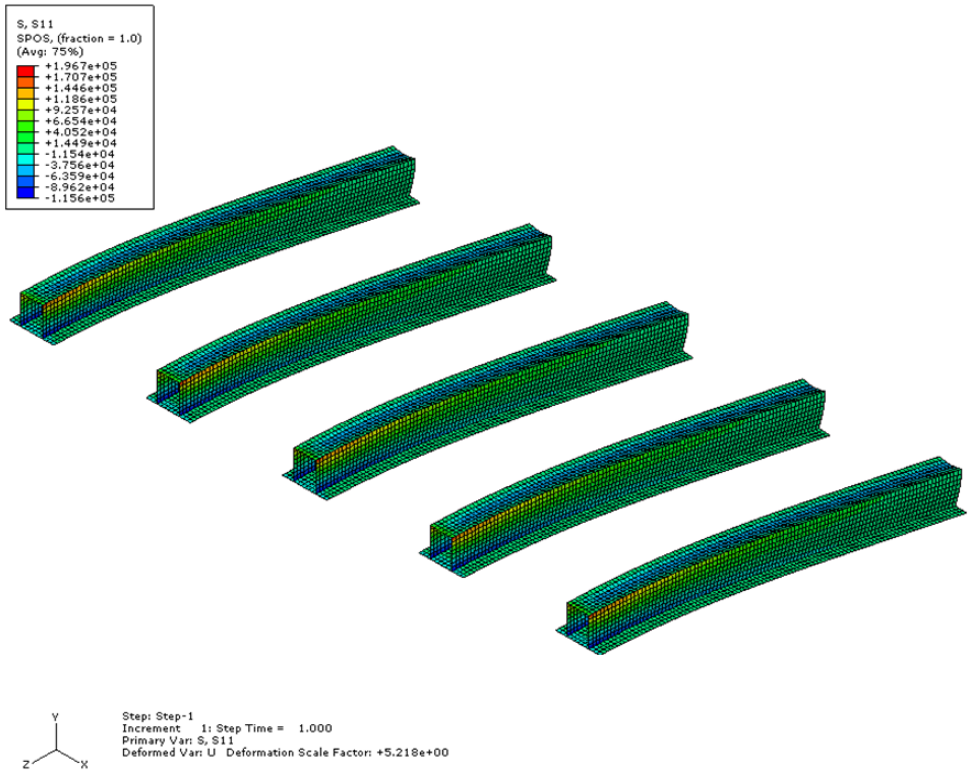


**Figure A2 - Stress Contour Plot for Constrained Beams**

The longitudinal stress along the bottom of the web is plotted for each of the beams in Figure A3. This plot indicates that the tied constraints provide a similar stress result to the single beam. Additionally, the beams behave the same way regardless of whether the surface-to-surface or surface-to-node constraint method is employed.

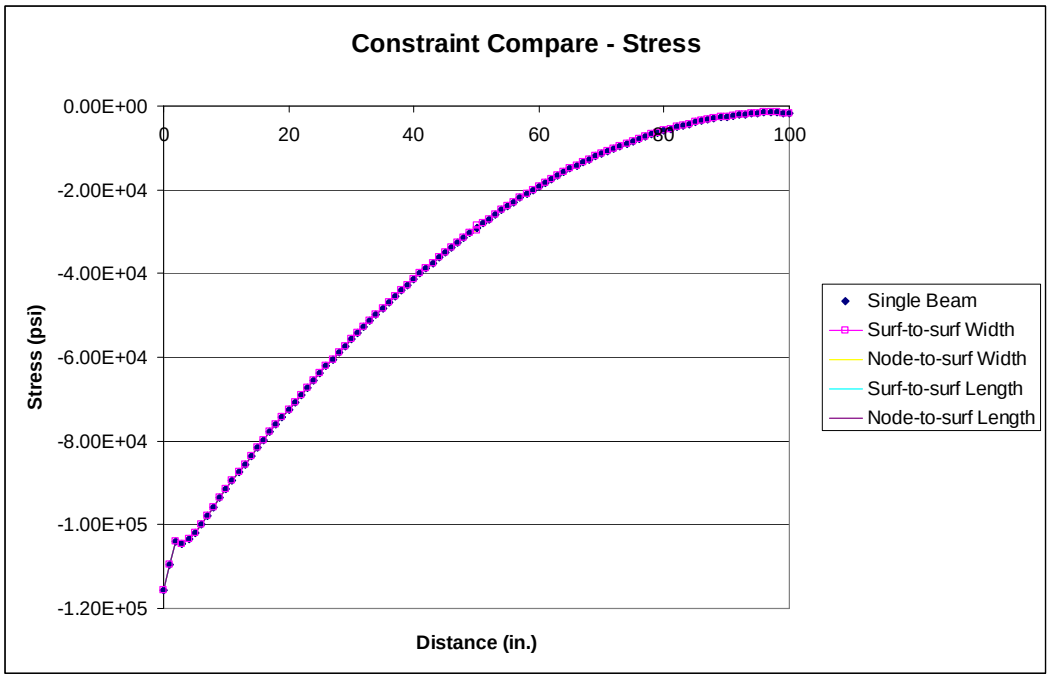


**Figure A3 - Stress Distribution for Test Beams**

Figure A4 plots the vertical displacement of the beams along their length. This plot also exhibits excellent agreement between the single part beam and each of the constrained beams.

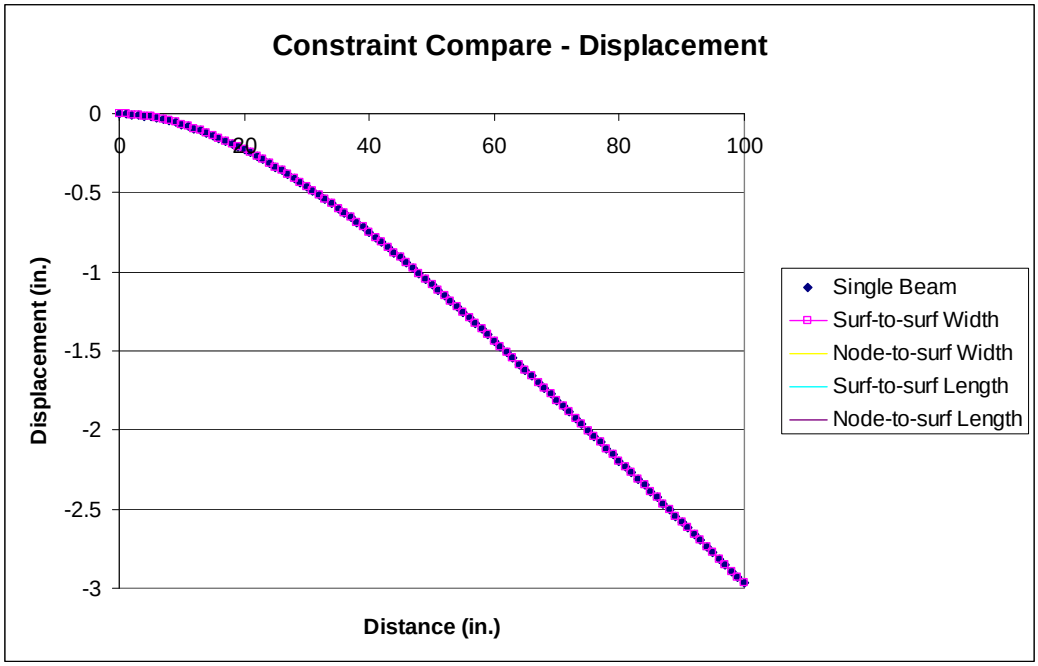


**Figure A4 – Vertical Displacement for Test Beams**

Through these test cases, it has been shown that beams assembled via the tied constraint method behave as if they were actually single parts. Care has been taken to ensure that in all cases demonstrated here, the meshes on the mating parts are such that the nodes on each part align with the nodes on the mating part. This same care has been taken during the meshing of the parts that make up the single and multilevel railcar models utilized elsewhere in this thesis.

## Appendix B – Calculation of Suspension Spring Stiffness

Suspension Stiffness - Single-level Car

Bounce Frequency

$F_b := 1.19\ Hz$ Bounce frequency measured in [29]

$F_{rad} := F_b \cdot 2 \cdot \pi$ $F_{rad} = 7.477\ \frac{radians}{second}$

Carbody Weight

$Weight_{T1} := 75000\ lbf$ Weight of car used in Full-scale Test 1 [23]

$Weight_{Tk} := 13700\ lbf$ Weight of truck used in Full-scale Test 1 [5]

$Weight_{carbody} := Weight_{T1} - 2 \cdot Weight_{Tk}$

$Weight_{carbody} = 4.76 \times 10^4\ lbf$ Weight of carbody used in Full-scale Test 1

$g := 386.4\ \frac{in}{s^2}$

$M_{carbody} := \frac{Weight_{carbody}}{g}$ $M_{carbody} = 123.188\ \frac{lbf \cdot s^2}{in}$

Spring Stiffness

$K_{eq} := M_{carbody} \cdot F_{rad}^2$ $K_{eq} = 6.887 \times 10^3\ \frac{lbf}{in}$ Equivalent spring stiffness for secondary suspension system

$n_{springs} := 16$ 16 springs used in finite element model

$K_{single} := \frac{K_{eq}}{n_{springs}}$

$K_{single} = 430.431\ \frac{\frac{lbf}{in}}{spring}$

Suspension Stiffness – Multilevel Car

Bounce Frequency

$F_b := 1.0 \quad Hz$ Frequency used in [33]

$F_{rad} := F_b \cdot 2 \cdot \pi \quad F_{rad} = 6.283 \ \frac{radians}{second}$

Carbody Weight

$Weight_{T1} := 137000 lbf$ Weight from [33]

$Weight_{Tk} := 12000 \ lbf$

$Weight_{carbody} := Weight_{T1} - 2 \cdot Weight_{Tk}$

$Weight_{carbody} = 1.13 \times 10^5 \ lbf$

$g := 386.4 \ \frac{in}{s^2}$

$M_{carbody} := \frac{Weight_{carbody}}{g} \qquad M_{carbody} = 292.443 \ \frac{lbf \cdot s^2}{in}$

Spring Stiffness

$K_{eq} := M_{carbody} \cdot F_{rad}^2 \qquad K_{eq} = 1.155 \times 10^4 \ \frac{bf}{in}$ [Equivalent spring stiffness for secondary suspension system]

$n_{springs} := 4$ [4 springs used in finite element model]

$K_{single} := \frac{K_{eq}}{n_{springs}}$

$K_{single} = 2.886 \times 10^3 \ \frac{\frac{lbf}{in}}{spring}$

## Appendix C – Symmetry of Results

The FE models of the single- and multilevel railcars were constructed to be symmetric about the longitudinal-vertical plane. For the results presented below, the loads and boundary conditions were applied in such a way that this symmetry was maintained. It is anticipated that future applications of the model may include asymmetric loading or boundary conditions, necessitating the construction of the model as a full car.

Due to this symmetry, the stress states in members on opposite sides of the car will be similar. This allows the stress values to be reported in only one member of a pair of members, such as the side sills, belt rails, or roof rails. Results from the single-level railcar body standing on its suspension in a normal gravity field (386.4 in/s$^2$) are presented in Figure A5, Figure A6, and Figure A7, for both center sill webs, both side sills, and both roof rails, respectively. In each case, the longitudinal stress is recorded at the lowest row of elements in the vertical web of the member.

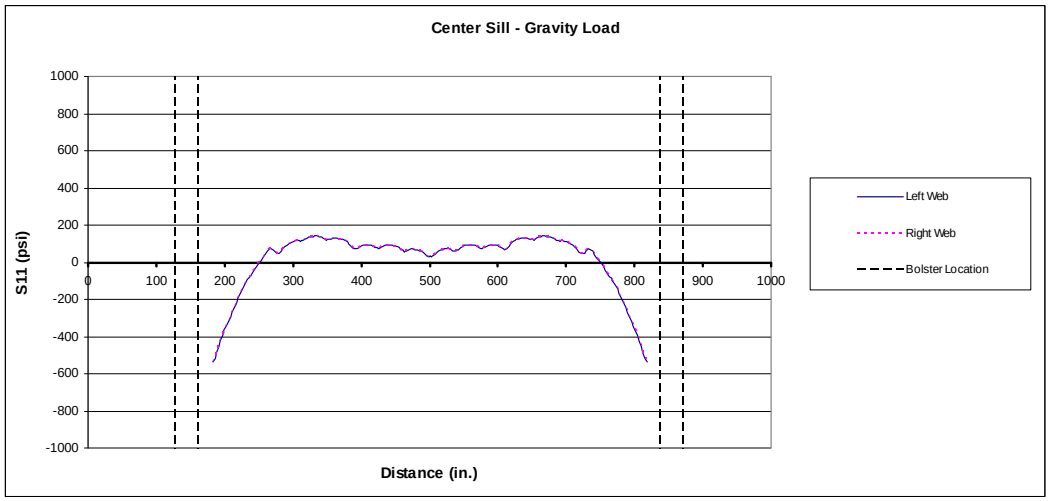


**Figure A5 - Longitudinal Stress in Left and Right Center Sill Webs, Standing Single-level Car**

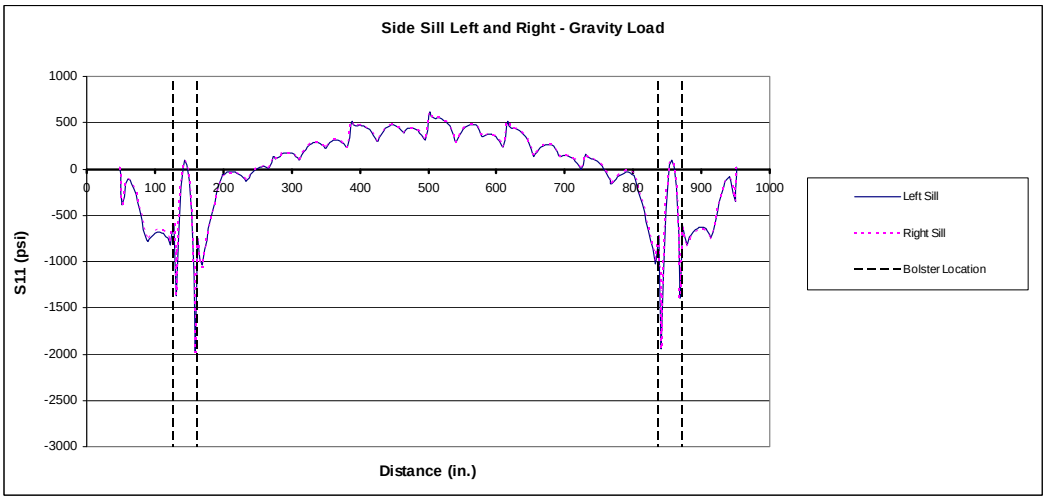


**Figure A6 – Longitudinal Stress in Left and Right Side Sills, Standing Single-level Car**

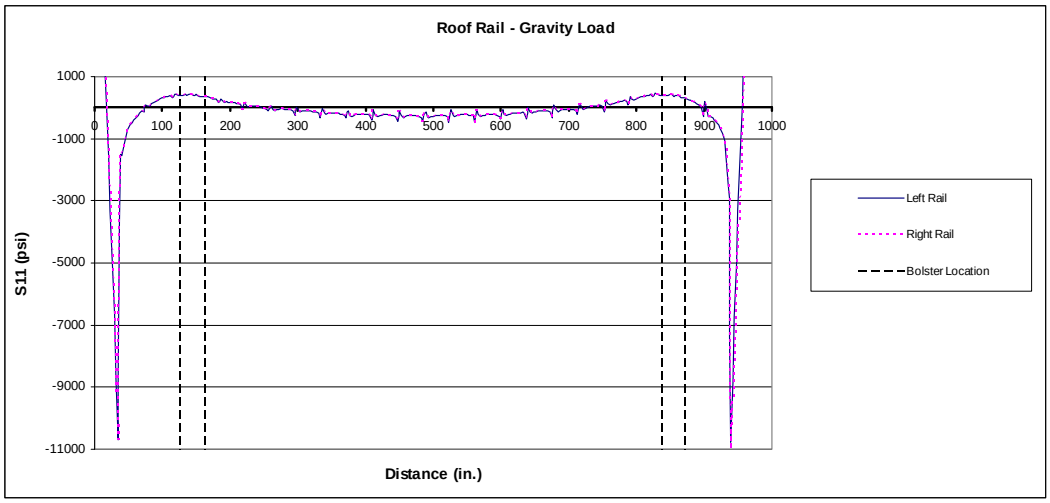


**Figure A7 – Longitudinal Stress in Left and Right Roof Rails, Standing Single-level Car**

As seen in these figures, the stress levels are equivalent for both left and right side members, verifying the symmetry of the model. Additionally, the structural frame of the railcar contains low stress levels under normal gravity loading. The periodic peaks in the stress level, most notable in the roof rail stress plot (Figure A7), correspond to the locations of the cross-members making up the skeleton of the car.

Under different loading conditions, the mesh of the single-level railcar remains the same and the area of load application varies. By extension, for any other loading condition symmetric about the longitudinal-vertical plane, the resulting stress distribution in corresponding left-right members will be the same. This allows the stress results reported in one member of a pair of members to represent the stress conditions in the member on the opposite side of the car.

The same series of investigations was run for the multilevel railcar model. The stress distribution was recorded along the length of the center sill, side sills,

and roof rails. For the center sill, the stress in the left and right web was compared. In the side sills and roof rails, the stresses in the left and right members were compared to one another. The stresses in the center sill, side sills, and roof rail are shown, respectively, in Figure A8**,** Figure A9**,** and Figure A10.

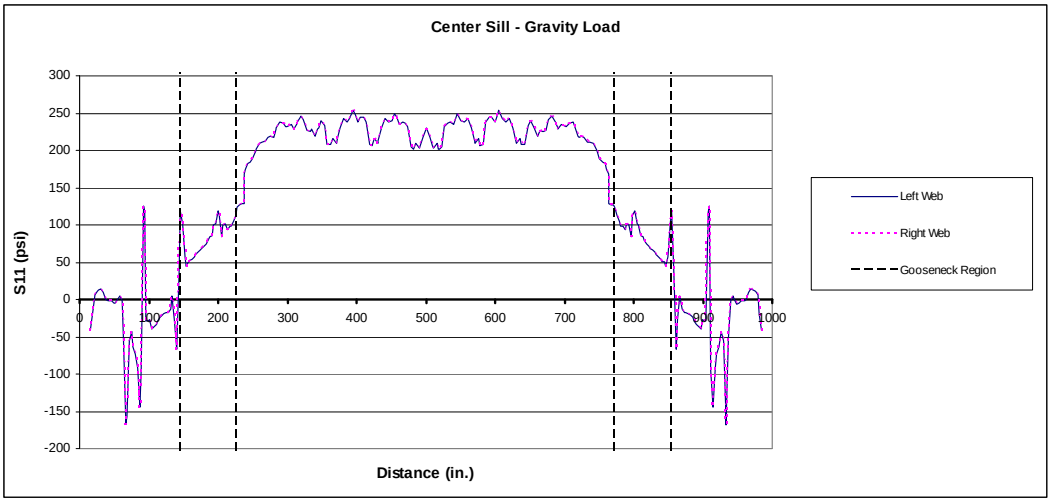


**Figure A8 - Stress Distribution in Left and Right Center Sill Webs, Standing Multilevel Car**

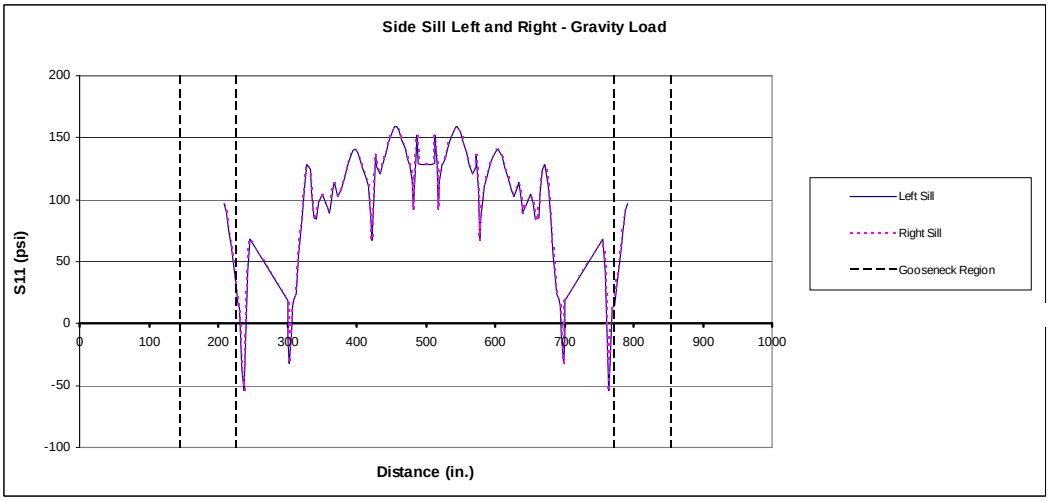


**Figure A9 - Stress Distribution in Left and Right Side Sills, Standing Multilevel Car**

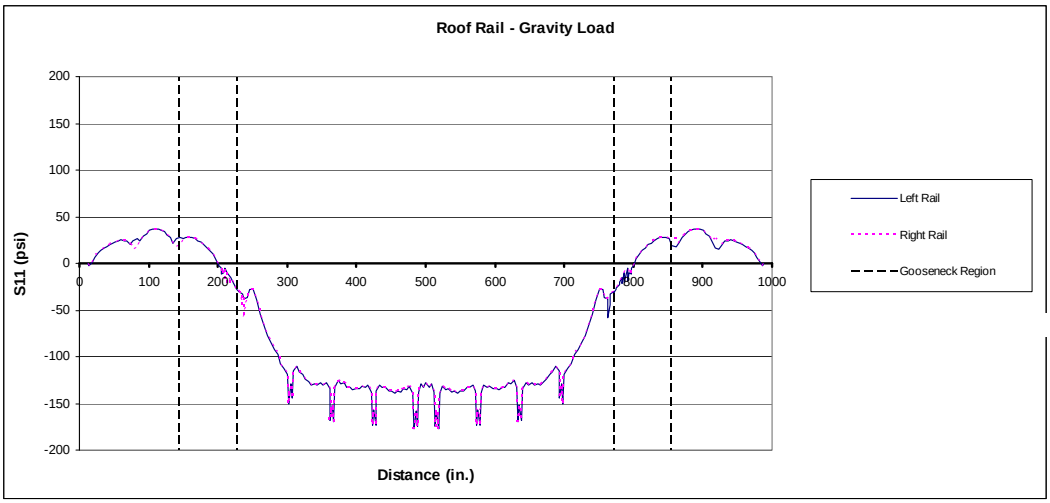


**Figure A10 - Stress Distribution in Left and Right Roof Rails, Standing Multilevel Car**

As in the single-level car, the mesh of the carbody exhibits left-right symmetry. Because of this, the stress distribution may be recorded in one member of a left-right pair during symmetric loading. These stress values can be taken as representative of both the left and right member, so long as the loading of the model is also symmetric.

## Appendix D – Stress Contour Plots for Various Load Cases

Figure A11 shows the contour plot of the entire single-level car during the AW0 load case. The car generally exhibits low levels of stress, without exceeding the yield stress for any member. The largest stress value, 57 ksi, is found in the side sill at the stepwell location. This coincides with the change in cross-section of the side sill when it spans the stepwell. The von Mises stress is the plotted result throughout this section, unless otherwise noted.

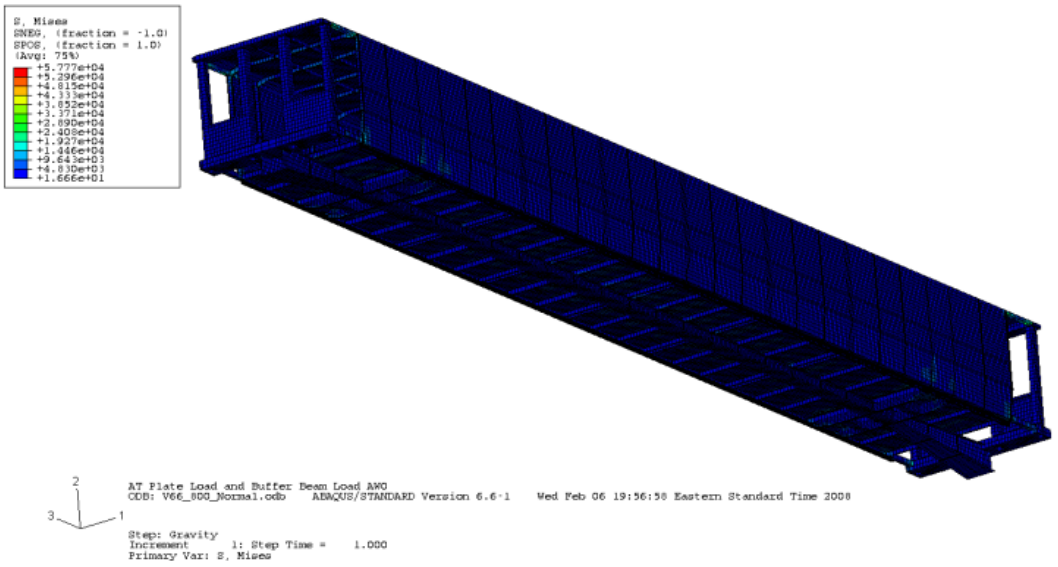


**Figure A11 – von Mises Stress Contour, AW0 Load**

The von Mises stress contours from the 800 kip load are shown Figure A12. The minimum contour value is set to 50 ksi, which corresponds to the yield stress of the wall skin. The complete listing of yield stresses for all the members that make up the model can be found in

Table 4. The areas of color seen in the plot correspond to stresses above yield stress. The areas of highest stress correspond to the draft sill surrounding

the buff stops, the attachment of the body bolster to the draft sill, the roof rail over the stepwell, and the change in cross-section in the side sill at the stepwell. Because of the simplified modeling used in this thesis, the connections between the draft sill and the lateral members are modeled as being perfectly welded at a right angle. The coarseness of the mesh also contributes to the appearance of a stress concentration at areas of sudden transition.

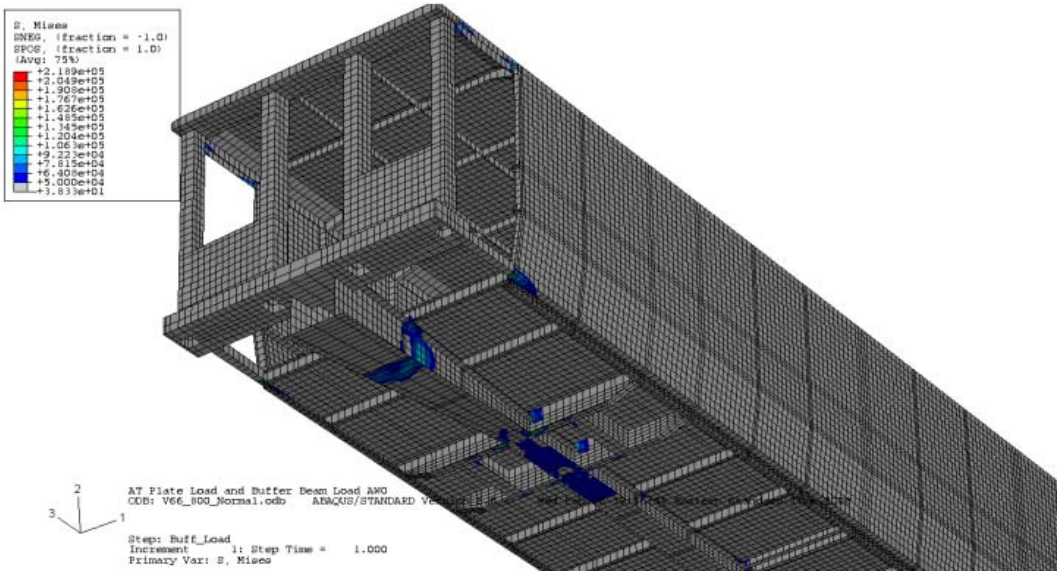


**Figure A12 – von Mises Stress Contour, 800 kip Load**

Figure A13 shows the contour plot of stress in the railcar subject to the 1,000 kip load across the buffer beam. The minimum stress contour is set to 50 ksi. The areas of stress concentration occur at the buffer beam, where the load is applied, as well as in the side sill at the end of the stepwell. There is also an increased level of stress at the body bolster's attachment to the draft sill.

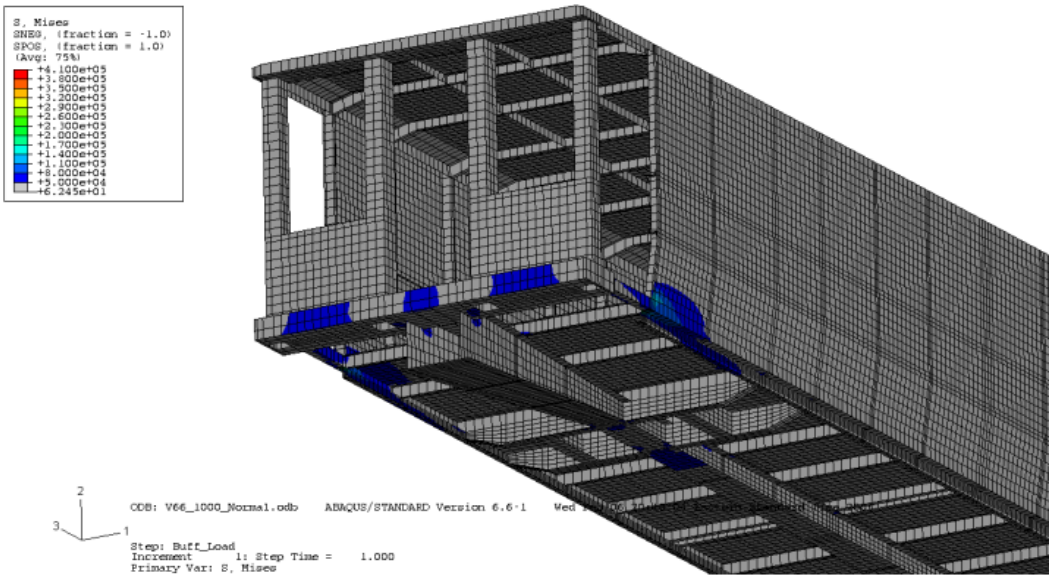


**Figure A13 – von Mises Stress Contour, 1,000 kip Load**

The von Mises stress contour plot from the 200 kip load across the AT plate is shown in Figure A14. The plot has a minimum contour level of 50 ksi. The highest levels of stress occur in the roof rail, purlins, and first lateral roof member inboard of the doorframe. The cross-section of the roof rail remains the same from AT plate to AT plate, but the wall skin ends at the inboard end of the doorframe.

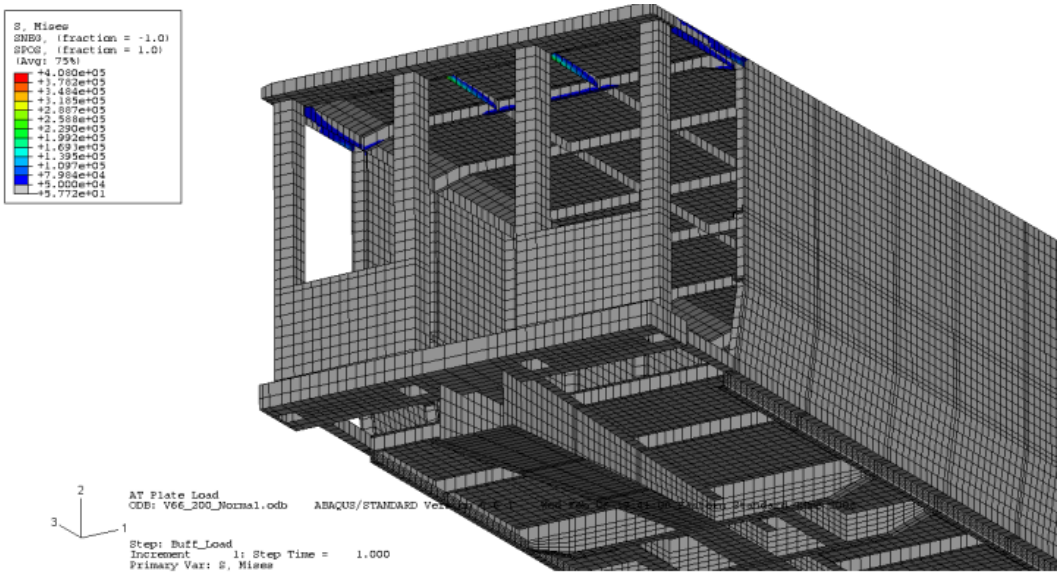


**Figure A14 – von Mises Stress Contour, 200 kip Load**

The von Mises stress contours are shown in Figure A15 for the 1,200 kip loading case. This load combines a 200 kip load at the AT plate with a 1,000 kip load at the buffer beam. The stress contours are similar to those from the individual applications of the 200 kip load and the 1,000 kip load. The 1,000 kip load causes the stress concentrations that occur in the lower members, while the 200 kip load at the AT plate cause the stress concentrations in the roof rail and the purlins.

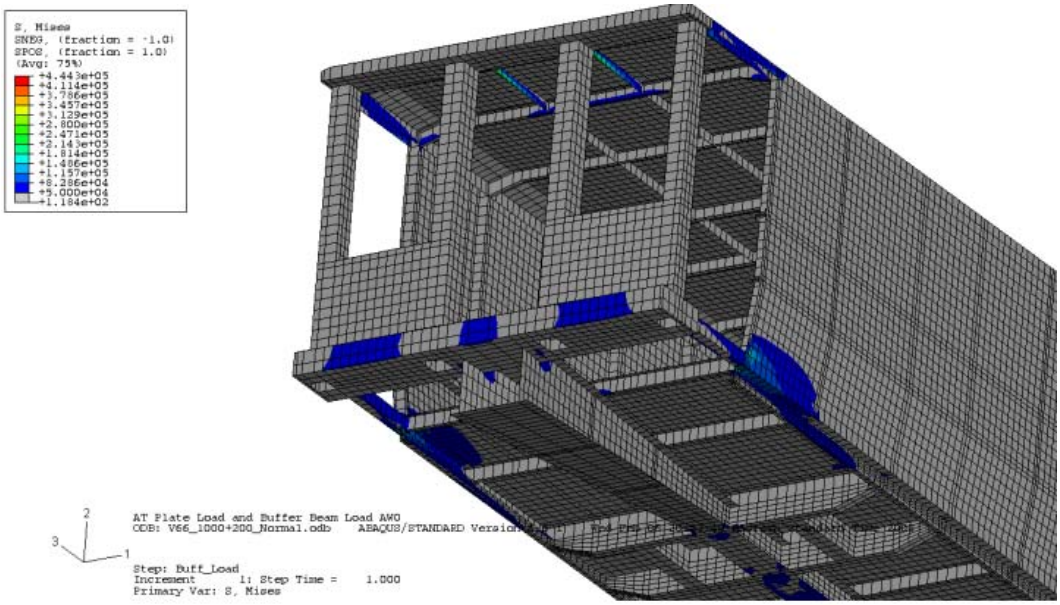


**Figure A15 – von Mises Stress Contour, 1,200 kip Load**

Following the analysis of the single-level car under the loading cases described above, the multilevel car model was also analyzed for its behavior subject to similar loads. The contour plots showing the areas of stress concentrations are shown in the following section. The first plot, presented in Figure A16, shows the entire carbody under AW0 load. The von Mises stress contours are plotted for the entire railcar. The figure shows the relatively low levels of stress present in the carbody when loaded only by its own weight. A list of yield stresses for the members in this model can be found in Table 7.

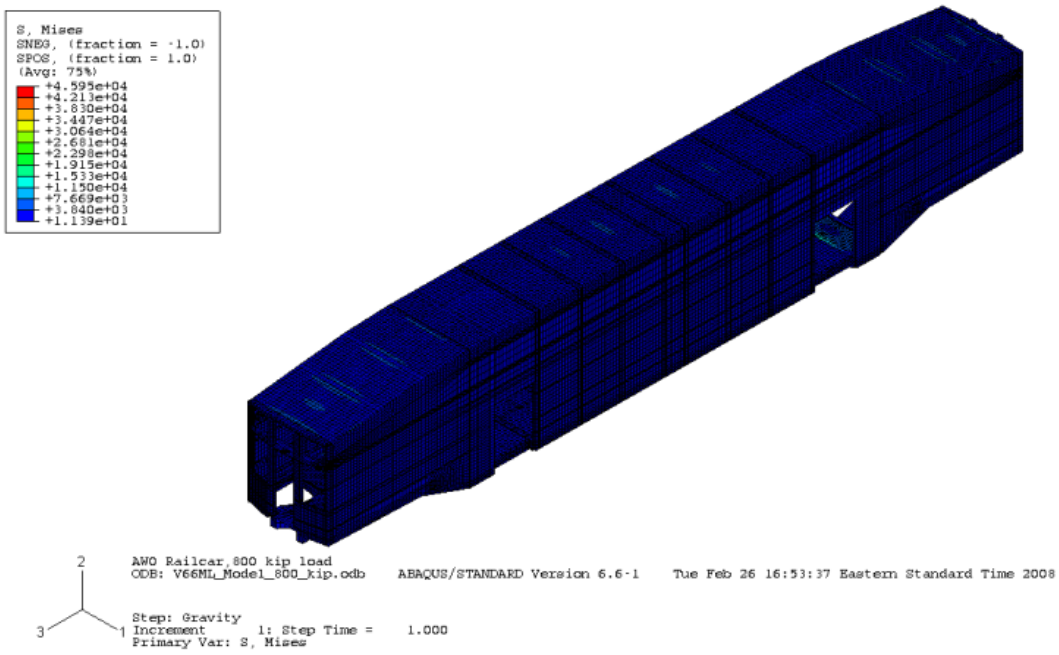


**Figure A16 – von Mises Stress Contour, AW0 Load, Multilevel Railcar**

The carbody was subject to an 800 kip compressive load at the buff stops. The von Mises stress was plotted for the entire car in Figure A17, with the lowest contour corresponding to a stress of 50,000 psi. This value was chosen because it is the yield stress of the steel members making up the underframe of the car. The

areas of stress higher than this value correspond to the draft sill surrounding the buff stops, connections between members, and the gooseneck region of the underframe. These apparent concentrations are likely caused by the coarse mesh of the model, which cannot capture the gooseneck transition in great detail.

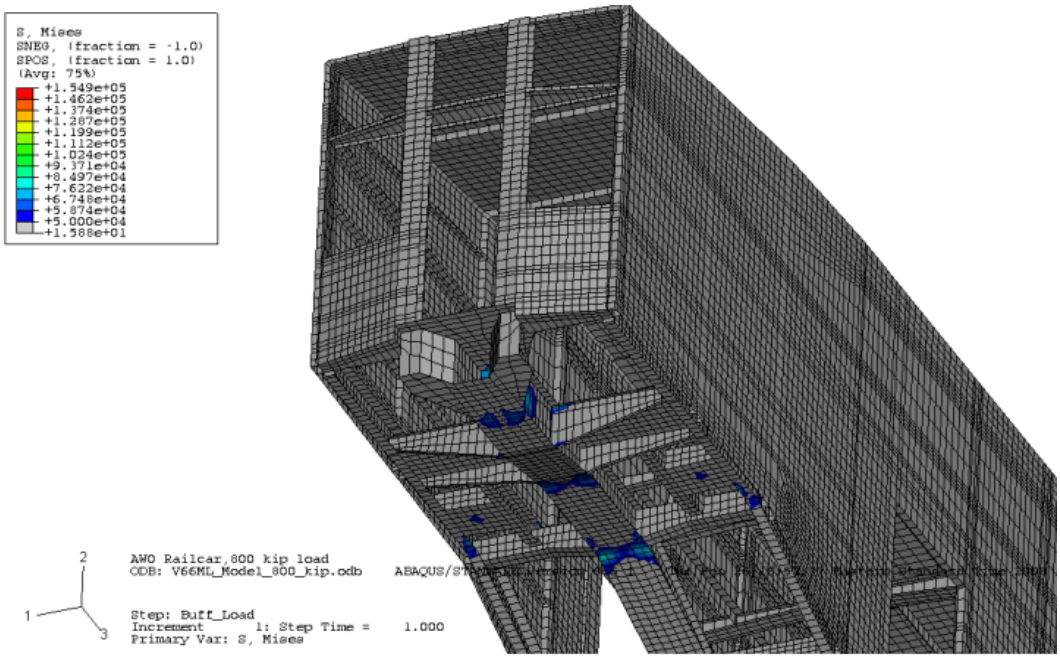


**Figure A17 – von Mises Stress Contour Plot, 800 kip Load, Multilevel Railcar**

The multilevel railcar was also subject to a 1,000 kip load, distributed across the buffer beam. The von Mises stress contours are plotted in Figure A18. The minimum contour level is 50,000 psi, the yield stress of the steel underframe members. The areas of stress above this value correspond to the face of the buffer beam where the load is applied, as well as the gooseneck transition in the center and side sills.

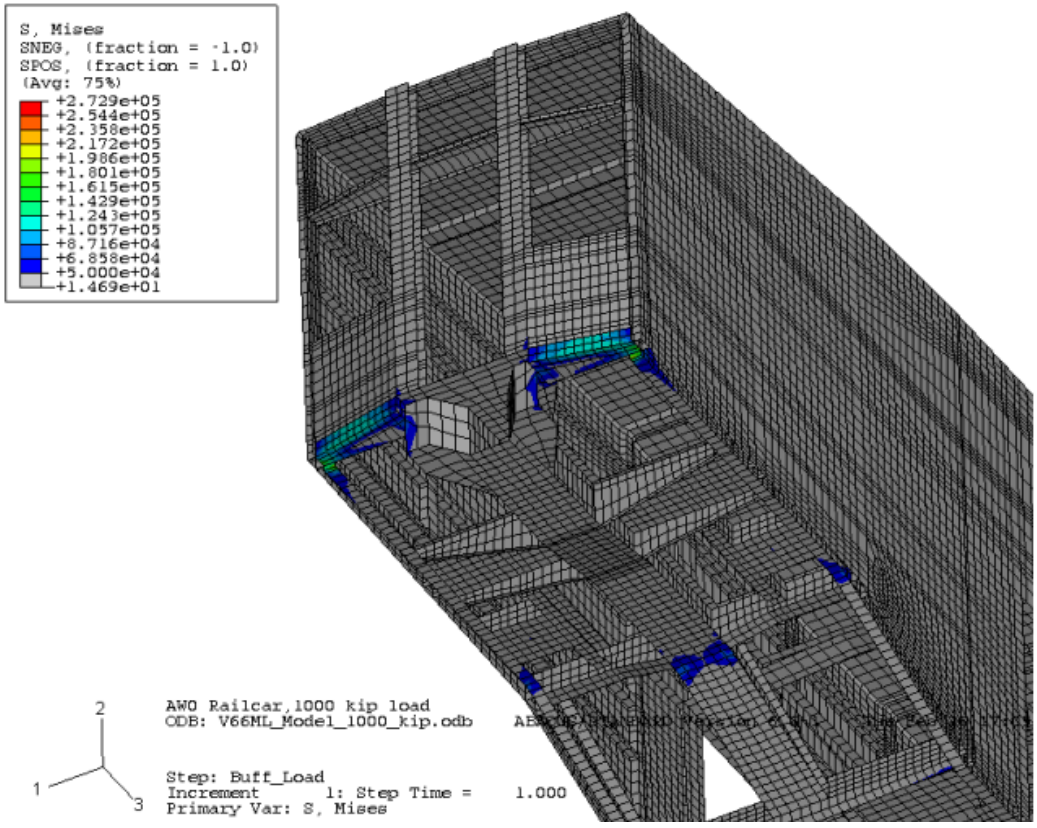


**Figure A18 – von Mises Stress Contour Plot, 1,000 kip Load, Multilevel Railcar**

The von Mises stress contour plot for the multilevel railcar subject to a 200 kip load across the endframe at the roof level is shown in Figure A19. This plot shows the endframe at the end of the car where the load is applied. In this plot, the minimum contour level is 23 ksi. This stress level corresponds to the yield stress of the roof skin. The areas of highest stress are concentrated around the load application area. The yield stress of the AT plate is 50 ksi, indicating the concentrated load causes yield in a smaller region of the model than indicated in Figure A19.

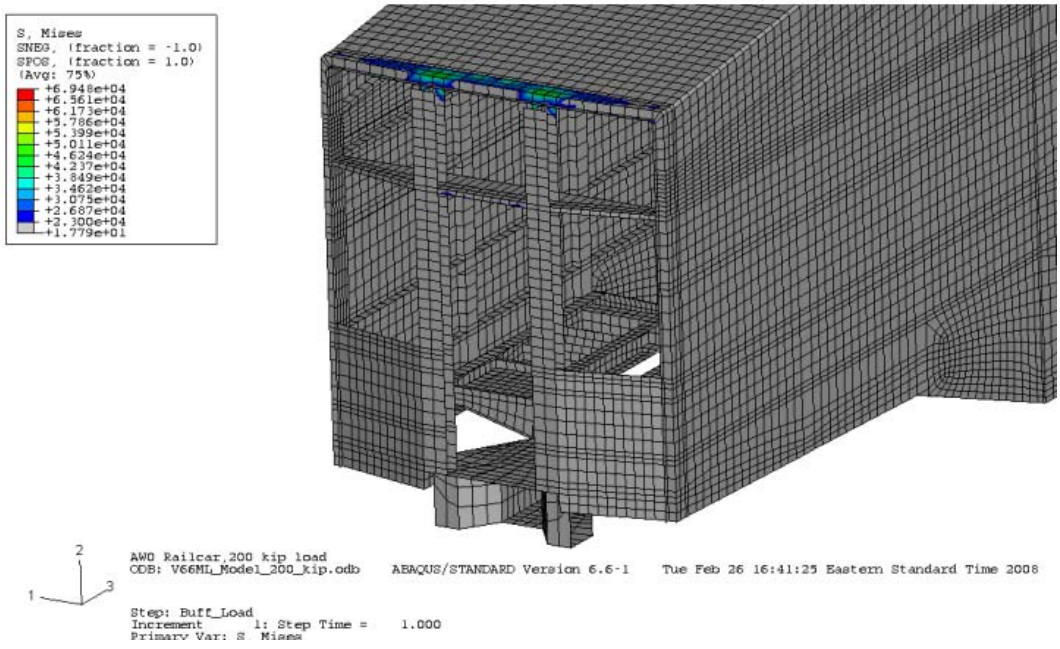


**Figure A19 – von Mises Stress Contour Plot, 200 kip Load, Multilevel Railcar Live End**

The fixed end of the railcar during application of the 200 kip load is shown in Figure A20. The contour levels have a minimum value of 23 ksi, the yield stress of the roof panels. This plot features stress concentrations occurring at the corners of the roof plate, in contrast to the concentration seen across the entire face of the AT plate seen in Figure A19.

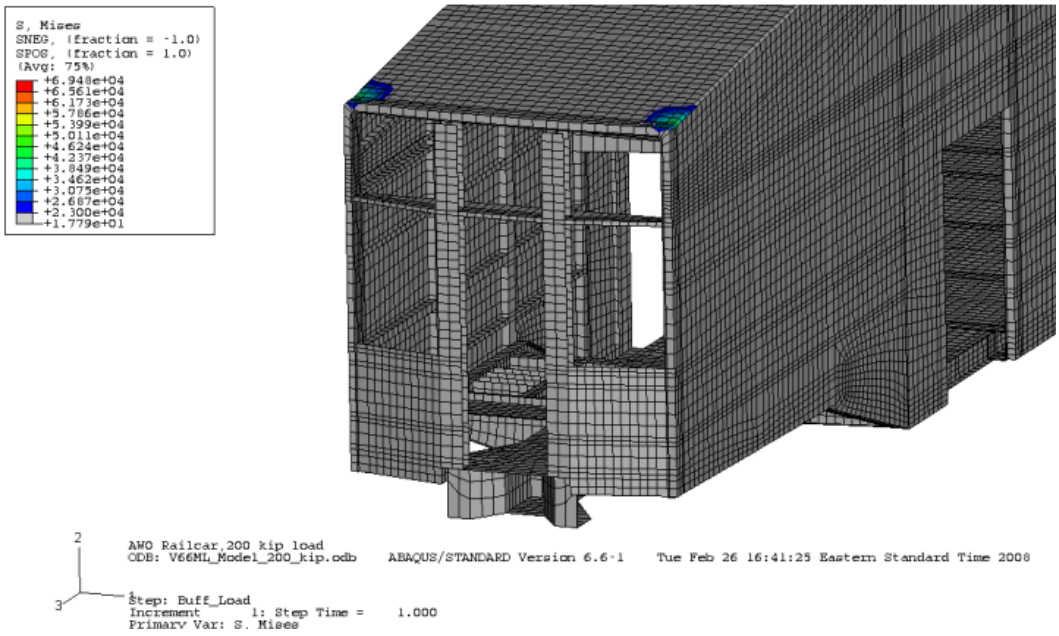


**Figure A20 – von Mises Stress Contour Plot, 200 kip Load, Multilevel Railcar Fixed End**

Figure A21 shows the von Mises stress contour levels present in the carbody during the application of the 1,000 kip load at the buffer beam at the same time as the 200 kip load at the AT plate. The minimum contour level has been set to 32 ksi. The areas of highest stress correspond to the loading locations across the buffer beam and at the intersection of the AT plate with the collision posts. These stress contours are similar to the stresses seen in the separate 200 kip and 1,000 kip loads.

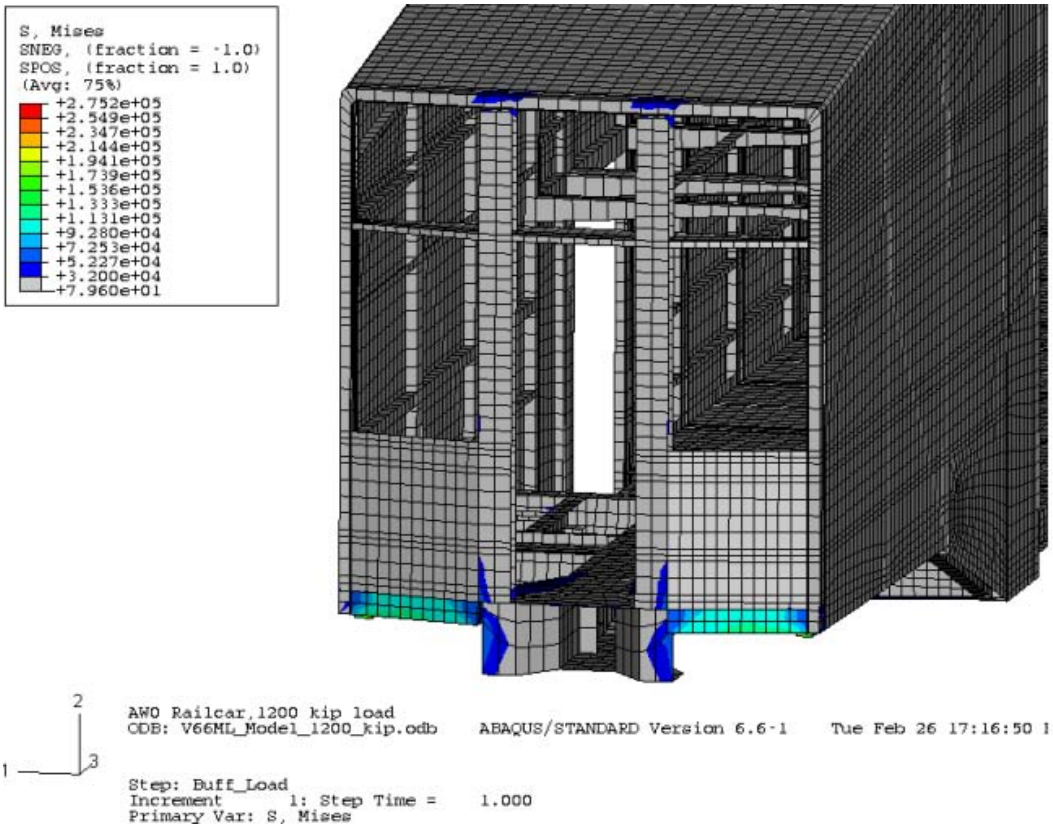


**Figure A21 – von Mises Stress Contour Plot, 1,200 kip load, Multilevel Railcar**

## Appendix E – Beam and Shell Model

The commercial software program ABAQUS/CAE was used to develop the geometry of the model [31]. This software package allows a model to be constructed of individual parts, with mesh and material properties associated with the individual parts. These parts are then assembled together via constraints, which can simulate various types of connections by removing certain degrees-of-freedom between constrained geometries.

For the particular model first constructed in this thesis, the structural members of the underframe and superstructure were represented as beam elements, with the outer skin of the railcar represented by shell elements. For the majority of the members, the length of the beam greatly exceeds both the height and width of the cross section of the beam, allowing the beam sections to be used reliably. B33 elements were used in meshing the beams, which are 2-node cubic formulation beam elements. The assembled beam and shell model contains 630 B33 elements and 316 shell (S4) elements. A quasistatic simulation ran in approximately 1 minute on a desktop computer.

In ABAQUS/CAE, the cross-section of a beam element can be defined via a series of (x,y) coordinates, allowing the user to specify an arbitrary geometry. The thickness of the segment between each consecutive pair of points is also user-defined. This method of input was used to define the majority of the members making up the passenger car. Figure A22 shows the cross section of the cross bearer that was defined in CAE. The x's represent the section points used to

define the geometry of the section, and the target represents the origin in the section's local coordinate system.

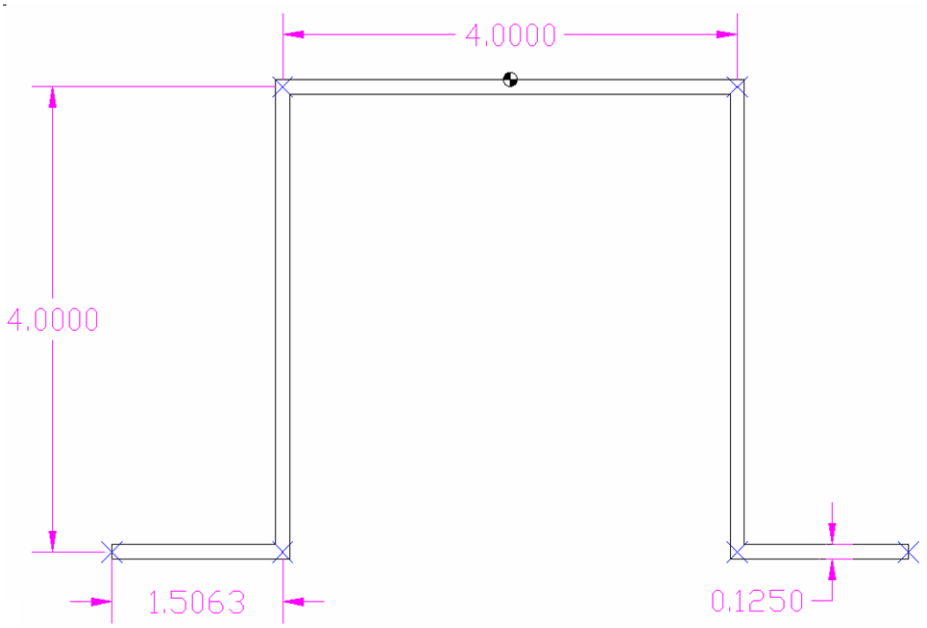


**Figure A22 - Cross Section View of Cross Bearer, Beam Model**

The assembly of the beams to form the frame of the car was accomplished through the use of a "tied" constraint. This constraint requires the user to specify a "master" and "slave" surface for the interaction. The slave surface's six degrees of freedom are restricted to the same displacements as the master surface, as if the slave and master was the same node. This effectively welds the slave surface to the master surface.

The tied constraint method was also utilized to attach the wall, floor, and roof skins to the respective framing members. Since 3-dimensional beams and 3-dimensional shells both have 3 translational degrees-of-freedom and 3 rotational degrees-of-freedom, the tied constraint was an obvious choice to constrain two

nodes on different parts to move as if attached. Additionally, the use of tied constraints allowed for parts to be altered or removed entirely from the assembly without affecting the other distinct parts of the assembly. Any constraints making reference to a part that had been removed from the assembly could merely be suppressed on the following simulation runs without difficulty.

Figure A23 shows the assembled underframe of the car. Each beam is represented by a 1-dimensional line in the assembly. The underframe consists of the center and side sills, body bolsters, cross bearers, and floor stiffeners.

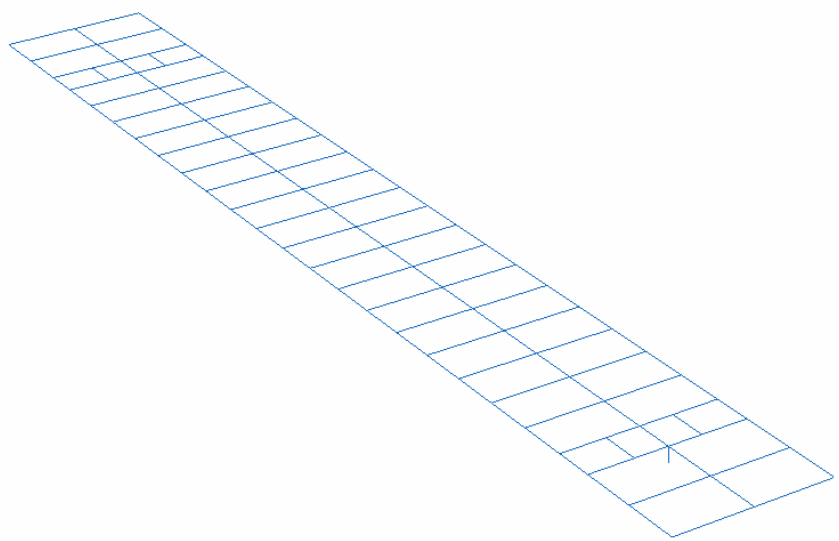

**Figure A23 - Beam Model Underframe**

The skeletal structure of the walls and roof are also modeled using beam elements. The belt rail, upper window rail, and roof rail are the longitudinal members in the superstructure. At the location of each cross bearer or floor stiffener is a vertical wall stiffener that intersects each of these longitudinal members. The structural members of one wall, attached to the underframe, are shown below, in Figure A24.

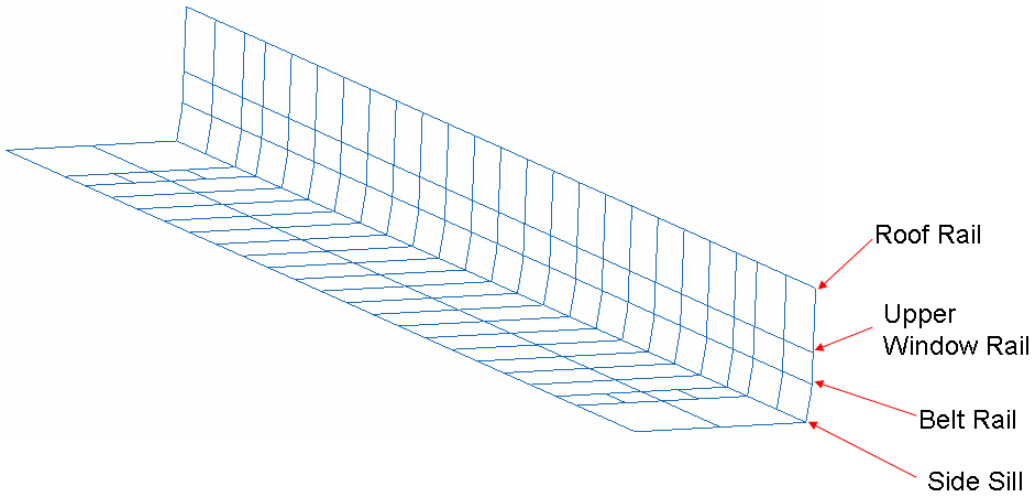


**Figure A24- Beam Model Underframe with One Wall**

The floor pans, wall panels, and roof panels were attached to the beam elements of the structural frame via tied constraints. The wall panels were left whole, without cutouts for the windows. This was done to simplify the modeling techniques used in this investigation. Because the windows are framed by the longitudinal and vertical structural members of the sidewall, the load path through the sidewall will be unaltered by this simplification. The beam and shell model with attached skin is shown below, in Figure A25.

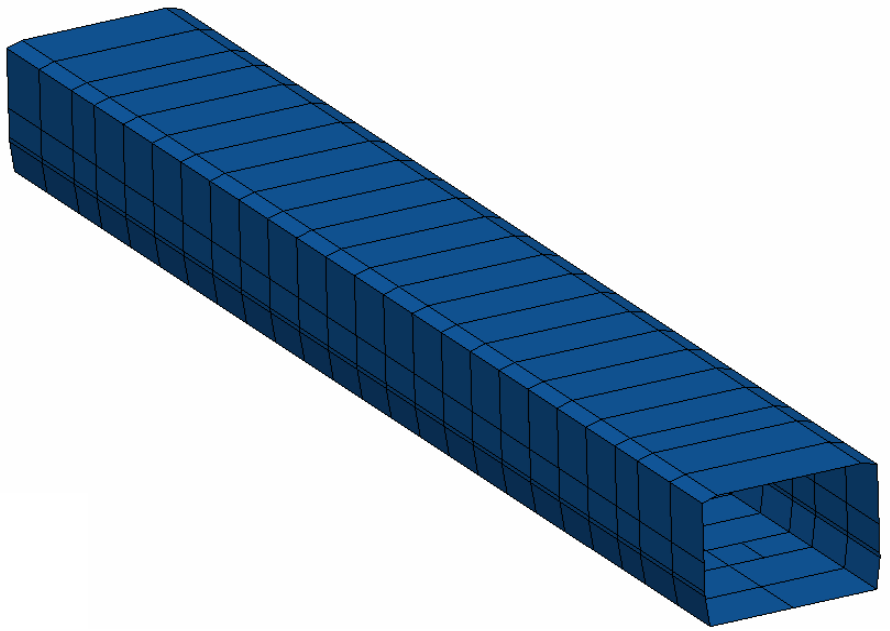

**Figure A25 - Beam Model with Floor, Walls, and Roof Attached**

This model had a length of 75 feet, 11 inches. This length represents the body of the railcar inboard from both stairwell vestibules. Since the area between the two stairwells in a railcar is the occupied area, the load path of the compressive load through this region is of particular interest. The endframe was not modeled for simplicity, but could easily be added to the assembly in the same manner as the rest of the components.

**Material Used**

The steel material used throughout this model is the same as is presented in

Table 3. Inelastic behavior was not included as part of the material behavior, as a passenger car that complies with the 800,000 pound strength requirement, by definition, does not exceed the elastic limit. Typical construction of this type of railcar utilizes stainless steels for the structural members. The yield stresses presented in Table A1 were obtained from previous finite element models as well as manufacturer drawings.

**Table A1- Yield Stresses for Structural Members, Beam and Shell Model**

| Member | Yield Stress ksi [GPa] |
|---|---|
| Belt Rail, Roof Rail, Upper Window Rail | 110 [760] |
| Body Bolster | 65 [450] |
| Center Sill | 100 [690] |
| Cross Bearer | 75 [520] |
| Draft Sill | 100 [690] |
| Floor Stiffeners | 110 [760] |
| Floor Pans | 32 [220] |
| Outer Skin | 50 [345] |
| Roof Stiffeners | 110 [760] |
| Side Sills | 75 [520] |
| Wall Stiffeners | 110 [760] |

**Weight**

The total weight of the carbody structure is 14,235 pounds. In order to simulate a carbody in empty, ready-to-run condition, the density of the steel material was increased. This artificially dense material brought the weight of the carbody up to 75,175 pounds. This weight simulates the weight of the carbody with interior fixtures, mechanical and electrical systems, but no passengers or truck assemblies. The addition of two 13,700 pound truck assemblies would bring the empty weight of the car up to 102,575 pounds. This weight is lighter than the values expected based on Reference 6, since this FE model features a

number of simplifications to the geometry and no endframes.

**Loading Conditions Examined**

One of the goals of this simple model was to determine the appropriate characteristics of the railcar as if it were a simple beam. Since the area between the body bolsters consists of a series of repeating cross sectional members, the assumption that the railcar exhibits beam-like behavior in this region is a reasonable one.

The first parameter to be examined was the neutral axis of the car. In order to simplify the loading, gravity was disabled for this step of the evaluation. This provided a railcar that was weightless. The extreme end of the car was fixed across its entire cross-section, as if the railcar was a cantilevered beam. The boundary condition as applied to the railcar is shown below, in Figure A26.

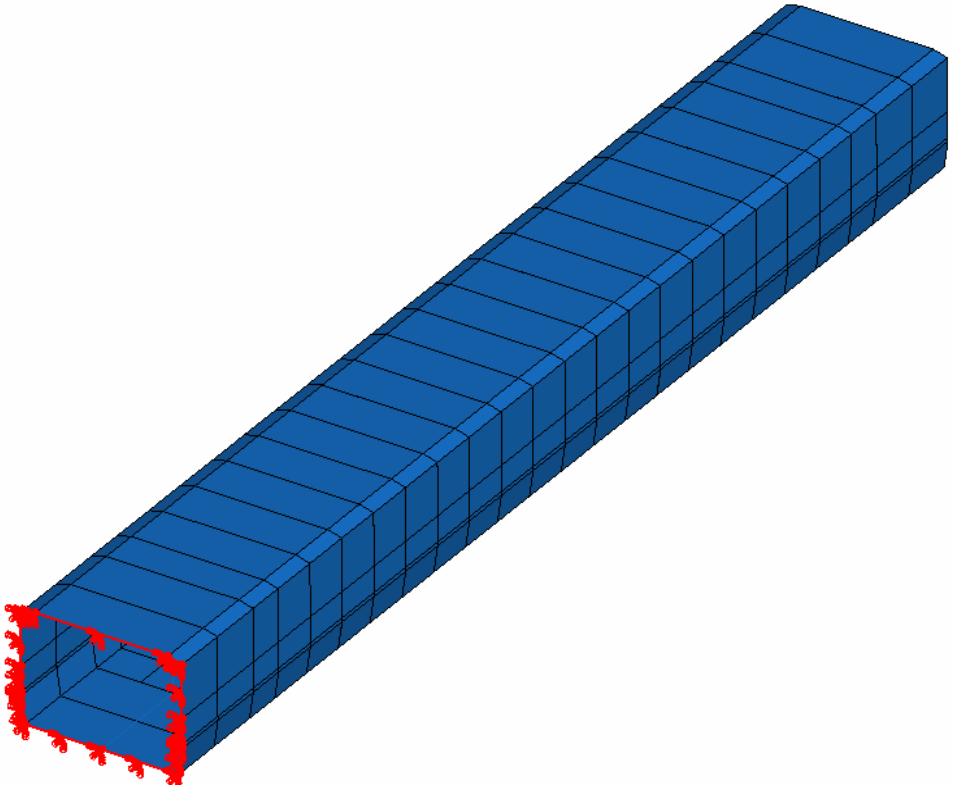

**Figure A26- Cantilever Boundary Condition Applied to Beam Model**

To evaluate the neutral axis location, a bending load was used as the simplest loading case. A series of point moments were applied across the far end of the body bolster, away from the cantilever end. The total moment applied to the car was 3.36 x $10^7$ in-lb, rotating about the lateral direction of the car.

Figure A27 shows a contour plot of the cantilevered carbody subject to this loading condition. The variable plotted is the displacement along the longitudinal direction of the car. In this plot, the contour bounds have been set very close to zero, so that all elements with a negative longitudinal displacement are black and all elements with a positive longitudinal displacement are plotted as gray.

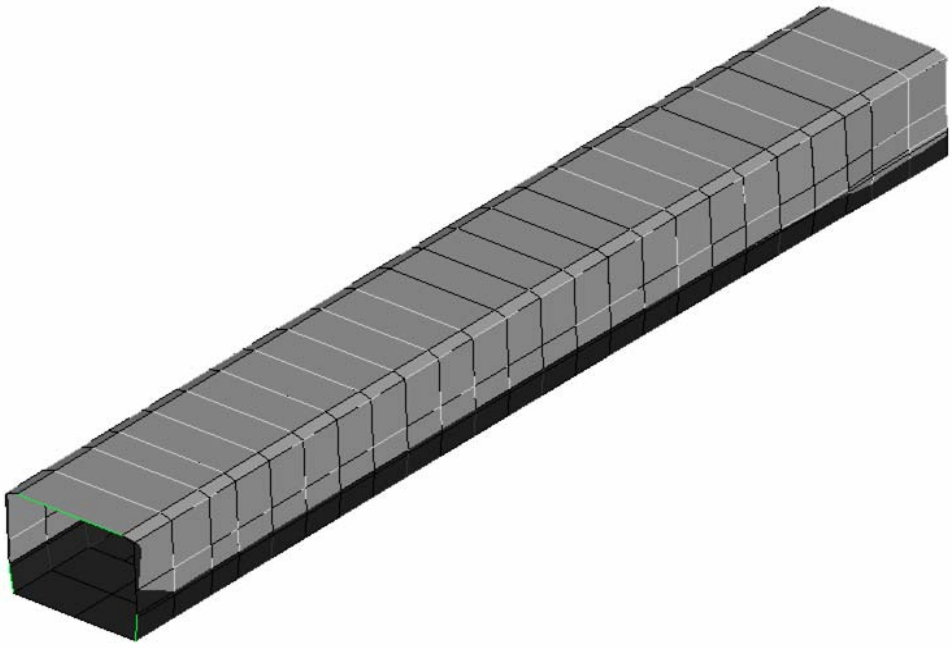

**Figure A27- Contour Plot of Longitudinal Displacement, Cantilevered Beam Model**

Since the neutral axis of a beam in bending represents the transition from tensile stress to compressive stress, it also represents the transition from positive displacement of the nodes to negative displacement of the nodes in an FE mesh. The longitudinal displacement of the nodes making up the wall stiffeners was plotted for each wall stiffener along the length of the car between the applied moment and the opposite body bolster. A plot of these displacements is shown below, in Figure A28. Each series represents the vertical wall support at a particular distance from the free end of the carbody.

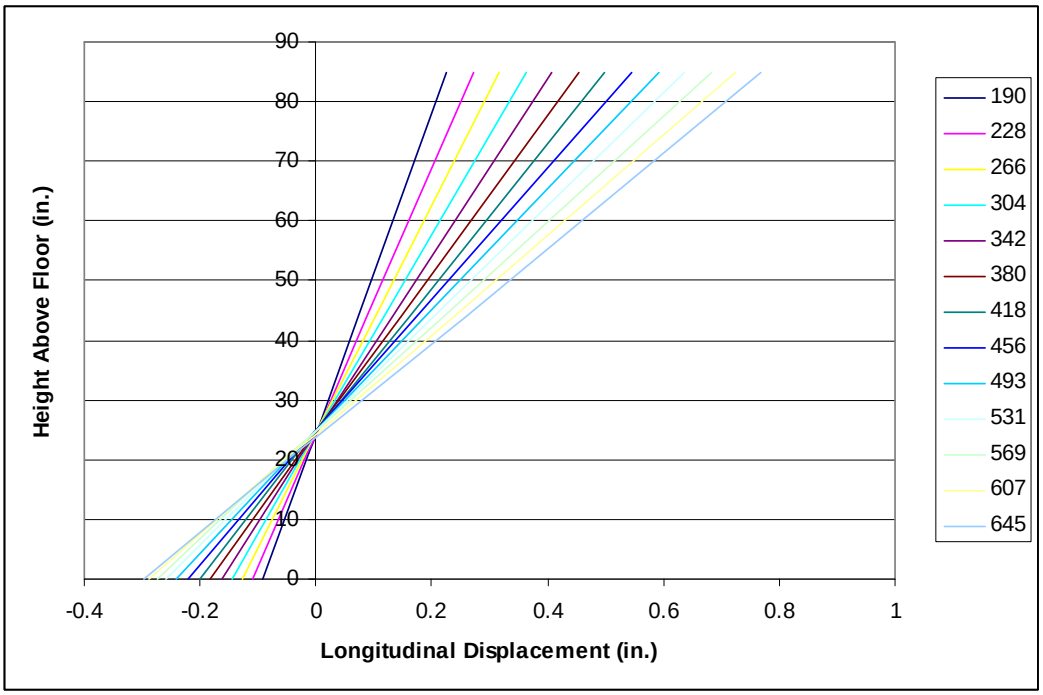


**Figure A28- Plot of Height Above Floor vs. Longitudinal Displacement for Varied Cross-sections**

Taking the average height at which the longitudinal displacement is equal to zero, the neutral axis is found to be approximately 24.4 inches above the top of the floor. The value of the neutral axis moves to a lower value as the cross-section being investigated gets closer to the applied moment. The value also fluctuates above and below the average value when the cross section is taken close to the fixed end. The value of 24.4 inches provides a reasonable estimate of the neutral axis height for the occupied volume, away from the end effects.

The beam and shell model offers a number of advantages over models that had been previously developed. The runtime is the most attractive feature of this model, being on the order of one minute to perform a quasi-static compressive load test on a model in a gravity field. This rapid runtime allowed a number of

simulations to be run on the model with varied boundary conditions, simulating loading conditions that are not able to be applied to the actual, physical railcar. This model adequately captured the overall behavior of the car as if it were a beam, allowing the neutral axis location of the car to be calculated.

There is a tradeoff in simplicity of the model for a rapid runtime. Because of the way beam sections are defined, a given beam is required to have a constant cross-section along its entire length. While the majority of the members used in passenger railcar designs are prismatic beams, there are some notable exceptions. The draft sill and the lateral members of the body bolster each feature a variable cross-section. These members contribute to the load path of the compressive load from the coupler, as the buff stops are located within the draft sill and the body bolster is the first lateral member inboard of the buff stops. This oversimplification of the geometry was the primary motivation for the decision to utilize shell FE models for the further stages of this work.

## Appendix F – Conventional Single-level Railcar Construction

### Car End Structure

In North American commuter and intercity passenger rail operations, it is possible to encounter two different heights of boarding platform along the same rail line. In some stations, the platform is at the same height as the floor of the railcar, allowing for level boarding through the doorways. In other stations, the platform height is below the height of the floor, necessitating the use of stairs to enter the railcar. Those railcars that service low-platform stations feature step wells built into the sides of the vehicle, which prevent the use of a continuous side sill running along the entire length of the car. These stepwells are typically placed at one or both ends of the railcar. In these cars, the center sill bears the majority of the longitudinal load, though some load is shed laterally into the side sills inboard of the stepwells [7]. The end portion of a typical conventional single-level car is shown below, in Figure A29.

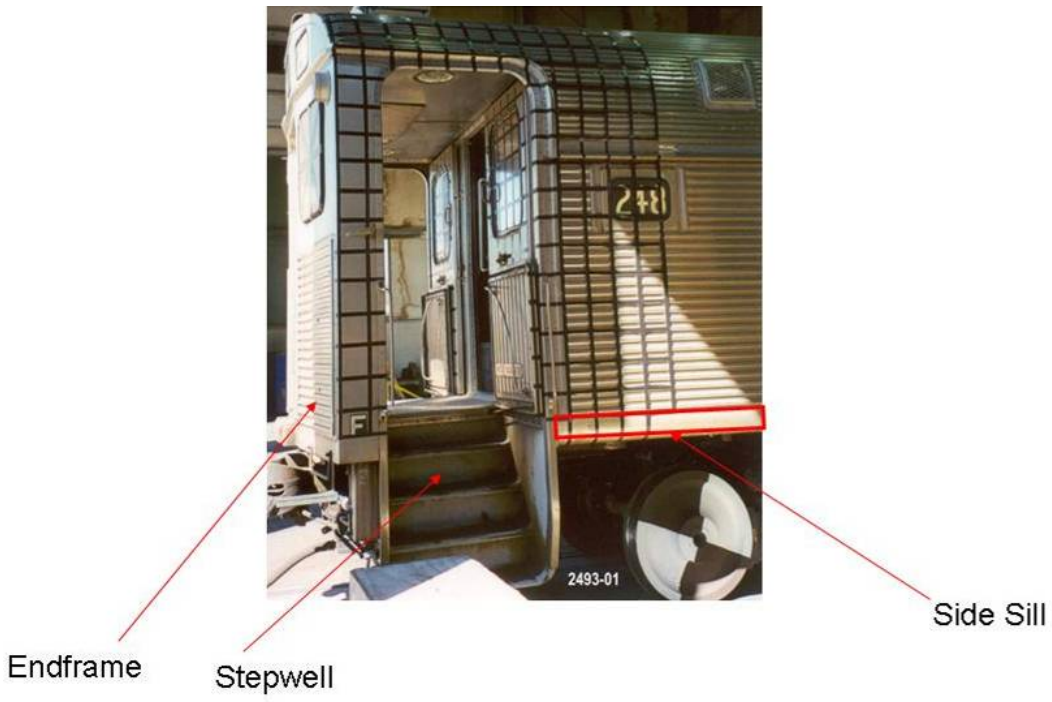


**Figure A29 - Conventional Car End Structure**

At each end of the car is an endframe, designed to withstand collision forces and prevent intrusion into the occupied volume of the car should an impact occur above the level of the underframe. A photograph of a state-of-the-art (SOA) endframe with the outer skin removed, taken from Reference 8, is shown in Figure A30. In this particular design, the side sills of the passenger car have been extended to run continuously from one endframe to the opposite endframe.

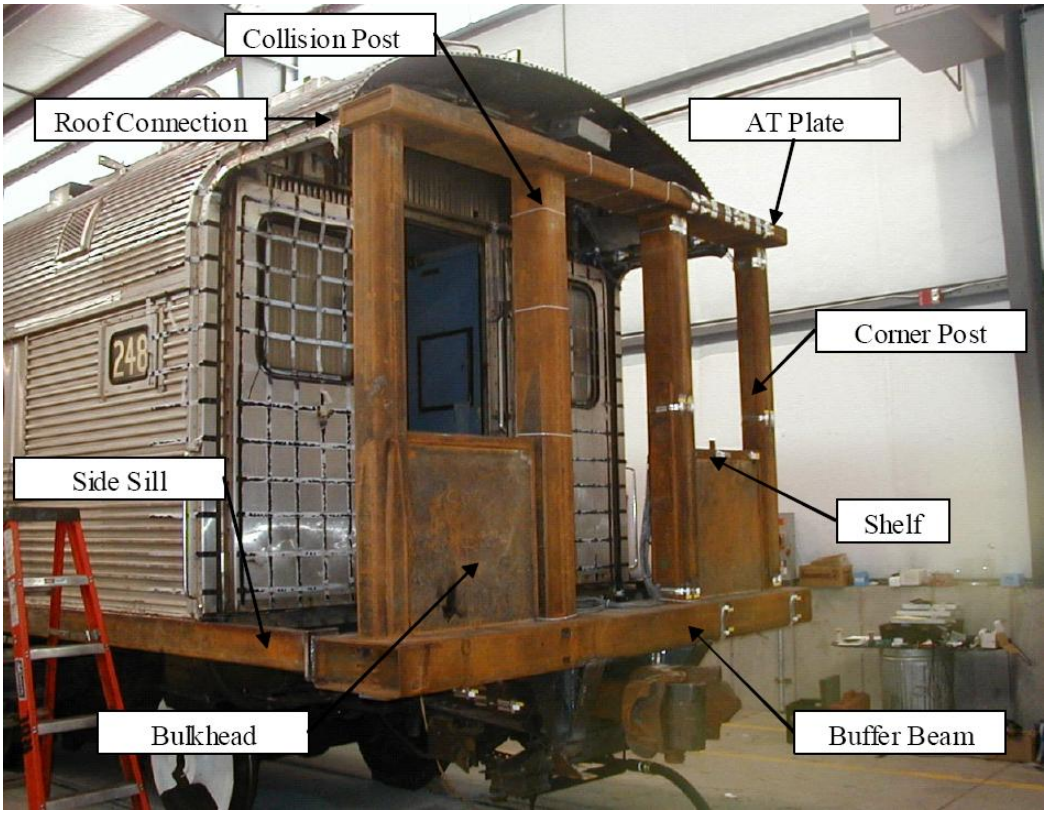


**Figure A30 - Annotated SOA Endframe Installed on Car**

In this endframe design, the buffer beam is a large, lateral member that is in line with the side sill and floor of the railcar. It connects to the anti-telescoping (AT) plate via four significant vertical members, the corner and collision posts. The AT plate, in turn, is attached to the roof rail at each end of the railcar. This endframe also features bulkheads that act as shear panels, as well as shelves connecting the corner and collision posts.

**Suspension Attachment**

The trucks of a railcar are composed of the wheels, axles, suspension components, and framing structures. In a passenger railcar, the carbody is connected to the truck via the secondary suspension. The secondary suspension is

typically made of either coil springs or airbag components, depending on the particular railcar [7].

As shown in Figure 1, the body bolsters are sizable lateral members within the underframe of the railcar. Typically, the secondary suspension of the trucks is attached to the body bolster just inboard of either side sill. Figure A31 shows a conventional, single-level railcar that has been disassembled outboard of the body bolster. The secondary suspension, an inflatable rubber bellows, is indicated on the near side of the car.

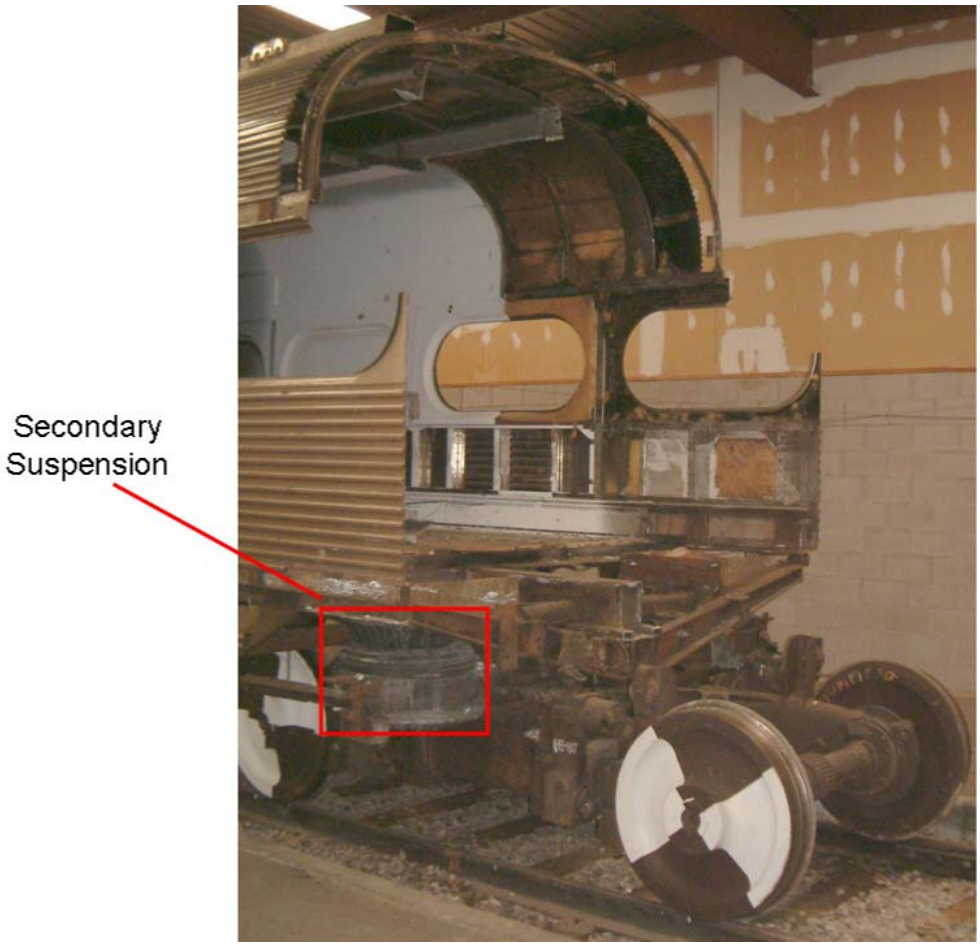


**Figure A31 - Sectioned Railcar Displaying Body Bolster and Truck Assembly**

**Underframe Construction**

In addition to the body bolsters, cross bearers and floor stiffeners also run laterally between the side sills, adding structural support. These members also serve to shed load laterally into the side sills of the car. In conventional car construction, it is typical for the cross bearers to be located above the center sill, so that the bottom surface of the cross members attaches to the top of the center sill. This places the top surface of the cross members at the same height as the top surface of the side sills. A cross-section of the underframe structure is shown schematically in Figure A32. This cross section is taken between the two body bolsters.

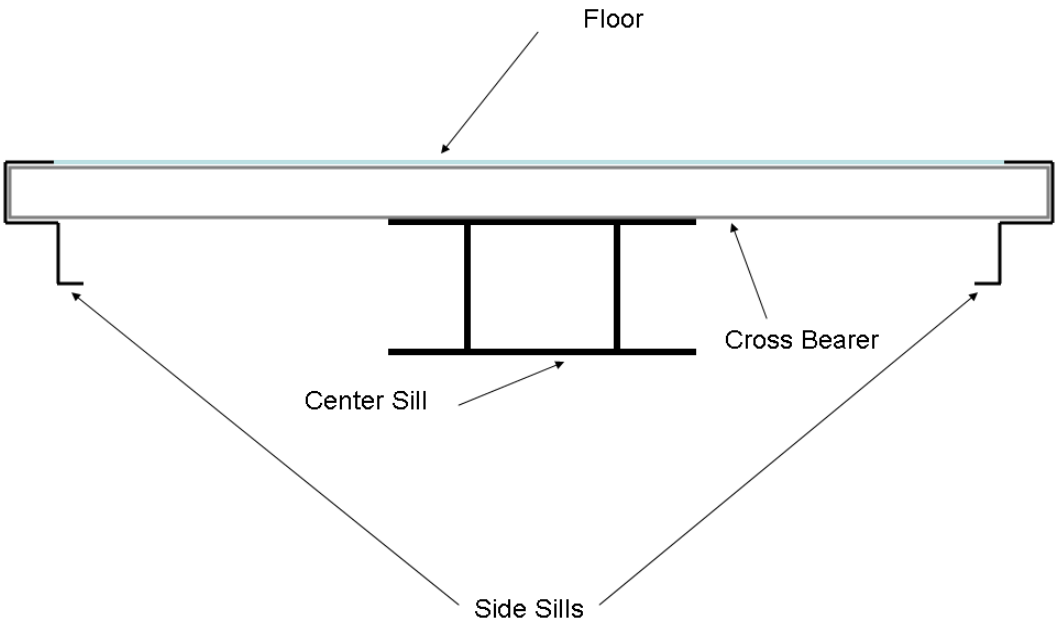


**Figure A32 - Schematic Cross-section of Underframe Structure**

**Carbody Superstructure**

The superstructure of the car, including the walls, the roof, and the framing, is situated atop the underframe. It is composed of a number of vertical

wall supports, longitudinal rails, and lateral members supporting the roof. By comparison, the superstructure is much weaker than the underframe, being composed of thinner, smaller members. Additionally, the wall skin itself contributes to the overall load sharing ability of the superstructure. Figure A33 shows a lateral cross-section of a typical passenger railcar, with the major structural members of the superstructure annotated. While not shown on this particular railcar, some designs also feature a longitudinal member at the center of the roof, known as the purlin.


**Figure A33 - Cross-section View Showing Typical Railcar Superstructure Members**

**Draft Sill Structure**

Passenger cars are linked together to form a consist by means of a coupler, located at each end of each car. The coupler is physically situated within the structure of the draft sill. In North America, passenger car couplers are of a type known as “tightlock” couplers [11]. This type of coupler includes features to prevent coupled cars from climbing above one another during rapid stops, such as during a collision. A tightlock coupler is shown below, in Figure A34, with different structures highlighted.

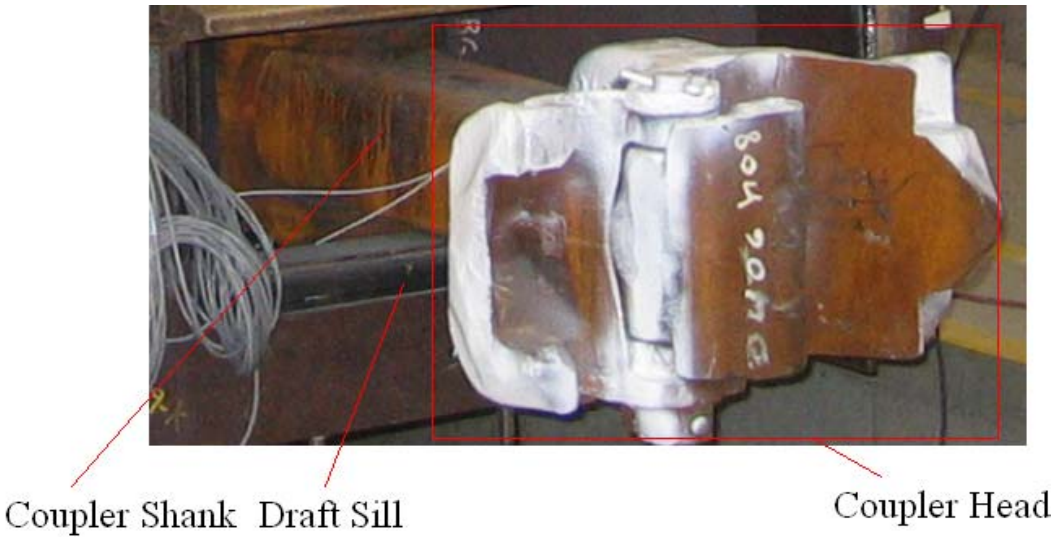


**Figure A34 - Annotated Tightlock Coupler**

The coupler is able to pivot about the vertical axis, enabling the cars to travel around curves. Additionally, the coupler can pivot up and down to allow small vertical motions between coupled cars. The coupler is attached to the draft sill of the car through a device known as the draft gear [11]. The draft gear attaches to the rear of the coupler’s shank, and acts as a shock absorber between the coupler and the carbody. This device is intended to dissipate the energy

associated with coupling the cars together, as well as the forces generated as the train accelerates and decelerates. The draft gear reacts against the buff stops when compressed, and the draft stops when in tension, thus transmitting the coupler load into the draft sill. A cutaway plan view of the draft sill is shown below, in Figure A35.

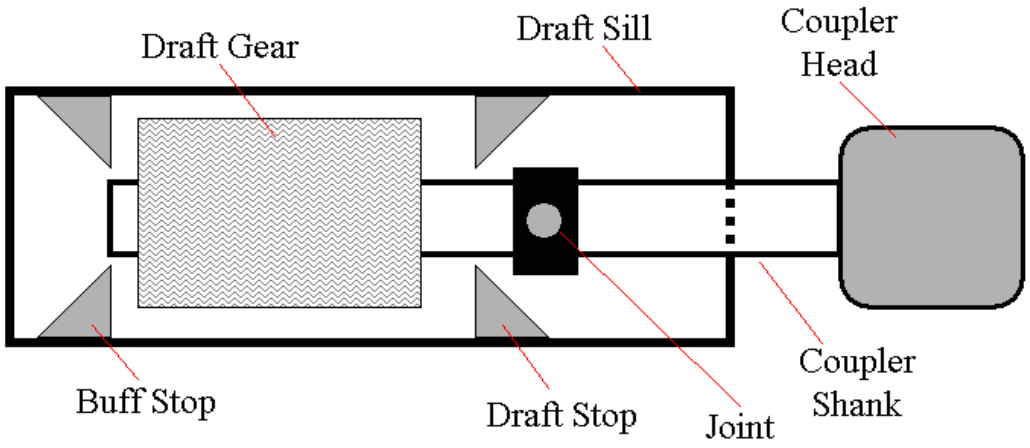


**Figure A35 - Schematic Plan View of Draft Sill Assembly**

**References**


1. Tyrell, D., "U.S. Rail Equipment Crashworthiness Standards," Journal of Rail and Rapid Transit, Proceedings Part F, Institute of Mechanical Engineers, August 2002.

2. Tyrell, D.C., Severson, K.J., Marquis, B.J., "Evaluation of Selected Crashworthiness Strategies for Passenger Trains," Transportation Research Record No. 1489, pp. 50-58, National Academy Press, 1995.

3. U.S. Department of Transportation, Federal Railroad Administration, "49 CFR Part 216 et al., Passenger Equipment Safety Standards; Final Rule," Federal Register, May 12, 1999.

4. Martinez, E., Tyrell, D., Perlman, A.B., "Development of Crash Energy Management Designs for Existing Passenger Rail Vehicles," American Society of Mechanical Engineers, Paper No. IMECE2004-61601, November 2004.

5. Severson, K.J, "The Development of Collision Dynamics Models to Estimate the Results of Full-Scale Rail Vehicle Impact Tests." Tufts University Master's Thesis, November 2000.

6. Stringfellow, R.G., Mayville, R.A., Rancatore, R., "A Numerical Evaluation of Protection Strategies for Railroad Cab Car Crashworthiness," American Society of Mechanical Engineers, AMD Vol. 237/BED Vol. 45, 1999.

7. Cassidy, R.J. and Romeo, D.J., March, 1975, "Final Report on Assessment of Crashworthiness of Existing Urban Rail Vehicles," U.S. Department of Transportation, DOT-TSC-681.

8. Mayville, R., Stringfellow, R., Johnson, K., Tyrell, D., "Rail Vehicle Cab Car Collision and Corner Post Designs According to APTA S-034 Requirements," American Society of Mechanical Engineers, Paper No. IMECE-2003-44114, November 2003.

9. *The Car and Locomotive Cyclopedia,* Simmons-Boardman Publishers, 1997 ed.

10. Priante, M., Tyrell, D., Perlman, A.B., "A Collision Dynamics Model of a Multi-Level Train," American Society of Mechanical Engineers, Paper No. IMECE2006-13537, November 2006.

11. White, J.H., "The American Passenger Railway Car," The John Hopkins University Press, 1978.

12. Woodbury, Clifford A., "Design and Operation of Passenger Cars and Locomotives," *The Car and Locomotive Cyclopedia*, Simmons-Boardman Publishers, 1997 ed.

13. Interstate Commerce Commission, "Report to the Chief of the Bureau of Safety Regarding Investigation of an Accident on the New York Central Railroad Near South Byron, N.Y., on January 12, 1919," File Number 577, March 4, 1919.

14. Interstate Commerce Commission, "Report of the Director, Bureau of Safety. Accident on the Southern Pacific Railroad, Tortuga, California, September 20, 1938," Investigation No. 2294, United States Government Printing Office, Washington D.C., 1939.

15. Interstate Commerce Commission, "Chicago, Burlington & Quincy Railroad Company Report in Regards to Accident at Naperville, IL, on April 26, 1946," Investigation No. 2988. United States Government Printing Office, Washington D.C., 1946.

16. Office of Safety and Office of Railroad Development, Federal Railroad Administration, "Report to the House and Senate Appropriations Committees: The Safety of Push-Pull and Multiple-Unit Locomotive Passenger Rail Operations," June 2006.

17. Aldrich, Mark, "Death Rode the Rails: American Railroad Accidents and Safety, 1828 – 1965." The Johns Hopkins University Press, Baltimore, MD, 2006.

18. American Passenger Transportation Association, "APTA SS-C&S-034-99, Rev. 2. Standard for the Design and Construction of Passenger Railroad Rolling Stock," June 15, 2006.

19. Erskine, Alastair. Research Programme, Engineering: Literature Review of Rail Vehicle Structural Crashworthiness. Rail Safety and Standards Board, United Kingdom, 2003.

20. Woodbury, Clifford A. "North American Passenger Equipment Crashworthiness: Past, Present, and Future," Published in "Proceedings of the Symposium on Rail Vehicle Crashworthiness, June 1996", US Department of Transportation, DOT/FRA/ORD-97/08, 1998.

21. Vantuono, William C. "Transit," *The Car and Locomotive Cyclopedia*, Simmons-Boardman Publishers, 1997 ed.

22. Tyrell, D., “Passenger Rail train-to-Train Impact Test Volume I: Overview and Selected Results,” DOT/FRA/ORD-03/17.1, U.S. Department of Transportation, Washington, DC, July 2003.

23. Tyrell, D., Severson, K., Perlman, A.B., “Single Passenger Rail Car Impact Test Volume I: Overview and Selected Results,” US Department of Transportation, DOT/FRA/ORD-00/02.I, March 2000.

24. Tyrell, D., Severson, K., Zolock, J., Perlman, A.B., “Passenger Rail Two-Car Impact Test Volume I: Overview and Selected Results,” US Department of Transportation, DOT/FRA/ORD-01/22.I, January 2002.

25. Carolan, M., “Performance Efficiency of Crash Energy Management Systems.” Tufts University Undergraduate Honors Thesis, May 2006.

26. National Transportation Safety Board, “Railroad Accident Report: Head-On Collision of Boston and Maine Corporation Extra 1731 East and Massachusetts Bay Transportation Authority Train No. 570 on Former Boston and Maine Corporation Tracks, Beverly, Massachusetts, August 11, 1981,” PB82-916301, NTSB-RAR-82-1, 1982.

27. Kirkpatrick, S.W., and Simons, J.W., “High-Speed Rail Collision Safety,” Rail Vehicle Crashworthiness Symposium, June 24-26, 1996, Cambridge, Massachusetts, DOT/FRA/ORD-97-08, pp. IIA-3-13 to IIA-3-27.

28. Stringfellow, R., Rancatore, R., Llana, P., Mayville, R., "Analysis of Colliding Vehicle Interactions for the Passenger Rail Train-to-Train Impact Test," American Society of Mechanical Engineers, Paper No. RTD2004-66037, April 2004.

29. Kirkpatrick, S.W. and MacNeill, R.A., "Development of a Computer Model for Prediction of Collision Response of a Railroad Passenger Car," Proc. JRC2002, The 2002 ASME/IEEE Joint Rail Conference, Washington D.C., Apr. 23-25, 2002.

30. Martinez , E., Zolock, J., Tyrell, D., “Crush Analysis of Multi-Level Equipment,” American Society of Mechanical Engineers, Paper No. IMECE2006-13214, November 2006.

31. ABAQUS/CAE Version 6.6-1, 2006, Abaqus, Inc. Providence, RI, USA

32. Martinez, E., Tyrell, D., Zolock, J., "Rail-Car Impact Tests with Steel Coil: Car Crush," American Society of Mechanical Engineers, Paper No. JRC2003-1656, April 2003.

33. Priante, M. “A Collision Dynamics Model of a Bi-Level Train.” Tufts University Masters Thesis, May, 2006.